ASTRONOMICAL LIBRARY
NEW PHYSICS BUILDING

MONTHLY NOTICES

OF THE

ROYAL ASTRONOMICAL SOCIETY

Volume 122 No. 1 1961

OHIO STATE UNIVERSITY
APR 20 1961
LIBRARY

Published and Sold by the

ROYAL ASTRONOMICAL SOCIETY
BURLINGTON HOUSE
LONDON, W.1

Price £1 4*s.* 0*d.* (*US* $3.50)

Subscription for volume £6 (*US* $18)

XUM

GEOPHYSICAL JOURNAL, VOLUME 4

Production of the extra volume of the *Geophysical Journal* (Volume 4), in honour of the seventieth birthday of Sir Harold Jeffreys, is now well advanced and publication will take place at the end of March.

The Geophysical Editors have obtained the co-operation of many of Sir Harold's distinguished colleagues and pupils, and believe that the contents of this special volume will represent the most advanced work in a number of fields in which Sir Harold has long been interested.

CONTRIBUTORS INCLUDE

S. Alterman	El Sayad M. Hassan	I. Lehmann
M. Båth	K. Hidaka	A. Marussi
F. Birch	U. Hochstrasser	R. H. Merson
E. C. Bullard	J. E. Jackson	W. H. Munk
K. E. Bullen	J. A. Jacobs	C. L. Pekeris
P. Caloi	H. Jarosch	F. Press
A. H. Cook	N. Jobert	R. Stoneley
A. Day	D. G. King-Hele	H. Takeuchi
F. F. Evison	L. Knopoff	C. Tsuboi
F. Gassman	R. L. Kovach	J. Verhoogen
A. L. Hales	E. R. Lapwood	P. L. Willmore

The complete volume, suitably bound in cloth boards, will also be available as a special publication.

Price £4 (US $ 12)

Orders, with remittance, should be sent to:
Assistant Secretary, Royal Astronomical Society, Burlington House, London, W.1

SPECIAL NOTICE TO FELLOWS

Fellows of the Society may obtain this bound volume of the *Geophysical Journal* at a specially reduced price of £1 10s. 0d. (US $ 4.50). It is particularly requested that Fellows wishing to receive a copy should send their orders, with remittance, as soon as possible to:

Assistant Secretary, Royal Astronomical Society, Burlington House, London, W.1

XUM

MONTHLY NOTICES
OF THE
ROYAL ASTRONOMICAL SOCIETY
Vol. 122 No. 1

A STUDY OF THE 30 DORADUS REGION OF THE LARGE MAGELLANIC CLOUD

M. W. Feast

(Communicated by the Radcliffe Observer)

(Received 1960 August 3)

Summary

The results are presented of a spectroscopic study of stars and nebulosity in the 30 Dor complex of the LMC. Intensity measurements of emission lines yield an electron temperature for the nebulosity of about 10^4 °K and electron densities ranging from, 2×10^2 to 20×10^2 cm^{-3} in different places. The Balmer decrement shows that no large amount of interstellar reddening is present in the region studied. The H/He ratio is normal. The variations in brightness within the nebulosity are probably caused by real variations in density.

Internal motions in the nebulosity are discussed from radial velocity measurements at 37 different points. The velocity dispersion, corrected for observational error is $11{\cdot}3 \pm 3{\cdot}2$ (s.e.) km/sec. Though this is larger than has been found in some other nebulae it is still sufficiently small so that a stable system of large mass may eventually be formed. Despite some indications of motions of an ordered nature the results are analysed on an hypothesis of turbulent motion. The difference in radial velocity (u) between two points is independent of their separation in the range 9–60 pc at least and thus Kolmogoroff's law does not apply in this range. u decreases at smaller separations.

The spectral types of 20 stars are given in Table V. There is a high proportion of W stars, all of which belong to the nitrogen sequence. The other stars are normal supergiants ranging from O8 to F7 Ia. A few stellar radial velocity results are listed. Some examples are given of stars showing an intimate connection with the structure of the nebulosity.

1. *Introduction.*—By far the most conspicuous object in the Large Magellanic Cloud is the diffuse nebula 30 Doradus (NGC 2070). The interest in a study of this structure lies not only in its membership of an extra-galactic system but also in its enormous size. According to Shapley and Paraskevopoulos (1) its total diameter is about 25′ or 400 pc (with a distance of 55 kpc for the LMC). The total gaseous mass has been estimated as 5×10^6 solar masses (2). Photographs with large scale reflectors have revealed the extremely complicated internal structure of the nebula and have led to the adoption by some authors of the names "great looped" nebula or "tarantula" nebula for 30 Dor. Furthermore the filamentary structure has suggested to some astronomers (e.g. (3), p. 291) the presence of large scale non-uniform magnetic fields. A large group of blue stars near the centre of the nebula was reported by Shapley and Paraskevopoulos (1).

Some years ago (4) a note on the spectrum of the bright star at the centre of the 30 Doradus complex was published and the existence of interstellar H and K and 3889 He I was reported. Since that time spectroscopic observations of individual stars and different parts of the nebulosity have gradually been

XUM

QB1
R8
V.122

accumulated. Recently the stellar observations were included in a general tabulation of spectral types and radial velocities in the Magellanic Clouds (**5**) and this therefore seems a suitable time to discuss these observations together with those of the nebulosity.

All the spectrograms were obtained with the two prism spectrograph at the Cassegrain focus of the 74-inch Radcliffe reflector. Either the *a*, *c* or *d* cameras were used (dispersions at Hγ, 21, 48 and 86 A/mm, slit widths 0·05, 0·09 and 0·20 mm). The first part of the paper is devoted to a discussion of some spectrophotometric work on the nebulosity, especially with regard to the determination of electron densities and temperatures. Secondly, radial velocity measurements at different points in the nebulosity are presented and the internal motions discussed. Thirdly, the spectral types of stars in the nebula are discussed together with some radial velocity results. Finally, some examples are given of the connection between stars and nebular structure.

2. *Spectrophotometry.*—The theoretical work carried out in recent years now enables the electron temperature, T_e, and electron density, N_e, in gaseous nebulae to be determined with a fairly high degree of confidence from the relative intensities of certain forbidden lines. From the observational point of view the easiest ratio to measure is that of the [O II] doublet 3729/3726 which yields N_e if a value of T_e is measured or adopted. Provided T_e is not far from 10^4 °K (the value expected theoretically for most nebulae) the actual value does not affect N_e greatly. T_e may be derived from the ratio of the [O III] lines 5007 + 4959/4363. Since these lines are fairly widely separated in the spectrum, photometric problems arise which are unimportant in the case of the [O II] doublet. In the following the results of line intensity measurements on plates suitably calibrated for heterochromatic photometry are first described including a determination of T_e from the [O III] intensities, and after this the determination of N_e from the [O II] doublet intensities on other plates is discussed.

The normal photometric procedure was followed, that is, spectra of a star with a known spectrophotometric gradient were obtained immediately before or after the nebular spectra. Either α Dor or o Vel (or sometimes both) were used, as these could be observed at a zenith distance close to that at which the nebular observations were made. The relative gradients of these stars have been measured by Gascoigne (**6**) and the absolute gradients may be deduced by a comparison with the work of Barbier and Chalonge (**7**). The brightness of the standard stars was reduced by about 4 magnitudes by a diaphragm placed over the collimator of the spectrograph. The plates were calibrated both by a spot sensitometer with a blue filter and by exposures in an auxiliary spectrograph using a rotating stepped sector to provide the calibration marks. All plates in any one series were taken from the same box and were developed together. The spectra were analysed with the Observatory's recording microphotometer*.

The calibration curves obtained from the exposures with the auxiliary spectrograph showed no wavelength dependence in the short wavelength region ($\lambda < 4500$A) and agreed with the results of the spot sensitometer. However in the 5000A region (103aO plates) the curves do depend on wavelength. In order to

* This has recently been improved by the provision of stabilized power supplies for the light source and phototube, designed and constructed in the National Physical Research Laboratory, Pretoria, under the direction of Mr J. D. N. v. Wyk. I am much indebted to him for his help and interest and also to Mr T. J. Deeming for help in testing the microphotometer in its present form.

cover the whole range of observed line intensities it was necessary to have several different exposures for each region of the nebula studied. It should be emphasized that the highest photometric accuracy is not claimed for these results and, in particular, difficulties may have been encountered with atmospheric dispersion in observing the standard stars, although a wide slit was used in all this work. However, for the purpose to which they are put, the results should be of sufficient accuracy. Line intensities have been derived in this way from a series of exposures at position A (see Plate 1 (*a*)) (*d* camera), two series at position D (one *c* and one *d* camera) and a series close to the central star R 136 (*d* camera). Apart from the [O II] doublet ratio (see below) there is no apparent variation in the relative intensities in these series and the means only are given in Table I. Hβ is taken arbitrarily as 100. The results for the fainter lines in this table depend mainly on the series at A and the quoted [O II] intensities are for this point. For comparison, Table I also gives the intensities determined by Johnson (**2**) from one plate at 298 A/mm and intensities measured photoelectrically in the Orion nebula by Aller and Liller (**8**).

The most likely place for error in the present work is near N_1 and N_2 where the sensitivity of 103aO plates is falling rapidly. In particular N_1 (5007) is quite near the limit of plate sensitivity. Since N_1 and N_2 originate in the same upper level their intensity ratio should equal the ratio of their transition probabilities. The computed value by Garstang (**9**) is 2·93 whilst the best measured (photoelectric) value is $3{\cdot}03 \pm 0{\cdot}11$ (see (**3**), p. 185). The results of Table I give the ratio N_1/N_2 as 4·1 which is about 30 per cent higher. This may be a result of an over-correction of N_1 for falling plate sensitivity. In fact, the uncorrected ratio is 2·8. It is interesting to note that Johnson's determination (**2**) in 30 Dor is correspondingly low (2·1). It should be noted that the strengths of N_1 and N_2 relative to Hβ are dependent on excitation and ionization conditions in the nebula.

TABLE I

Line intensities in 30 Doradus

Line (λ)	30 Dor	30 Dor (**2**)	Orion (**8**) Nebula	Theoretical Balmer decrement (**10**)
3726 [O II]	102	155	127	
3729 [O II]	98			
H9		10		
3871 [Ne III]	33	58	19·7	
3889 He I + H8	26	41	18·1	
3967 [Ne III]	11	53	24·4	
Hϵ	16			21
4026 He I	3·0	4	2·7	
Hδ	30	38	25	31
Hγ	56	63	41	51
4363 [O III]	3·5		1·55	
4471 He I	4	6	4·6	
Hβ	100	100	100	100
4957(N_2) [O III]	182	140	113	
5007(N_1) [O III]	741	296	342	

Also in Table I are the intensities of the Balmer lines calculated by Baker and Menzel (**10**) for "case B" (nebula optically thick in Lyman alpha) at an electron temperature of 10^4 °K. This theoretical Balmer decrement has frequently been used together with the observed decrement to estimate the amount of interstellar

reddening present. However, recent work by Pottasch (**11**) taking into account radiative excitation from the second level of the hydrogen atom shows that the theoretical decrement requires a correction which is a function of the optical depth of the nebula to Hα, and which has the effect of increasing the strength of later members of the Balmer series relative to Hβ. The accuracy of the present results does not warrant a detailed comparison with theory. The important point to note is that the ratio Hβ/Hγ has probably not been greatly affected by interstellar reddening so that the ratio $(N_1+N_2)/4363$ can be used directly to determine T_e without applying any reddening correction.

The ratio $4363/(N_1+N_2)$ $(=r')$ is strictly a function of both N_e and T_e but at low densities (as found in 30 Dor) we may with sufficient accuracy write

$$r' = 0{\cdot}113 \times 10^{-14\,300/T_e}$$

(see (**3**), p. 193).

Using the figures in Table I we obtain

$$T_e = 9700\ ^\circ\mathrm{K}.$$

In view of the previous discussion of the ratio N_1/N_2 it may be preferable to omit N_1 and to use N_2 together with the theoretical value of the ratio N_1/N_2. This was, in fact, the procedure adopted by Andrillat (**12**) for planetary nebulae. In this case we obtain

$$T_e = 10\,500\ ^\circ\mathrm{K}.$$

Clearly the electron temperature is close to $10^4\ ^\circ$K and this is the value adopted in this paper. Johnson (**2**) obtained the higher value of 14 000 °K. However, he did not observe λ4363 directly since at the dispersion he used it was blended with Hγ and he was forced to deduce its intensity from the departure of the measured intensity of Hγ from a theoretical Balmer decrement. The present determination should therefore be of higher accuracy.

TABLE II

Measured ratio $r = 3729/3726$ [O II] *in 30 Dor and deduced electron density* N_e.

Position	r	$N_e(\mathrm{cm}^{-3})$
A	0·95	$8{\cdot}5 \times 10^2$
B	1·26	$2{\cdot}4 \times 10^2$
C	1·05	$5{\cdot}9 \times 10^2$
R140	0·98 :	$7{\cdot}6 \times 10^2$:
R136 (Central star)	0·71	20×10^2
R136 (to side of continuum)	1·15	$4{\cdot}0 \times 10^2$
	1·35 :	$1{\cdot}3 \times 10^2$:

PLATE 1 (*see facing page*)

(*a*) *Reproduction of inner region of 30 Dor from a 74-inch Radcliffe reflector Newtonian plate* (*K*103*aE*+*W*12, 3^m *exposure*). *All points for which radial velocities of the nebulosity have been measured are marked except* X *and* Y *which are in the outer parts* (*see Plate 2*). *Some positions are indicated in black on the position and some in white to the side of the star used as a reference point. Most of the stars for which spectral types are given in Table V are also indicated. Maps for these stars have previously been published* (**5**). *There is a plate defect 14 mm from the N side and 39 mm from the following side.*

(*b*) *The region of star R*143 (*F*7 *Ia*) *showing filaments discussed in text;* (*c*) *Star* V *showing surrounding nebular structure* (*see text*); *and* (*d*) *Star* I *showing surrounding "Strömgren sphere"* (*see text*).

(*b*), (*c*) *and* (*d*) *are reproduced from a 74-inch photograph* (*K*103*aE*+*W*12 30^m *exposure*). *Throughout Plate 1, south is at the top, preceding to the right and the scale of the reproductions is 2·2 sec of arc per mm.*

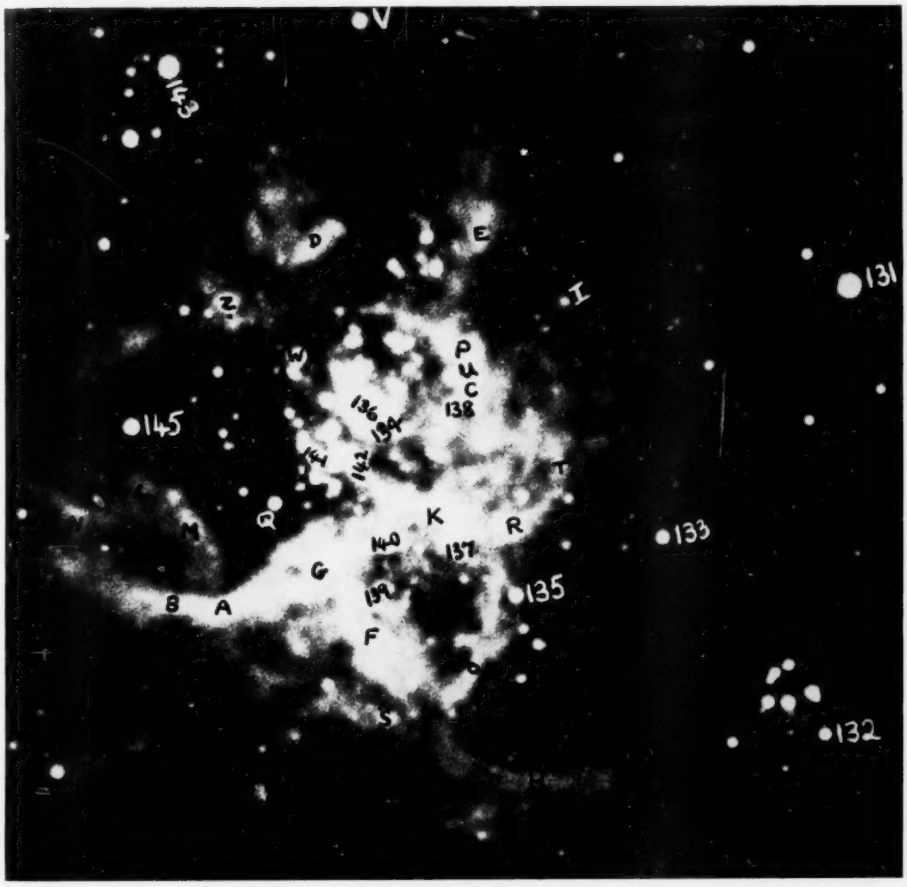

(*a*)

(*b*)

(*c*)

(*d*)

M. W. Feast, A study of the 30 Doradus region of the Large Magellanic Cloud

Reproduction of 74-inch photograph of 30 Dor (K103aE+W12, 30^{m} exposure). South is at the top and preceding to the right. The scale is 8·2 sec of arc per mm. Star X is 89 mm from the north side and 25 mm from the following side. Star Y is 97 mm from the north side and 32 mm from the preceding side. The long curved filament referred to in the text may be seen on the north side of the main nebulosity stretching from star AB (25 mm from north side and 46 mm from following side) to star AA (42 mm from north side and 54 mm from following side). The great loop (LMNAB of Plate 1 (a)) is over-exposed on this plate—its centre lies 86 mm from the north side and 45 mm from the following side.

In principle the ratio of He 4471 and He 4026 to Hβ can be used to estimate the abundance of He relative to H (**13**). A detailed discussion is not warranted but the agreement of the 30 Dor intensities with those measured in the Orion nebula suggests a similar He/H ratio, a conclusion reached also by Johnson (**2**).

The ratio 3729/3726 ($=r$) has been measured at a number of places in the nebula and the results are listed in Table II. Generally for these measurements the plates were calibrated by means of the spot sensitometer. The lines are so close together that heterochromatic corrections from standard stars are not required.

According to Seaton and Osterbrock (**14**)

$$r = 1{\cdot}5\left[\frac{1+0{\cdot}33\epsilon+2{\cdot}30x(1+0{\cdot}75\epsilon+0{\cdot}14\epsilon^2)}{1+0{\cdot}40\epsilon+9{\cdot}9x(1+0{\cdot}84\epsilon+0{\cdot}17\epsilon^2)}\right]$$

where $\epsilon = e^{-1{\cdot}96/t}$, $x = 10^{-4}N_e/t^{1/2}$, $t = 10^{-4}T_e$. Putting T_e as 10^4 °K the values of N_e given in Table II are obtained. This calculation assumes that the observed radiation is coming from a region of constant N_e and T_e. This is probably incorrect (at least so far as N_e is concerned). If a nebula has a regular structure, some attempt can be made to correct for variations in N_e along the line of sight (cf. Osterbrock and Flather (**15**)) but it is unlikely that this could be done for so complicated a structure as 30 Dor, at least not without very many more observations.

Whilst the values of N_e given in Table II are thus only some kind of weighted mean along the line of sight they are still of some considerable interest. The average value of N_e is quite low and corresponds roughly to that found in the outer parts of the Orion nebula (in this nebula N_e varies from $1{\cdot}8\times10^4$ to $2{\cdot}6\times10^2$ cm^{-3} (**15**)). No densities as high as that observed in the centre of the Orion nebula have been found but the highest value in 30 Dor is actually in the "central star". This "star" is found in good seeing to be distinctly diffuse and probably has a diameter of the order of 2·to 3 seconds of arc. The observation of the [O II] doublet is difficult at this position since there is a strong stellar continuum present but it appears that N_e is higher here than at other points investigated. The dense inner region of the Orion nebula is only about 4 minutes of arc in diameter (see (**15**), Plate 4). Adopting with Osterbrock and Flather (**15**) a distance of 450 pc for the Orion nebula and 55 kpc (corrected distance modulus $18^m{\cdot}7$, see (**5**)) for the LMC, the size of this inner region in the Orion nebula would be about 2 seconds of arc at the distance of 30 Dor or about the size of the central "star". In the Orion nebula it is only within this region that very high densities ($r \leqslant 0{\cdot}7$) occur. It is quite possible that in limited regions of 30 Dor (of the order of 1 second of arc diameter) the electron density may rise to as high as 10^4 cm^{-3}, as in the centre of the Orion nebula, but since we are integrating over a large volume such high densities would probably go undetected.

In discussing the structure of so complex a nebula as 30 Doradus it is possible to adopt two extreme views. Either the variations in brightness across the nebula are due to variations in density or else the density remains essentially constant and the variations in brightness are due to some other cause (e.g. distribution of dark obscuring clouds; distribution of exciting stars; emission originating in regions of widely different depth in the line of sight). A comparison of density measurements with surface brightness observations could distinguish between these two extremes. The present measurements do indeed suggest that regions of greater

XUM

brightness are also regions of higher density (cf. the results of Table II with Plate 1 (*a*)). Note the decrease in N_e from point A to the adjacent and fainter point B. The nebulosity is fairly bright near points C and R140 but is relatively weak near the central "star" (outside the small dense core).

Johnson (**2**) has attempted to estimate the mass of 30 Dor from the limited data at his disposal. The mass derived, 5×10^6 solar masses, must be considered quite uncertain. The new observations of N_e reported above could be used to extend this type of calculation but in view of the complex structure of the nebula it is doubtful if any simple model will give a good approximation to the actual nebula and the derived mass depends largely on the model adopted. However, the present density determinations are of the same order of magnitude as Johnson's single determination and it seems therefore that the mass of 30 Dor must be extremely large and probably of the order of magnitude calculated by Johnson.

No attempt has been made to study the nebular continuum though a long exposure at point B shows it quite strongly. Note that the spectrum reproduced in (**5**) refers to point B of 30 Dor.

3. *Radial velocities of the nebulosity.*—Internal motions in diffuse nebulae have been studied in only a very limited number of cases and the Orion nebula is the only one in which extensive investigations with slit spectrographs have been undertaken. The present radial velocity observations in 30 Dor comprise 56 spectrograms referring to 37 different points within the nebula. These points are all indicated in Plates 1 (*a*) and 2. In some cases stars were used as reference points; in other cases no stars were visible at the position observed. The spectra were measured in the usual way on the Observatory's Casella projection measuring machine. Laboratory wavelengths were used for H and He lines and the wavelengths of forbidden lines were taken from Bowen's paper (**16**). Most of the observations were made with the *c* or *d* cameras but a few were made with the *a* camera. In the case of the *a* and *c* cameras all the lines visible on a plate (generally Kodak 103aO) were used in determining the mean velocity. However, in the case of the *d* camera the lines N_1 and N_2 are generally very strong and in a region both of low dispersion and where the iron arc is usually rather unsuitable for measurement. These lines were therefore omitted from the mean. Since the number of lines measured may vary considerably from spectrum to spectrum the following system of weights has been adopted:

d camera, unit weight per line;
c camera, double weight per line;
a camera, quadruple weight per line.

At 11 points in 30 Dor there are observations with the *c* (and/or *a*) and *d* cameras. It is found that

$$\Delta V(c-d) = +2{\cdot}9 \pm 3{\cdot}2 \text{ (s.e.) km/sec.}$$

There is thus no evidence of a systematic difference between the *d* camera and the higher dispersions. In earlier work on *stars* at about the same declination as 30 Dor it was found that

$$\Delta V(c-d) = +11{\cdot}4 \pm 2{\cdot}7 \text{ km/sec (5)}$$
$$\Delta V(c-d) = +10{\cdot}0 \pm 3{\cdot}5 \text{ km/sec (17)},$$

and a correction of +10 km/sec was applied to all *d* camera velocities. Whilst the standard errors of the various differences are quite large it is of interest that the

30 Dor nebulosity results do not indicate any significant difference. Since these results apply to an extended source for which, if uniform, atmospheric dispersion should be negligible, they lend support to the view previously advanced that the differences observed in the case of stars are due to the effect of atmospheric dispersion on guiding at a wide slit. In the following the *d* camera velocities are used without any correction.

TABLE III

Velocities of 30 Doradus nebulosity

Position	Velocities from individual plates			Mean velocity	Weigh
R132	+225: (1*d*)	+244: (1*d*)		+234	2
R133	+266(4*d*)			+266	4
R134	+254(7*d*)	+300(3*d*)		+268	10
R135	+279(4*d*)	+278(5*c*)		+278	14
R136	+267(4*c*)	+280(3*c*)	+254(9*d*)	+265	23
R137	+277(8*c*)	+270(7*d*)		+275	23
R138	+242(3*d*)	+242(4*c*)	+230(8*d*)	+237	19
R139	+248(4*c*)	+264(3*d*)		+252	11
R140	+268(10*d*)	+267(8*d*)		+268	18
R141	+261(4*d*)			+261	4
R142	+239(3*d*)			+239	3
R143	+251(1*d*)			+251	1
A	+250(5*c*)			+250	10
B	+242(10*d*)	+251(3*a*)	+252(3*d*)	+248	25
C	+234(10*d*)			+234	10
D	+261(1*a*)	+257(5*c*)		+258	14
E	+262(3*c*)	+252(3*d*)		+259	9
F	+269(4*c*)			+269	8
G	+264(4*c*)	+260(8*d*)	+258(6*d*)	+261	22
H	+244(3*d*)			+244	3
I	+247(2*d*)			+247	2
K	+264(4*d*)			+264	4
L	+291(3*d*)			+291	3
M	+287(3*d*)			+287	3
N	+283(3*d*)			+283	3
O	+289(5*d*)	+274(5*c*)		+279	15
P	+243(6*c*)			+243	12
Q	+266(2*d*)			+266	2
R	+265(6*c*)			+265	12
S	+236(9*d*)	+245(5*c*)		+241	19
T	+275(5*c*)			+275	10
U	+239(7*d*)			+239	7
V	+234(3*d*)			+234	3
W	+276(2*d*)			+276	2
X	+258(2*d*)			+258	2
Y	+275(3*d*)			+275	3
Z	+268(8*d*)	+275(4*c*)		+272	16

Description of Table III

Column

1 The position of the nebulosity observed is identified (cf. Plates 1 (*a*) and 2). The numbered positions refer to stars listed in (5).

2, 3, 4 The individual plate velocities. The number of lines measured and the camera used are given in brackets.

5, 6 The adopted mean velocity and its weight. The unit is km/sec.

The measured velocities are listed in Table III. The weighted mean of these velocities is then found to be $+259{\cdot}7$ km/sec. An unweighted mean is insignificantly different from this value.

de Vaucouleurs (**18**) gives $+273 \pm 19$ (s.e.) km/sec for a point near the central star and $+269 \pm 12$ (s.e.) km/sec for a "bright arch" from low dispersion spectrograms (s.e. computed from published p.e.) Wilson (**19**) gives a mean velocity of $+275$ km/sec for the nebula from 4 plates. Apart from de Vaucouleurs' measurement near the central star, which agrees within the quoted error with the present value, direct comparison is not possible since the exact positions observed by Wilson and de Vaucouleurs are not known.

The velocity dispersion in the nebula corrected for observational error was obtained from the equation (**20**):

$$\sigma^2 = \sigma_e^2 - \sum_i \nu_i \sigma_0^2 / i \qquad (1)$$

where σ = the true velocity dispersion,

σ_e = the observed velocity dispersion giving equal weight to each point in the nebula observed,

σ_0 = the internal dispersion per unit weight which is derived from those points with more than one spectrum each (15 points)

ν_i = the fraction of points with weight i.

In this way the observations give

$\sigma^2 = 256{\cdot}7 - 128{\cdot}4 = 128{\cdot}3$ (km/sec)^2

and $\sigma = 11{\cdot}3 \pm 3{\cdot}2$ (s.e.) km/sec.

These results indicate that there is a considerable velocity dispersion in the nebula. Velocity dispersions of the order of 3 km/sec have been reported for some nebulae (**21**) (note that the mean deviations given in (**21**) must be multiplied by $1{\cdot}25$ to be comparable with the present dispersion) though certain nebulae (e.g. radio sources) have much larger velocity dispersions. The deviations of the velocities from the mean are plotted in Fig. 1.

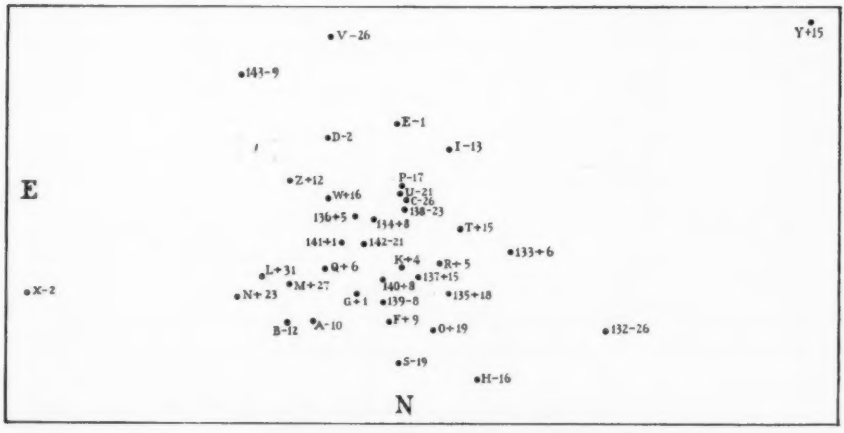

FIG. 1.—*Velocities of the 30 Dor nebulosity. The dots indicate the positions measured. The letter or number of the point observed is followed by the difference of the radial velocity from the mean (+260 km/sec). For identification of the points compare with Plates 1 (a) and 2.*

It is not clear *a priori* whether this dispersion is the result of large scale turbulent motion or whether some ordered motion such as a general expansion is dominant. In the case of a simple spherical expanding mass of gas the radial velocity dispersion should decrease from the centre to the edge of the nebula. The present observations neither confirm nor deny this hypothesis. It is interesting to note, however, that in the central region of 30 Dor the radial velocities with respect to the central star range up to about 30 km/sec. This would correspond on an expansion hypothesis to the maximum velocity of expansion. The prominent arc of which position X is a part on the following side of the nebula is about 65 pc. from the central star (cf. Plate 2). If it were expanding at 30 km/sec in the plane of the sky it would have reached this distance in $\sim 2 \times 10^6$ years, a length of time one might expect for the age of 30 Dor. (Compare the age of AE Aur and μ Col ($2{\cdot}6 \times 10^6$ years) derived from their motions away from the Orion nebula (**22**).)

This calculation neglects the possible effects of magnetic and gravitational forces. The possible existence of appreciable magnetic fields has been suggested ((**3**), p. 291) in order to account for the structure of the nebula. If the mass is as high as estimated by Johnson (**2**) then the velocity of escape becomes of the same order as the observed range of velocities and gravitational forces may appreciably modify the motions. This is in contrast to the situation that probably exists in the Orion nebula.

Indeed it is of interest to note that gravitational forces may be sufficiently strong to stabilize at least the inner parts of 30 Dor. This may be illustrated by assuming equilibrium and applying the virial theorem to determine the mass of the system. Adopting the virial theorem in the form given by Chandrasekhar (**23**)*

$$\overline{V^2} = \frac{GM}{2R} \qquad \begin{array}{l} G = \text{gravitational constant.} \quad M = \text{mass.} \\ R = \text{"average" radius of system.} \end{array}$$

$$\overline{V^2} = 3\sigma^2 \quad (\sigma \text{ as above}).$$

Since most of the radial velocities refer to points in the inner part of the nebula within a projected distance of about 25 pc of the centre, this value for R was adopted. Then using the value of σ given above, the total mass of the inner region becomes

$$M = 4{\cdot}4\,(\pm 2{\cdot}6 \text{ s.e.}) \times 10^6 \text{ solar masses.}$$

Adopting a model for 30 Dor based on the Orion nebula, Johnson (**2**) obtained for the mass of gas in the entire system

$$M_{\text{gas}} = 5 \times 10^6 \text{ solar masses.}$$

The agreement between these two figures (fortuitously close) suggests that the nebula may approach the conditions of stability fairly closely and that eventually a stable system of considerable mass may be formed.

Perhaps the most conspicuous feature of the nebula, at least on short exposure photographs, is the great loop on the N following side of the nucleus. It is probably this structure which accounts for 30 Dor being known as the "great

* The apparent difference by a factor two from the equation given by Schwarzschild (**24**) is due to a different definition of R. Examination of several possible density distributions suggests that the form given by Chandrasekhar is more likely to be appropriate when R is a radius estimated from direct photographs.

XUM

looped nebula". Radial velocities have been measured at several different points around this loop and comparison of Fig. 1 and Plate 1 (*a*) shows that there are marked changes in velocity from one side to the other. Radial velocity differences of 30 or 40 km/sec occur for diametrically opposed points so that, at least in its present form, it must be an extremely short lived structure. It will also be seen that the fainter portions of the loop have a higher velocity of recession than that measured anywhere else in the nebula. Clearly so far as the gas in this loop is concerned, ordered motion of some kind (e.g. expansion of the loop) is more important than a general turbulent motion. If more results were available it might be possible to detect other examples of the relationship of radial velocity to the detailed filamentary structure of the nebula.

However, despite the above conclusions, it is of interest to apply the theory of turbulence to the nebula as a whole. This is particularly so since there has been a good deal of interest in recent years in turbulence in the interstellar medium. Furthermore the great linear dimensions of 30 Dor should allow the spectrum of turbulence to be extended to much smaller wave numbers than has previously been possible.

Von Hoerner (**25**) has subjected the velocities measured in the Orion Nebula by Campbell and Moore (**26**) to an analysis for turbulent motion and it will be convenient to follow his procedure here.

It was shown by Kolmogoroff (**27**) that the equilibrium spectrum for isotropic, homogeneous, incompressible turbulence is

$$F(k) \propto k^{-5/3}$$

where $F(k)$ is the spectrum of turbulence and k the wave number ($1/k$ may be pictured as defining the size of the turbulent elements). Von Hoerner ((**25**), eq, II, 10) finds that under these conditions the radial velocity difference (u) between any two points in a nebula varies approximately as the cube root of their projected distance (Λ) for distances large compared with the effective depth of the nebula and approximately as $\Lambda^{5/6}$ for smaller distances. Campbell and Moore's observations were found by von Hoerner to show the dependence $u \propto \Lambda^{1/3}$ and this was taken as confirmation of the Kolmogoroff law (the coefficient actually found was 0·4 which was explained by von Hoerner as the effect of optical depth).

Courtès, from measurements with an interferometer (**21**), (**28**) showed that a similar dependence of u on Λ occurred in the inner parts of the λ Ori nebula but that in the outer parts of this nebula u became more or less independent of Λ. This was taken to indicate a transitional region in the spectrum of turbulence towards the von Karman region where for large turbulent elements (small k) the law $F(k) \propto k^4$ should apply.

The recent beautiful and very detailed measurements of internal motions in the inner part of the Orion nebula by Wilson, Münch, Flather and Coffeen (**29**) have not yet been submitted to a detailed analysis. A preliminary analysis by Münch (**30**) confirmed that $u \propto \Lambda^{1/3}$ as found from the earlier observations. This, according to Münch, does not, however, imply that the Kolmogoroff law applies since the $\Lambda^{1/3}$ dependence holds to such small values of Λ that an effective depth of the nebula is indicated which is inconsistent with line breadth measurements. Furthermore, since relative velocities in excess of the velocity of sound (~ 12 km/sec) are measured in the nebula, the turbulence cannot be incompressible, a necessary condition for the applicability of the Kolmogoroff law. Since

no comprehensive theory of compressible turbulence exists, this effectively reduces us to a purely descriptive level.

In 30 Dor the radial velocity difference V and the projected distance Λ have been measured for all possible pairs of points. Since velocities were measured at 37 points, this gives 666 point pairs. Von Hoerner discussed the inner and outer regions of Orion separately with 49 points in the former and 36 points in the latter. Dividing the point pairs into distance groups the mean square velocity $\overline{V^2}$ was determined for each group. Then $\overline{u^2}$ the true mean square value corrected for observational error is given by

$$\overline{u^2} = \overline{V^2} - 2\sum \nu_i \sigma_0^2 / i \qquad (2)$$

(cf. eq. (1) above) where, in this case, summation is carried out over all points in each distance group. Table IV lists the values of $\overline{V^2}$ and $\overline{u^2}$.

TABLE IV

"Point pair" turbulence analysis in 30 Doradus

Range of Λ (sec. of arc)	Mean Λ (sec. of arc)	Mean Λ (pc)	No. of point pairs	$\overline{V^2}$ (km/sec)^2	$\overline{u^2}$ (km/sec)^2
0–20	14·1	3·8	17	140·5	−8·4
21–42	33·2	8·8	62	414·2	211·6
43–64	53·2	14·2	104	489·8	310·3
65–86	75·9	20·2	108	480·5	270·3
87–108	97·5	26·0	88	625·0	390·1
109–130	119·7	31·9	77	498·6	280·7
131–152	142·1	37·9	51	506·4	179·9
153–196	172·9	46·1	60	663·3	289·8
197–284	235·8	62·9	55	685·9	272·5
285–614	356·8	95·1	44	424·6	80·6

The original analysis was carried out with Λ in mm, as measured on a photograph ; the limits given in sec. of arc are approximate.

Two other corrections to the observed quantities are discussed by von Hoerner. The first takes into account the effect of finite slit width. This is important only for point pairs with distances comparable to the slit width. The effect is not important in the present case, partly because the measures do not extend to quite so small a value of Λ (sec. of arc) as in the Orion nebula and, to a larger extent, because the scale of the Radcliffe reflector is more than six times that of the Crossley reflector with which Campbell and Moore worked. The other correction is for the widths of each distance group. This is negligible for the present purpose. The statistical uncertainty of $\overline{u^2}$ is given (**25**) by the equation

$$\sigma(\overline{u^2}) = 1{\cdot}414\,\overline{V^2}\sqrt{\frac{1}{\nu} + \frac{1}{N}}$$

where N = the total number of point pairs,
and ν = the number of different points in each group.

In Fig. 2 $\log\sqrt{(\overline{u^2})}$ is shown plotted against $\log\Lambda$. The vertical lines indicate the limits of $\sigma(\log\sqrt{(\overline{u^2})})$. The point for the smallest distance group, $\Lambda = 14$ sec

of arc ($\doteqdot 4$ pc, and $0 < \Lambda < 20$ sec of arc), is omitted since $\overline{u^2}$ is negative. Whilst the uncertainty in this value would easily allow $\overline{u^2}$ to take on a positive value it is clear that the velocity dispersion is significantly less than for the more distant groups. It might be argued that the motions of individual clouds of the order of size of 4 pc are here being measured and that their internal turbulent motion is small compared with the observational errors. In this connection it should be mentioned that of the 17 point pairs with $\Lambda < 20$ sec of arc, 6 refer to the four points (P, U, C, R138). These four points have velocities which do not differ significantly from one another and direct photographs give the impression that they all refer mainly to one elongated cloud (about 4 pc long) (cf. Plate 1 (*a*)).

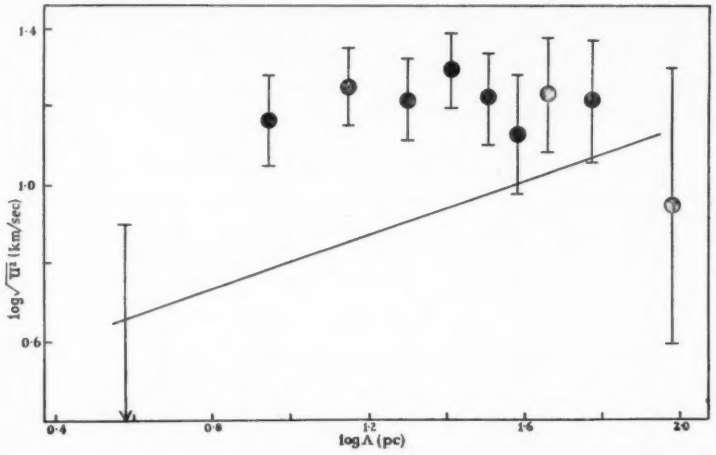

FIG. 2.—*Analysis for turbulence in* 30 *Dor. Relation between log* $\sqrt{(\overline{u^2})}$ *(km/sec) and log* Λ *(pc). The lengths of the vertical lines are twice the standard errors. The point for the smallest value of* Λ *has* $\overline{u^2}$ *negative (see text). The sloping line shows the relationship* $u \propto \Lambda^{1/3}$ *(Kolmogoroff's law).*

Apart from this one distance group it is clear from Fig. 2 that u is practically independent of Λ. This is the state of affairs found in the outer parts of the λ Ori nebula (**21**). Whether it is proper to describe this as a transition in the turbulence spectrum from the Kolmogoroff to the von Karman regions as suggested by Courtès is uncertain both as a result of Münch's work (**30**) (see above) and also because of possible systematic motions in the nebulae as previously mentioned. Such systematic motions would affect the interpretation of Courtès' work equally with the present results.

It will be noticed that there is a slight indication that u may decrease again for very large Λ. Whilst this would be in line with a transition to the von Karman region the result has little weight especially since the point pairs in the largest distance group depend heavily on the combination of the two outer points (Y, X) with the other points and the velocities at many more outer points would be needed to confirm the effect.

According to Courtès (**21**) the change from a linear dependence of log $\sqrt{(\overline{u^2})}$ on log Λ occurs at about 8 pc in the λ Ori nebula. Courtès (**21**) also reported a similar effect in the outer parts of the Orion Nebula setting in at about 1 pc. However a more recent publication (**28**) whilst reproducing the λ Orionis results

unchanged, shows a linear dependence of log $\sqrt{(\overline{u^2})}$ on log Λ out to at least 2 pc (the largest separation reported) in the Orion nebula.

In 30 Dor it is clear that log $\sqrt{(\overline{u^2})}$ must drop fairly steeply between 9 pc (33 sec of arc) and 4 pc (14 sec of arc). We may, therefore, conclude for these nebulae that whatever the theoretical interpretation of the results may be, the value of u shows an increase with increasing Λ (probably as $\Lambda^{1/3}$ approximately) up to values of Λ of the order of 5 pc after which u becomes independent of Λ, out to at least 60 pc in the case of 30 Dor.

4. *Spectral types and radial velocities of stars in the 30 Dor region.*—Precise determination of spectral type and radial velocity is extremely difficult for many of the stars in the 30 Dor region, since it often happens that the stellar spectrum is overlaid by strong nebular emission lines. Spectral types of some 20 stars have been obtained as well as radial velocities for a few of these stars. These results were included in the recent compilation of Magellanic Cloud observations (**5**). They are listed here in Tables V and VI for convenience where the numbering is from (**5**). The stars were partly selected from the HDE catalogue and partly from direct photographs.

TABLE V

Spectral types in the region of 30 Doradus

Star	Type	HD	Star	Type	HD
R129	Bo Ia :	269896	139	WN7+O :	
130	Bo :+W?		140	WN6	
131	B9 I	269902	141	Bo.5 :	
132	B—A		142	B	
133	O8		143	F7 Ia	
134	WN7		144	WN7	38282
135	WN7		145	WN6–7	269928
136	O+WN	38268 (central star).	146	WN5	269926
137	Bo.5 Ia :		147	WN5+	38344
138	Ao : I :		151	A5 Ia :	269982

F103 is a foreground star in the direction of 30 Doradus. Full notes on these spectral types are given in (**5**).

The outstanding feature of the spectral types is the presence of a considerable number of Wolf-Rayet stars; 9 out of the 21 stars studied. It is to be expected that many more W stars await discovery in this region, but even with the present number 30 Dor represents the richest group of these stars in the sky. All the W stars so far found belong to the nitrogen sequence. Roberts (**31**) has shown that in the galaxy there is a tendency for the W stars in cluster and associations to be of the nitrogen rather than the carbon sequences though some WC stars do occur in clusters and it is noteworthy that in some groups of stars (e.g. NGC 6231) both a WC and a WN star occur. Roberts has suggested that all W stars are formed in clusters or associations and that his results imply a greater age for WC stars than for WN stars. The possibility that WN stars might evolve into WC stars has been discussed previously (**32**) in connection with the observation that some novae

XUM

resemble WN stars at one stage of their evolution and WC stars at a later stage. The W stars observed in 30 Dor cover the whole range of WN spectral types. Rough magnitude estimates for these stars from direct photographs using an iris diaphragm photometer, indicate that they scatter over at least a magnitude with no indication of any magnitude spectral type relationship.

TABLE VI

Radial velocities in 30 Doradus

Stellar Velocities		Interstellar H and K	
Star	Radial Velocity (km/sec)	Star	Radial Velocity (km/sec)
R129	+273	R134	+287
R131	+269	R136	+295
R133	+235 :	R139	+307
R136	+251 :		
R143	+263		
Mean	+262	Mean	+296

Mean nebular velocity = +260 km/sec.
He I 3889 (R136) = +240 km/sec.
Individual plate velocities are given in (5)

The spectral types of the other stars in the region of 30 Dor are all normal supergiants ranging from O8 to F7 Ia. The A5 Ia star (R151) which is on the outskirts of the cluster might, of course, be a member of the general field of the LMC but R143, F7 Ia, the latest type found in the region is intimately connected with nebulosity (see Section 5) and thus there is no doubt that it must be considered a member of the 30 Dor complex. Whilst there is no direct proof for later type members of 30 Dor a number of red irregular variables have been found scattered over a wide region around the nebula (**33**). These stars have been assumed by Sharpless (**34**) to represent M-type supergiant members of 30 Dor and to be similar to the M supergiants in h and χ Per. This seems quite likely but it would be desirable to observe some of the stars spectroscopically and photoelectrically. At $\overline{m_{pg}} = 15^{m}{\cdot}2$, however, they are below the magnitude limit of the present programme.

There are only five stars in 30 Dor for which radial velocities have so far been obtained and three with interstellar lines suitable for measurement. These few results are listed in Table VI where the means are given for stars, interstellar H and K, nebular emission lines and the nebular absorption line He I 3889 in the central star. The H and K lines seem to indicate a velocity systematically higher than the other sets of measures, but the data are clearly insufficient for a proper discussion.

5. *The relationship between the stars and the nebulosity.*—Whilst the 30 Dor nebulosity must clearly be excited by the many early-type stars it contains there is, in the main, no obvious relationship between the distribution of these stars in the sky and the intricate structure of the nebulosity. Indeed in the inner region of the nebula the main region of star clustering (around the central "star") is

displaced, S following from the brightest extended region of nebulosity. Despite this there are a few noteworthy examples of obvious connections between individual stars and the structure of the surrounding nebulosity.

Perhaps the most striking of these examples is the case of star R143, the only late-type (F7 Ia) star studied in this region and one of the five known late type super-supergiants in the LMC (**5**), (**35**). An enlargement of the region around this star is shown in Plate 1 (*b*). There are at least four, and possibly more, curved filaments of nebulosity starting on or near the star and ending either on knots of nebulosity or faint stars. This remarkable structure gives good evidence that star R143 is actually associated with the 30 Dor complex and is not just a superposed star from the LMC general field. The filaments are quite long in linear measure ($\sim 3{\cdot}5$ pc) so that this is a large-scale structure by galactic standards. It may be recalled that there is some evidence that the spectrum of star R143 varies from F5 Ia to F8 Ia (**5**).

Star V lies at the centre of a butterfly shaped region of nebulosity (see Plate 1(*c*)) also of considerable linear dimensions (major axis about 4·8 pc). The spectral type of this star is unknown but one weak plate suggests an early-type continuum.

Between stars AA and AB, neither of which have known spectral types, there appears to be a very long filament (projected length ~ 44 pc) (see Plate 2). The filament appears to start on or near star AA and to project beyond star AB; there is also other structure near the former star. It might be that this is just a chance projection effect but there would appear to be a fairly good probability of real connection.

Finally around the Star I there is what appears to be a beautiful example of a Strömgren sphere, perhaps the only really regular geometrical shape in the entire 30 Dor complex (see Plate 1 (*d*)). The spectral type of the central star is not known. The diameter of the sphere is about 2·5 pc which, if the density is of the order of 10^2 H atoms/cm^{-3}, as in those regions of the nebula discussed in Section 3, could be excited by a main sequence star of early O-type. Spectra taken with this nebulosity stationary at the centre of a long slit show that whilst the H lines are markedly strengthened compared with the surrounding area the strengthening of [O III] N_1 and N_2 is much less noticeable. This could be explained in two ways: either (1) the central star has bright H lines in its spectrum, or (2) the level of excitation and ionization changes from the centre outwards in this nebulosity. Since guiding is rather difficult on this faint object of only some $4\frac{1}{2}$ secs of arc radius, it is not possible to decide between these two alternatives, but perhaps the second is the more likely.

In conclusion it should be pointed out that the above are only a few examples of the connection between stars and nebular structure. A detailed study of direct photographs of the nebula has not been made but might be very rewarding.

Acknowledgments.—I should like to thank Dr A. D. Thackeray for allowing me to use some of his direct photographs of the 30 Dor region (including those reproduced in Plates 1 and 2) in this work and also for his comments on the manuscript.

Radcliffe Observatory,
Pretoria:
1960 *July.*

XUM

References

(1) H. Shapley and J. S. Paraskevopoulos, *Ap. J.*, **86**, 340, 1937.
(2) H. M. Johnson, *P.A.S.P.*, **71**, 425, 1959.
(3) L. H. Aller, *Gaseous Nebulae* (London : Chapman and Hall 1956).
(4) M. W. Feast, *Observatory*, **73**, 255, 1953.
(5) M. W. Feast, A. D. Thackeray and A. J. Wesselink, *M.N.*, **121**, 337, 1960.
(6) S. C. B. Gascoigne, *M.N.*, **110**, 15, 1950.
(7) D. Barbier and D. Chalonge, *Ann. d' Astrophys.*, **4**, 30, 1941.
(8) L. H. Aller and W. Liller, *Ap. J.*, **130**, 45, 1959.
(9) R. H. Garstang, *M.N.*, **111**, 115, 1951.
(10) J. D. Baker and D. H. Menzel, *Ap. J.*, **88**, 52, 1938.
(11) S. R. Pottasch, *Ap. J.*, **131**, 202, 1960.
(12) H. Andrillat, *Ann. d' Astrophys.*, Suppl. No. 1, 1955.
(13) J. S. Mathis, *Ap. J.*, **125**, 328, 1957.
(14) M. J. Seaton and D. E. Osterbrock, *Ap. J.*, **125**, 66, 1957.
(15) D. E. Osterbrock and E. Flather, *Ap. J.*, **129**, 26, 1959.
(16) I. S. Bowen, *Ap. J.*, **121**, 306, 1955.
(17) M. W. Feast and A. D. Thackeray, *M.N.*, **120**, 463, 1960.
(18) G. de Vaucouleurs, *Ap. J.*, **131**, 265, 1960.
(19) R. E. Wilson, *Pub. Lick Obs.*, **13**, 187, 1918.
(20) R. J. Trumpler and H. F. Weaver, *Statistical Astronomy* (University of California Press, 1953), p. 126.
(21) G. Courtès, *Gas Dynamics of Cosmic Clouds* (I.A.U. Symposium No. 2) (North Holland, Amsterdam, 1955), p. 131.
(22) A. Blaauw and W. W. Morgan, *Ap. J.*, **119**, 625, 1954.
(23) S. Chandrasekhar, *Principles of Stellar Dynamics*, (University of Chicago Press, 1942), equation 5.209.
(24) M. Schwarzschild, *A.J.*, **59**, 273, 1954.
(25) S. von Hoerner, *Z. f. Astrophys.*, **30**, 17, 1951.
(26) W. W. Campbell and J. H. Moore, *Pub. Lick Obs.*, **13**, 77, 1918.
(27) A. N. Kolmogoroff, *C.R. Acad. Sci. U.S.S.R.*, **30**, 301, and **32**, 16, 1942; c.f. for a brief resume, C. de Jager, *l'Etude optique de l'atmosphere terrestre* (1951 Liege Colloquium), p. 223.
(28) G. Courtès, *Ann. d' Astrophys.*, **23**, 115, 1960.
(29) O. C. Wilson, G. Münch, E. M. Flather and M. F. Coffeen, *Ap. J.*, Suppl. 4, 199, 1959.
(30) G. Münch, Third Symposium on Cosmical Gas Dynamics (I.A.U. Symposium No. 8), *Rev. Mod. Physics*, **30**, 1035, 1958.
(31) M. S. Roberts, *Etoiles à Raies d'emission* (1957 Liege Colloquium), p. 76.
(32) M. W. Feast, *Observatory*, **73**, 256, 1953.
(33) H. Shapley and V. McK. Nail, *Proc. Nat. Acad. Sci.*, **34**, 173, 1948, (H.R. 306).
(34) S. Sharpless, *P.A.S.P.*, **70**, 392, 1958.
(35) M. W. Feast and A. D. Thackeray, *M.N.*, **116**, 587, 1956.

SEMI-EMPIRICAL TRACKS FOR THE CLUSTER M67

J. Crampin

(Communicated by F. Hoyle)

(Received 1960 September 3)

Summary

Calculations by Sandage of the quantity of hydrogen burned at various stages along the M67 sequence have been repeated, using more recent theoretical data. The fraction of the hydrogen burned turns out to be systematically larger than Sandage's values. On the basis that the upper limit of the giant branch of the sequence occurs at $M_V = 0{\cdot}00$, the fraction burned at the top of the sequence is about 0·5. Adding the fraction appropriate for the horizontal branch, at least some sixty per cent of the initial hydrogen present in the M67 stars must be burned by nuclear processes, before the horizontal branch reaches $B-V = 0{\cdot}00$. The proportion burned could be higher still. This would be the case if the true upper limit of the giant sequence extends beyond that found by observation for M67—this could turn out to be the case in a more populated cluster of similar stars. It therefore appears reasonable to suppose that not more than thirty per cent of the total mass of M67-type stars is lost by shedding into space during the extreme giant phase of their evolution. With a mass loss of this order, the masses of the stars in the horizontal branch are about $0{\cdot}7\odot$.

---

1. *Introduction.*—Sandage (**1**) has compared star counts along the colour-magnitude sequence of the cluster M67 with star counts along the main-sequence. Then by using a theoretical evolutionary track, and making a plausible homology assumption, he has obtained interesting information concerning the quantity of hydrogen burned at different stages along the colour-magnitude diagram.

In the present paper, Sandage's calculations will be repeated using the more recent theoretical data obtained by Hoyle (**2**). According to the following calculations it turns out that at any particular evolutionary stage a greater fraction of a star's hydrogen is burned than was the case according to Sandage's investigation (cf. Fig. 3).

2. *The necessary observational data.*—It will be more convenient, in relation to the following paper, to work in the M_V, $B-V$ plane, rather than in the M_{Bol}, $\log T_e$ plane used by Sandage. The zero-age main-squence, for $+3{\cdot}5 < M_V < +7{\cdot}0$, and for stars with chemical composition similar to the stars of M67, will be taken as the line

$$B-V = 0{\cdot}154\, M_V - 0{\cdot}1344. \qquad (1)$$

Values of M_V, $B-V$ have been determined (**3**) by Johnson and Sandage for the individual stars of M67. By placing a mean curve through the individual points a unique sequence in the H–R diagram can be obtained. This is plotted in Fig. 1. Pairs of values of M_V, $B-V$ along this sequence are given in Table I.

TABLE I

M_V	$B-V$	M_V	$B-V$
7·29	0·988	2·57	1·000
6·94	0·940	1·15	1·100
6·73	0·908	0·52	1·200
6·47	0·870	0·11	1·300
6·18	0·829	0·00	1·330
5·92	0·791	0·64	1·1
5·58	0·746	0·92	1·0
5·28	0·706	1·17	0·9
4·95	0·660	1·40	0·8
4·62	0·619	1·54	0·7
4·22	0·574	1·63	0·6
3·90	0·545	1·64	0·5
3·41	0·524	1·62	0·4
3·20	0·542	1·58	0·3
3·01	0·592	1·54	0·2
2·97	0·635	1·50	0·1
3·28	0·868	1·40	0·0
3·25	0·900	...	...

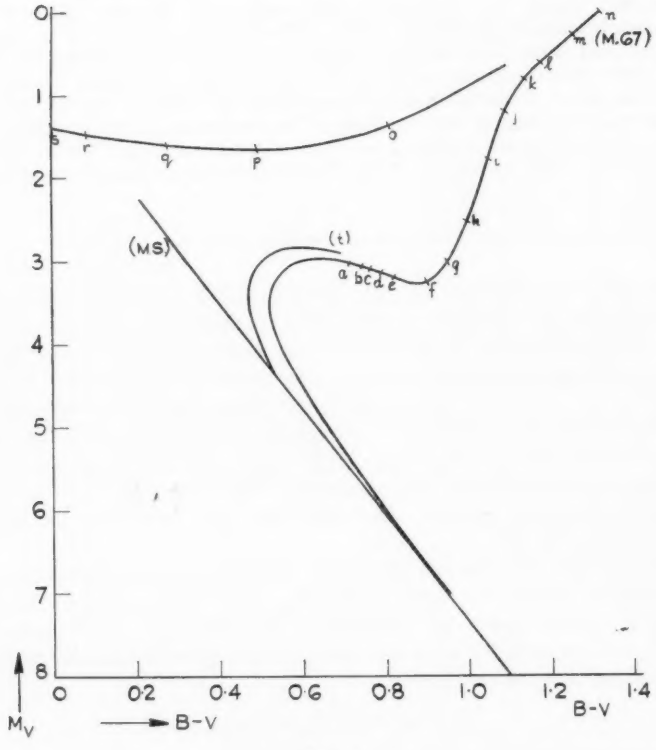

FIG. 1.

The number of stars ΔN_ϕ in various magnitude ranges along the M67 sequence are given in Table II (these values are read off from a curve drawn through the measured histogram (cf. 1)). Values ΔN_ϕ derived from the Salpeter

luminosity function for the relevant part of the main-sequence are given in Table III. These latter values have been normalized in a manner that will be explained below.

TABLE II

M_V (M67)	ΔN_ϕ	M_V (M67)	ΔN_ϕ	M_V (M67)	ΔN_ϕ
7·0		3·25		1·5	
	7		18		3
6·75		2·99		1·0	
	16		6		6
6·25		3·02		0·5	
	19		10		2
5·75		3·15		0·0	
	24		5		1
5·25		3·25		1·17	
	30		3		3
4·75		3·0		1·63	
	36		3		3
4·25		2·5		1·58	
	41		2		4
3·75		2·0		1·50	
	39		2		2
3·25		1·5		1·40	

TABLE III

M_V (M.S.)	7·0	6·5	6·0	5·5	5·0	4·5	4·0
ΔN_ϕ	233	223	199	177	156	139	

3. *The theoretical data.*—Table IV gives the theoretical evolutionary track on which the present paper is based. The theoretical calculations give M_{Bol}, $\log T_e$, of course, not M_V, $B-V$. The values of M_V in Table IV were obtained from M_{Bol} by using the bolometric corrections given in the table. Over a limited range of T_e the colour index $B-V$ may be taken as connected with $\log T_e$ by an equation of the form

$$B-V = a \log_{10} T_e + b. \qquad (2)$$

For the range of T_e from 5000° to 6000°, the constant $a \cong -3{\cdot}184$. The value of b is somewhat uncertain, however, partly due to an inherent uncertainty in the relation of $B-V$ to $\log T_e$, and partly because this relation is known to depend on the chemical composition of the star in question. This situation is dealt with by choosing b to be such that at the beginning of the evolutionary track the star lies on the main-sequence (1). The appropriate form of (2) is

$$B-V = -3{\cdot}184 \log_{10} T_e + 12{\cdot}65. \qquad (3)$$

The values of $B-V$ in Table IV were obtained with the aid of (3) from the theoretical values of $\log T_e$.

The values of M_V, $B-V$ given in Table IV are plotted in Fig. 1, the resulting track being denoted by t. It is satisfactory that the shape of t is closely similar to the shape of the lower part of the M67 sequence.

To effect further progress it is necessary to introduce an assumption of homology. The track t starts on the main-sequence at $M_V = 4{\cdot}33$. It is assumed that stars initially on the main-sequence at values of M_V fainter than about 4·0

TABLE IV

M_V	4·33	4·11	3·69	3·44	3·26	3·12	3·03	2·95
$B-V$	0·532	0·519	0·484	0·478	0·478	0·487	0·503	0·522
B.C.	−0·04	−0·03	−0·02	−0·02	−0·03	−0·03	−0·05	−0·06
T	0	3·868	6·446	7·617	8·158	8·468	8·666	8·803
Xq	0	0·041	0·079	...	0·119	...	...	0·142
M_V	2·90	2·86	2·84	2·85	2·86	2·88	2·91	...
$B-V$	0·541	0·567	0·599	0·634	0·662	0·681	0·700	...
B.C.	−0·08	−0·10	−0·13	−0·16	−0·18	−0·19	−0·21	...
T	8·901	8·977	9·035	9·080	9·116	9·131	9·145	...
Xq	...	...	...	0·156	...	...	0·160	...

all possess evolutionary tracks homologous to t, as far to the right in the H–R diagram as $B-V=+0·7$. That is to say, all such tracks are obtained from t by a shift of t parallel to the main-sequence.

Definition:

Let t_1, t_2... be a set of such tracks, and let an arbitrary line drawn parallel to the main-sequence (i.e. parallel to (1)) intersect the respective tracks at P_1, P_2,.... The points P_1, P_2,... are defined as *equivalent evolutionary stages.*

TABLE V

M_V (M.S.)	M_V (M67)	ΔN_ϕ	ΔN_ϕ	f
4·45	3·03			
		15	15	1·00
4·50	3·05			
		14	14	1·00
4·55	3·31			
		14	15	0·93
4·60	3·48			
		13	15	0·87
4·65	3·64			
		11	16	0·69
4·70	3·78			
		9	15	0·60
4·75	3·89			
		8	14	0·57
4·80	4·00			
		32	65	0·49
5·00	4·39			
		31	86	0·36
5·25	4·82			
		22	91	0·24
5·50	5·20			
		17	97	0·18
5·75	5·59			
		11	102	0·11
6·00	5·84			
		21	223	0·09
6·50	6·41			
		17	233	0·07
7·00	6·9½			

The assumption involved in our homology concept is that the physical structures of a set of stars, of similar chemical composition but of differing masses, are homologously similar when they lie at the points $P_1, P_2 \ldots$ of the H–R diagram.

By taking points on the main-sequence fainter than $M_V = 4{\cdot}33$ evolutionary tracks can be obtained, from the homology postulate, that intersect the M67 sequence. Such tracks associate values of M_V on the main-sequence with values of M_V on the M67 sequence. This association is illustrated by the values given in Table V, the significance of the association being that stars now at M_V(M67) have evolved from M_V(M.S.)—for example, stars at $M_V(\text{M67}) = 3{\cdot}03$ lie at zero-age at M_V (M.S.) $= 4{\cdot}45$.

The normalization used for ΔN_ϕ in Table III can now be explained. If the magnitude ranges of Table V are used instead of those of Tables II and III, the star numbers ΔN_ϕ, ΔN_ψ take on the values given in Table V. The ratio $f = \Delta N_\phi / \Delta N_\psi$ is unity at the highest luminosity, *viz.* at $M_V(\text{M67}) = 3{\cdot}03$, $M_V(\text{M.S.}) = 4{\cdot}45$. The ΔN_ψ values were indeed normalized so that this is the case. As the M_V values increase, f decreases, implying that the population of the M67 cluster has been weakened by the escape of stars at magnitudes fainter than about 3·1. On the basis of independent estimates by van den Bergh, Sandage gave $f = 1$ for $M_V < 3{\cdot}7$ and $f < 1$ for $M_V > 3{\cdot}7$. The present estimate of the weakening of the M67 cluster through the escape of stars is therefore comparable with, although somewhat more stringent than, the values adopted by Sandage.

4. *A test of the homology hypothesis, and a determination of the age of M67.*—The times required, T, for evolution from the main-sequence to various points of the track t are given in Table IV in units of 10^9 years. For tracks homologous to t the evolution times at corresponding evolutionary stages differ according to the factor $\mathcal{M}/L$(M.S.), where $\mathcal{M}$ is the stellar mass and L(M.S.) is the luminosity at zero age. For stars of about solar mass, $\mathcal{M}$ is proportional to about $L^{1/4}$(M.S.), so that the evolution times are proportional to about $L^{-3/4}$(M.S.). Since the bolometric corrections are small, the visual part of the luminosity, L_V say, can be used as an adequate approximation in place of the total luminosity. Thus the evolution times to corresponding evolutionary stages are proportional to about $L_V^{-3/4}$(M.S.), i.e. to $10^{0{\cdot}3 M_V(\text{M.S.})}$.

We now introduce the requirement that all stars of M67 have the same age. This demands that the evolution times shall be the same along all the tracks connecting pairs of values in Table V. Since the M67 sequence is not parallel to the main-sequence, different evolutionary stages are involved along the M67 sequence. Our requirement is that the age differences arising from the different evolutionary stages shall be just compensated by the factor $10^{0{\cdot}3 M_V(\text{M.S.})}$. Whether this is so or not gives a test of the homology hypothesis.

To find the appropriate evolutionary stage for any pair of values in Table V, we simply seek the point on the track t at which the visual magnitude has increased by $M_V(\text{M67}) - M_V(\text{M.S.})$—i.e., by the difference between the particular pair of values selected from Table V—above the starting point 4·33 of track t on the main-sequence. We then read off the evolution time T for this particular point of t. Our requirement is that

$$10^{0{\cdot}3 M_V(\text{M.S.})} . T \qquad (4)$$

be constant for all pairs of values M_V(M.S.), M_V(M67) selected from Table V. The age of M67 itself is given by

$$10^{0{\cdot}3 M_V(\text{M.S.}) - 4{\cdot}33} . T. \qquad (5)$$

XUM

By plotting a graph of $M_V(t) - M_V(\text{M.S.})$ against T for the points of track t, it is easy to read off the value of T corresponding to any assigned pair of values from Table V. The values of T so obtained turn out to satisfy very closely the relation

$$\log_{10} T = -0{\cdot}298\, M_V(\text{M.S.}) + 2{\cdot}2872,$$

T being measured in units of 10^9 years. This gives T essentially proportional to $10^{-0{\cdot}3M_V(\text{M.S.})}$, so that (4) is indeed almost exactly constant. Substituting

$$T = 10^{2{\cdot}2872 - 0{\cdot}3M_V(\text{M.S.})}$$

in (5) gives an age

$$T_0 = 9{\cdot}93 \times 10^9 \text{ years}$$

for M67, a value close to that obtained by Hoyle (**2**).

5. *Sandage's method of estimating the quantity of hydrogen burned along the M67 sequence.*—Define the functions $N_\phi(M_V)$, $N_\psi(M_V)$, for $M_V < 7$, by

$$N_\phi(M_V) = \sum_{M_V}^{7} \Delta N_\phi,$$

$$N_\psi(M_V) = \sum_{M_V}^{7} \Delta N_\psi. \tag{6}$$

By summing the values of ΔN_ϕ, ΔN_ψ given in Tables II and III, N_ϕ, N_ψ are easily obtained for the particular values of M_V entered in these tables. Fig. 2 is a plot of N_ϕ and of $0{\cdot}3\, N_\psi$ constructed from these particular M_V. Values of N_ϕ, N_ψ at other M_V can then be read off from the curves, and ΔN_ϕ, ΔN_ψ can also be read off for any specified range of M_V.

We proceed now to use Sandage's method for determining associated pairs of values $M_V(\text{M.S.})$, $M_V(\text{M67})$ at luminosities higher than those of Table V.

Start with the brightest associated pair of values in Table V, namely $M_V(\text{M.S.}) = 4{\cdot}45$, $M_V(\text{M67}) = 3{\cdot}03$. Take an interval of $0{\cdot}01$ mag. along the main-sequence and determine ΔN_ψ from Fig. 2 for the range from

$$M_V(\text{M.S.}) = 4{\cdot}45 \text{ to } M_V(\text{M.S.}) = 4{\cdot}44.$$

Now use the criterion

$$\Delta N_\psi = N_\psi[M_V(\text{M67})] - N_\psi(3{\cdot}03) \tag{7}$$

to determine the value of $M_V(\text{M67})$ to be associated with $M_V(\text{M.S.}) = 4{\cdot}44$. This is easily done with the aid of Fig. 2. The resulting point is shown as *b* in Fig. 1. (The point *a* is just the 'starting value' $3{\cdot}03$.) Proceeding similarly, we obtain a series of associated pairs of values of $M_V(\text{M.S.})$, $M_V(\text{M67})$. These pairs are given in Table VI. The relevant points on the M67 sequence are those marked *c*, *d*, ... in Fig. 1.

It will be noticed that (7) assumes no escape of stars at the relevant luminosity levels. This is in accordance with the discussion of Section 3

$$(f = 1 \text{ for } M_V(\text{M67}) < 3{\cdot}1),$$

and also with Sandage's discussion.

It is of interest to notice that, although the track *t* is close to the M67 sequence, it does not actually intersect the sequence until $M_V(67) = +0{\cdot}28$—i.e. until nearly the top of the sequence—the point *m* of Fig. 1. This is an indication of how closely similar the individual evolutionary tracks are for all stars beyond the point *a* of Fig. 1. This in turn indicates that the masses of all such stars are nearly

equal. The evolution time for passage through the stages beyond *a* is of course short compared with the total evolution time from the main-sequence.

TABLE VI

M_V (M.S.)	4·45	4·44	4·43	4·42	4·41	4·40	4·39
M_V (M67)	3·03	3·07	3·10	3·14	3·20	3·23	3·00
M_V (M.S.)	4·38	4·37	4·36	4·35	4·34	4·33	4·327
M_V (M67)	2·53	1·77	1·21	0·83	0·62	0·28	0·00
M_V (M.S.)	4·32	4·31	4·30	4·29	4·28	...	...
M_V (M67)	1·38	1·64	1·57	1·46	1·37	...	...

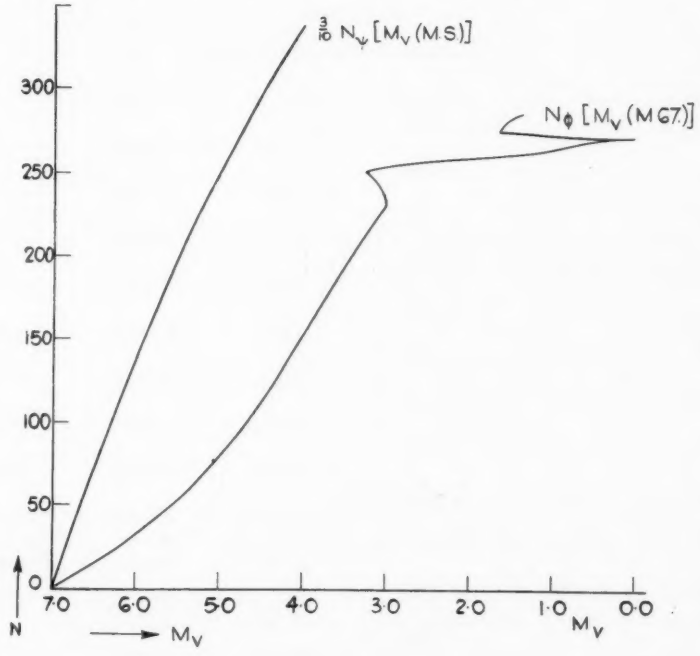

FIG. 2.

We again use the homologous property of neighbouring tracks. Consider, as an example, the tracks joining two neighbouring pairs of values: M_V(M.S.) = 4·38, M_V(M67) = 2·53; and M_V(M.S.) = 4·37, M_V(M.S.) = 1·77, for example. These tracks reach the M67 sequence at the points *h* and *i* of Fig. 1. The homology condition requires the upper track to be systematically brighter than the lower track by 0·01 mag. as far to the right on the upper track as the evolutionary point corresponding to *h*. (According to the definition of Section 3, the join of corresponding evolutionary points is parallel to the main sequence.) Now the evolution time along the lower track up to the point *h* is just the age T_0 of the M67 cluster. And the evolution time along the upper track as far as the evolutionary point corresponding to *h* is less than T_0 by the factor $10^{-0·003}$. But since the evolution

time to the point i must be just T_0, it follows that the last part of the evolution along the upper track, from the evolutionary point corresponding to h up to i, is

$$T_0(1-10^{-0\cdot003})=\Delta T \text{ say.} \tag{8}$$

The amount of hydrogen in grams that must be burned in order to maintain a luminosity level L_{Bol}(M67) erg sec^{-1} for a time interval ΔT seconds is

$$(6\cdot2\times10^{18})^{-1}.L_{Bol}(\text{M67}).\Delta T.$$

This can be equated to $\mathscr{M}X\Delta q$, where $\mathscr{M}$ is the stellar mass in grams, X is the initial hydrogen concentration at zero age, and Δq is the fraction of the star's hydrogen that is burned. If $\mathscr{M}$ and L_{Bol} are measured in solar units, and (8) is used for ΔT, then

$$X\Delta q=0\cdot00955(1-10^{-0\cdot003})L_{Bol}(\text{M67})T_0/\mathscr{M}. \tag{9}$$

TABLE VII

$X=0\cdot75$ in theoretical calculation

M_V (M67)	*B.C.*	$L_{Bol}/\mathscr{M}$	$L_{Bol}/\mathscr{M}$	$X\Delta q$	Xq
3·03	−0·21	4·937			
			4·910	0·00318	0·163
3·07	−0·24	4·883			
			4·853	0·00315	0·166
3·10	−0·26	4·824			
			4·776	0·00310	0·169
3·14	−0·28	4·727			
			4·656	0·00302	0·172
3·20	−0·31	4·585			
			4·645	0·00301	0·175
3·23	−0·37	4·705			
			5·392	0·00350	0·179
3·00	−0·42	6·078			
			7·933	0·00514	0·184
2·53	−0·47	9·787			
			14·933	0·00968	0·194
1·77	−0·53	20·079			
			28·385	0·01841	0·212
1·21	−0·59	30·691			
			46·317	0·03003	0·242
0·83	−0·67	55·943			
			63·417	0·04112	0·283
0·62	−0·72	70·890			
			89·425	0·05799	0·341
0·28	−0·84	107·960			
			134·95	0·02629	0·368
0·00	−1·00	161·940			
			40·397	0·01833	0·386
0·92	−0·65	50·274			
			26·913	0·01745	0·403
1·38	−0·57	30·521			
			24·160	0·01567	0·419
1·64	−0·54	23·306			
			26·438	0·01714	0·436
1·57	−0·55	25·014			
			29·166	0·01891	0·455
1·46	−0·56	27·862			
1·37	−0·57	30·470			

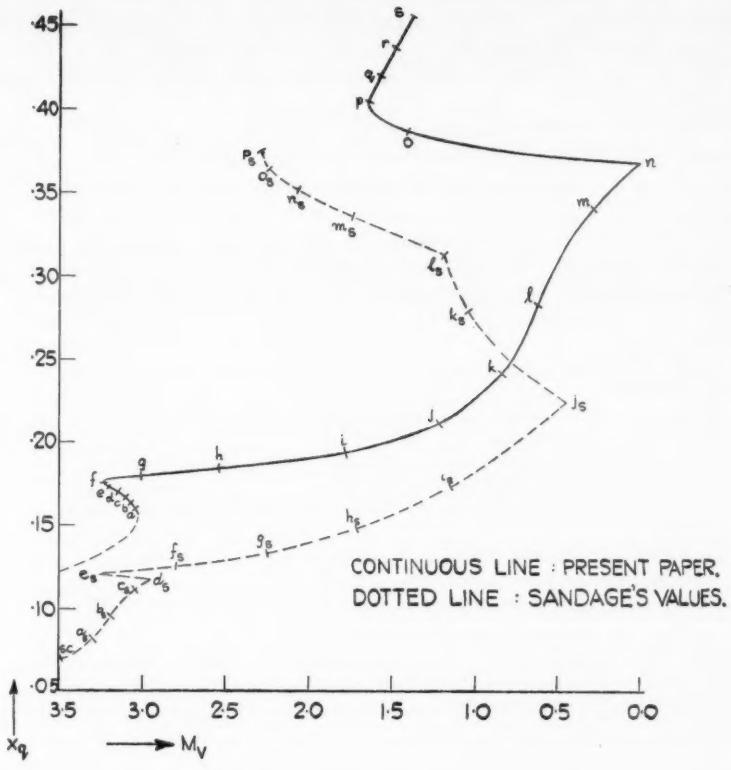

FIG. 3.

Since the evolutionary tracks are nearly parallel to the M67 sequence, the expression (9) gives the fraction of hydrogen burned between the points *h* and *i* of the M67 sequence.

Given the appropriate bolometric corrections, $M_{I'}$(M67) can be converted into L_{Bol}(M67), expressed in solar units. The mass $\mathcal{M}$ is determined by noting that $\mathcal{M} \propto L_V^{1/4}$(M.S.) approximately, and that $\mathcal{M} = 1{\cdot}093\odot$ at M_V(M.S.)$=4{\cdot}33$, this being just the mass for which the theoretical track *t* was calculated. Table VII gives L_{Bol}(M67)/$\mathcal{M}$, with L_{Bol}(M67) and $\mathcal{M}$ in solar units.

For the steps *a* to *b* to *c*..., the values of L_{Bol}(M67)/$\mathcal{M}$ vary appreciably between adjacent points. To take account of this, L_{Bol}(M67)/$\mathcal{M}$ has been averaged between the beginning and end of each interval. Results for $X\Delta q$ are given in Table VII. The value of Xq at the last point of the track *t* was 0·160. The value of Xq at the point *a* of the M67 sequence must lie close to this. Summing the values of $X\Delta q$ we obtain the values of Xq at the points *a*, *b*,... of the sequence. These are given in Table VII. They are also plotted in Fig. 3, together with the corresponding values of Sandage.

6. *Discussion of results.*—Remembering that in the theoretical calculations for the track *t* the value of *X* was 0·75, the results given in Table VII show that $q \cong 0{\cdot}5$ at the top of the giant sequence, and that $q \cong 0{\cdot}6$ at $B-V = 0{\cdot}0$ on the horizontal

branch. This implies that at least 60 per cent of the original hydrogen is burned by nuclear processes. The percentage of hydrogen burned would be higher if the upper limit of the giant sequence were extended beyond $M_V = 0{\cdot}00$. It is true that no stars are found in M67 beyond this upper limit. But this could be a population effect.

At the most, it seems therefore as if only about 40 per cent of the original hydrogen is likely to be unaccounted for by nuclear processes. This 40 per cent might be lost by shedding into space during the extreme giant phase of the evolution.

The values of Xq given in Table VII are systematically higher than those obtained by Sandage. The differences between the present results and those of Sandage arise largely from the different theoretical calculations used here.

Girton College,
Cambridge:
1960 *September.*

References

(1) Sandage, A. R., *Ap. J.*, **126**, 326, 1957.
(2) Hoyle, F., *M.N.*, **119**, 124, 1959.
(3) Johnson, H. L. and Sandage, A. R., *Ap. J.*, **121**, 616, 1955.

ON THE CHANGE WITH TIME OF THE INTEGRATED COLOUR AND LUMINOSITY OF AN M67-TYPE STAR GROUP

J. Crampin and F. Hoyle

(Received 1960 September 3)

Summary

The integrated colour of an M67-type cluster is determined, on the basis of no escape of stars from the cluster, as about $\overline{B-V}=+0\cdot8$. By making plausible homology hypotheses, the integrated colours of a similar star group at different moments of time have been determined. The colours range from about $\overline{B-V}=+0\cdot63$ for a star group of age 5×10^9 years to about $\overline{B-V}=+0\cdot95$ for a group of age 2×10^{10} years.

The colour appears to be insensitive to age for values of $\overline{B-V}$ close to $+0\cdot85$, which is the colour of typical elliptical galaxies. Hence it seems that the near constancy of the colours of elliptical systems is not necessarily an indication of a constancy of age. The observational data appear to be consistent with age variations from 10^{10} years to about 2×10^{10} years.

The present work could be much improved by more extensive theoretical integrations of stellar evolutionary tracks, and by star counts in groups more populous than M67, for example in the cluster 47 Tucanae. The possibility arises that, with sufficient theoretical and observational accuracy, integrated colours might be used as an index of age for certain extragalactic systems—elliptical galaxies and perhaps the nuclei of Sa and Sb spirals.

1. *Introduction.*—Since star counts are available along the M67 sequence, the integrated colour and magnitude of the whole cluster can readily be determined by addition of the effects of the separate stars. If we could calculate how such a sequence looks at earlier and later times, and how the stars are distributed along it, we should evidently be able to work out the change of integrated colour and magnitude with time.

Such an investigation might well turn out to have importance in cosmology. The work of Morgan (1), on the integrated spectra of extragalactic systems, suggests that the stars of elliptical galaxies, and those of the nuclei of Sa and Sb spirals, are probably similar to the stars of M67. From the observed integrated colours of such systems we might therefore expect to infer their ages. Are all the ages similar, or are there substantial differences? This is the type of question it may be possible to answer.

At the present moment, neither the observational data nor the theoretical calculations are sufficient for definitive results to be obtainable. The stars of M67 are too few in number at the high luminosity levels on the 'giant branch', and along the 'horizontal branch', for results obtained from M67 to be extrapolated with complete confidence to a much larger population of similar stars. And in the absence of the many theoretical evolutionary tracks necessary to provide full theoretical data we are obliged to extrapolate from the few known results by means of homology postulates.

Even so, interesting results can already be obtained. The accuracy of the present investigation is probably sufficient to establish that the near constancy, at $\overline{B-V}=+0\cdot85\pm0\cdot05$, of the colours of elliptical galaxies is not an indication of a constancy of age.

2. *The homology postulate for the lower part of the evolutionary sequence.*—The M67 sequence possesses a maximum (with respect to M_V) at $B-V \cong +0{\cdot}6$ and minimum at $B-V \cong +0{\cdot}83$. By the lower part of the sequence we mean the part that lies at colours earlier than the minimum—the part that lies to the left of the point E of Fig. 1.

Our homology assumption is that the sequence at earlier and later times, up to the corresponding minimum point, is to be obtained by displacing the M67 sequence in the H–R diagram in a direction parallel to the main-sequence. This is illustrated in Fig. 1, the main-sequence being drawn in accordance with equation (1) of the previous paper (**2**), viz.

$$B-V = 0{\cdot}154 M_V - 0{\cdot}1344.$$

By the present criterion we can define a series of sequences (each one up to its minimum point) by the parameter $p = 0, \pm 1, \pm 2, \ldots$, the meaning of p being that the sequence S_p is related to the M67 sequence, S_0, in the following way: there is a point D_p on S_p corresponding to D on the M67 sequence, such that

$$M_V \text{ at } D_p = 0{\cdot}2p + M_V \text{ at } D, \quad (1)$$

$$B-V \text{ at } D_p = 0{\cdot}0308p + B-V \text{ at } D. \quad (2)$$

Writing $B = M_B$, in analogy to $V = M_V$, equations (1) and (2) can be combined to yield

$$M_B \text{ at } D_p = 0{\cdot}2308p + M_B \text{ at } D. \quad (3)$$

The sequences S_5, S_{-5} are shown in Fig. 1. The present discussion deals only with the definitions of these sequences up to the minimum points E_5 and E_{-5}, however. The forms of the sequences for later colours are decided by a criterion still to be discussed (Section 3 below).

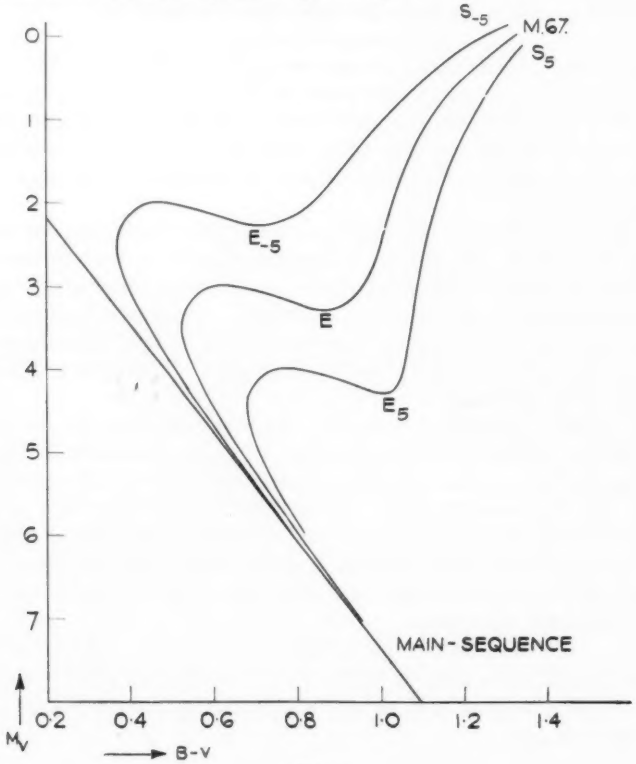

FIG. 1.

It is emphasised that the hypothesis implied in (1) and (2) is not the homology hypothesis used in the preceding paper. Here we are assuming a homologous similarity of the forms of the sequences occupied by a group of stars at different moments of time, whereas formerly it was assumed that individual stars of different masses follow homologous tracks.

When the homology hypothesis of the preceding paper is added to the hypothesis contained in (1) and (2), a procedure becomes available for determining the distribution of stars along S_p, as far to the right as the minimum point E_p. This procedure will now be discussed.

Take a set of evolutionary tracks t_1, t_2, ... all homologous to the theoretical track t of the preceding paper. Let the series of tracks leave the main-sequence at the points $C(1)$, $C(2)$, ... For definiteness, let M_V at $C(1)$ be $+7{\cdot}0$, and let M_V increase by $0{\cdot}1$ mag. along the sequence $C(1)$, $C(2)$, ...

Suppose that t_k cuts the sequence S_p at the point $D_p(k)$, and that it cuts the *M*67 sequence at $D_0(k)$. Then our homology hypotheses are such that $D_p(k)$ and $D_0(k+2p)$ are related by equations (1), (2), and (3),

$$M_V \text{ at } D_p(k) = M_V \text{ at } D_0(k+2p) + 0{\cdot}2p,$$

$$M_B \text{ at } D_p(k) = M_B \text{ at } D_0(k+2p) + 0{\cdot}2308p.$$

This follows because S_p is obtained from S_0—i.e., the M67 sequence—by displacement parallel to the main-sequence, whereas the tracks t_1, t_2, ... also differ from each other by displacements parallel to the main-sequence.

The number of stars, $\Delta N_\psi(k+0{\cdot}5)$, associated with the segment of the main-sequence between $C(k)$ and $C(k+1)$ is obtained from the function N_ψ, plotted in Fig. 2 of the preceding paper. Then, taking the escape factor f to be unity, the number of stars between the points $D_p(k)$ and $D_p(k+1)$ of the sequence S_p is $N_\psi(k+0{\cdot}5)$. It will be recalled that the function N_ψ is normalized for the case of M67. The procedure of putting $f=1$ is not strictly correct for M67 itself, but it is correct if we wish to carry the theory over to galactic systems. In this connection, it is of course the case that only the quantities which are substantially independent of the actual number of stars in M67 can be carried over in this way. The integrated colour is such a quantity, whereas the integrated magnitude obviously is not.

Instead of giving the star distribution explicitly for each value of p, a simplification can be introduced by using the circumstance mentioned above, that $D_p(k)$ and $D_0(k+2p)$ are corresponding points in that they satisfy (1), (2), and (3). The total visual luminosity contributed by the stars on the lower part of S_p is

$$\sum_k \Delta N_\psi(k+0{\cdot}5)\ 10^{-0{\cdot}4M_V[D_p(k+0{\cdot}5)]} \qquad (4)$$

where $D_p(k+0{\cdot}5)$ is taken mid-way between $D_p(k)$ and $D_p(k+1)$, and $M_V[D_p(k+0{\cdot}5)]$ is the visual magnitude at this mid-point. (The use of the mid-point gives better accuracy when $C(1)$, $C(2)$... are not infinitesimally spaced.)

The total blue luminosity for the lower part of S_p is likewise given by

$$\sum_k \Delta N_\psi(k+0{\cdot}5)\ 10^{-0{\cdot}4M_B[D_p(k+0{\cdot}5)]} \qquad (5)$$

where $M_B[D_p(k+0{\cdot}5)]$ is the blue magnitude at $D_p(k+0{\cdot}5)$. The luminosity of a star of zero magnitude is taken as unit in (4) and (5). The range of summation

with respect to k must be appropriately chosen. How this is to be done will be discussed below. Now by (1) and (3) we have

$$M_V[D_p(k+0{\cdot}5)] = M_V[D_0(k+0{\cdot}5+2p)] + 0{\cdot}2p,$$

$$M_B[D_p(k+0{\cdot}5)] = M_B[D_0(k+0{\cdot}5+2p)] + 0{\cdot}2308p.$$

Substituting in (4) and (5) gives

$$10^{-0{\cdot}08p} \sum_k \Delta N_\psi(k+0{\cdot}5)\ 10^{-0{\cdot}4M_V[D_0(k+0{\cdot}5+2p)]}, \tag{6}$$

$$10^{-0{\cdot}09232p} \sum_k \Delta N_\psi(k+0{\cdot}5)\ 10^{-0{\cdot}4M_B[D_0(k+0{\cdot}5+2p)]}. \tag{7}$$

These formulae have the advantage that $D_0(k+0{\cdot}5+2p)$ are points on the M67 sequence, so that the situation for S_p is now referred to the situation on the M67 sequence. When $p=0$, (6) and (7) give results for the M67 sequence.

Table I gives values of M_V at the points $C(n)$ of the main-sequence for $n=1, 2, \ldots 27$, together with the values of M_V, M_B at $D_0(n+0{\cdot}5)$, and the values of $\Delta N_\psi(n+0{\cdot}5)$, for $n=1, 2, \ldots 26$.

TABLE I

n	$M_V[C(n)]$	$M_V[D_0(n+0{\cdot}5)]$	$M_B[D_0(n+0{\cdot}5)]$	$\Delta N_\psi(n+0{\cdot}5)$
1	7·0	6·89	7·82	46·3
2	6·9	6·78	7·69	46·7
3	6·8	6·67	7·57	47·0
4	6·7	6·56	7·44	46·8
5	6·6	6·46	7·33	46·6
6	6·5	6·35	7·20	46·2
7	6·4	6·24	7·07	45·5
8	6·3	6·13	6·95	44·7
9	6·2	6·02	6·82	43·8
10	6·1	5·90	6·69	42·6
11	6·0	5·78	6·55	41·5
12	5·9	5·66	6·41	40·5
13	5·8	5·53	6·29	39·7
14	5·7	5·40	6·12	38·9
15	5·6	5·27	5·97	38·1
16	5·5	5·13	5·81	37·3
17	5·4	4·98	5·65	36·4
18	5·3	4·83	5·48	35·4
19	5·2	4·66	5·28	34·4
20	5·1	4·48	5·08	33·6
21	5·0	4·29	4·87	32·7
22	4·9	4·10	4·66	31·9
23	4·8	3·89	4·43	31·2
24	4·7	3·64	4·17	30·5
25	4·6	3·31	3·84	29·8
26	4·5	3·03	3·75	29·1
27	4·4			

We shall be concerned with values of $|p| \leqslant 5$. For such values, $C(1)$ has been chosen sufficiently low on the main-sequence (at $+7{\cdot}0$) for the contribution of fainter stars to be negligible in assessing the integrated colour of S_p. Hence we can take the sums (6) and (7) as possessing $k=1$ as first term, whatever the value of p.

The situation concerning the upper limit of k in these sums is more complicated. Consider first the case of the M67 sequence itself. The point $D_0(27)$ has $M_V = +3{\cdot}23$, lying very close to the minimum point E of Fig. 1. Hence $k=26$ represents the upper limit (to high accuracy) for the M67 sequence (it will be recalled that, so far, we are only considering the portion of the sequence up to the minimum point). For S_p, the corresponding upper limit falls at $k+2p=26$. Explicitly then, our sums are

$$10^{-0{\cdot}08p} \sum_{k=1}^{k=26-2p} \Delta N_\psi(k+0{\cdot}5)\ 10^{-0{\cdot}4M_V[D_0(k+0{\cdot}5+2p)]} \tag{8}$$

for the visual luminosity, and

$$10^{-0{\cdot}09232p} \sum_{k=1}^{k=26-2p} \Delta N_\psi(k+0{\cdot}5)\ 10^{-0{\cdot}4M_B[D_0(k+0{\cdot}5+2p)]} \tag{9}$$

for the blue luminosity.

Table I includes all the necessary values of M_V, M_B. It does not include, however, all necessary values of $\Delta N_\psi(k+0{\cdot}5)$ for cases where $p<0$. For p down to -5, we evidently require $\Delta N_\psi(k+0{\cdot}5)$ for values of k up to 36. These are given in Table II, actually up to $k=37$ for a reason that will appear in the following section.

TABLE II

k	27	28	29	30	31	32	33	34	35	36	37	38
M_V at $C(k)$	4·4	4·3	4·2	4·1	4·0	3·9	3·8	3·7	3·6	3·5	3·4	3·3
$\Delta N_\psi(k+0{\cdot}5)$	28·5	27·9	27·3	26·7	26·1	25·5	25·0	24·4	23·9	23·4	23·0	

3. *The upper parts of the sequences.*—It would be wrong to define the upper part of S_p in accordance with (1) and (2), for the sequence S_p must converge towards the M67 sequence in the giant region. This is known from a study of the colour magnitude diagrams of galactic clusters of different ages—the convergence has been termed the 'funnelling effect' by Sandage. To take account of this, the sequences in Fig. 1 are shown as converging near $M_V=0{\cdot}0$.

To estimate the contribution to the integrated visual and blue luminosities of the stars of the giant branch, consider first the case of M67 itself. In Table III we have values of M_V(M67), M_D(M67) corresponding to stars evolving from the main-sequence at $M_V=4{\cdot}40$, $4{\cdot}39, \ldots, 4{\cdot}30$—i.e., steps of 0·01 magn. along the main-sequence in place of the steps of 0·1 magn. used in the previous section. The appropriately normalised values of ΔN_ψ for each of these steps are all close to 2·8. The average $10^{-0{\cdot}4M_V}$ and $10^{-0{\cdot}4M_B}$ are therefore easily computed from Table III. They are 0·3132 and 0·1220 respectively.

TABLE III

M_V on main-sequence	M_V on M67 sequence	M_B on M67 sequence
4·40	3·23	4·315
4·39	3·00	3·95
4·38	2·53	3·53
4·37	1·77	2·83
4·36	1·21	2·305
4·35	0·83	1·98
4·34	0·62	1·80
4·33	0·28	1·53
4·32	1·38	2·185
4·31	1·64	2·24
4·30	1·57	1·82

XUM

Putting $p=0$ in (8) and (9), and adding $28\times0{\cdot}3132$ to (8) and $28\times0{\cdot}1220$ to (9) gives the total integrated visual and blue luminosities for the M67 sequence.

Turning now to the giant branch of S_p, we notice that the upper part of S_p lies close to the upper part of the M67 sequence, whereas the lowest part is related to the lowest part of the M67 sequence by the conditions (1), (2), and (3). Taking this into account, a reasonable approximation for the average effect of the stars on the giant branch of S_p is given by using the following condition:

The average visual magnitude of the stars on the giant branch of S_p differs from the average visual magnitude of the stars on the giant branch of M67 by $0{\cdot}1p$ magn. The corresponding difference for the average blue magnitude is $0{\cdot}0154p$.

The quantities $0{\cdot}1p$, $0{\cdot}0154p$ give a shift parallel to the main-sequence, but of half the amount used in the previous section. This is to take an average between the situation at the top of the giant branch and the situation at the bottom.

On this basis we must add

$$0{\cdot}3132\times10^{-0{\cdot}04p}.\quad\Delta N_{\psi}(27{\cdot}5+2p)$$

to (8) in order to obtain the total visual luminosity, and

$$0{\cdot}1220\times10^{-0{\cdot}0061p}.\quad\Delta N_{\psi}(27{\cdot}5+2p)$$

to (9) to obtain the total blue luminosity. When $p=-5$ we therefore require $\Delta N_{\psi}(37{\cdot}5)$; this is the last entry of Table 2.

Writing $\mathscr{L}_p(V)$ and $\mathscr{L}_p(B)$ for the resulting quantities, the integrated colour $\overline{B-V}$ of the sequence S_p is given by

$$\overline{B-V}=2{\cdot}5\log_{10}[\mathscr{L}_p(V)/\mathscr{L}_p(B)]. \tag{10}$$

4. *The age of the sequence* S_p.—The age $T_0=9{\cdot}93\times10^9$ years was obtained for M67 in the preceding paper. The age T_p of S_p differs from T_0 by the factor $10^{0{\cdot}06p}$. This follows from the result obtained in the preceding paper, that the age is proportional to $10^{0{\cdot}3M_V}$, where M_V is the visual magnitude at any representative point on the lower part of the sequence—for example at the minimum point E_p of Fig. 1. The difference between M_V at such a representative point of S_p and the value at the corresponding point of M67 is $0{\cdot}2p$ (cf. equation (1)), which leads immediately to the factor $10^{0{\cdot}06p}$. Thus

$$T_p=T_0\,10^{0{\cdot}06p}=9{\cdot}93\times10^{9+0{\cdot}06p}\text{ years}. \tag{11}$$

5. *Results.*—Table IV gives T_p, $\overline{B-V}$, and $\mathscr{L}_p(V)/\mathscr{L}_0(V)$ for $p=0,\ \pm1,\ \pm2,\ \pm3,\ \pm4,\ \pm5$. It is particularly to be noticed that these quantities are independent of the actual numerical population of M67. The population of M67 is relevant only in so far as low number counts may well have introduced statistical errors, particularly near the tip of the giant branch and on the horizontal branch.

TABLE IV

p	$\mathscr{L}_p(V)/\mathscr{L}_0(V)$	$\overline{B-V}$	T_p (10^9 years)
−5	1·74	0·628	5·00
−4	1·56	0·663	5·73
−3	1·39	0·696	6·58
−2	1·24	0·729	7·54
−1	1·11	0·765	8·65
0	1·00	0·794	9·93
1	0·90	0·825	11·4
2	0·81	0·858	13·1
3	0·73	0·889	15·0
4	0·66	0·921	17·2
5	0·60	0·953	19·7

The present results are not intended as definitive. They have been obtained in order to indicate the sort of consideration that can be brought to bear on the time variations of colour and magnitude of large star groups, particularly of galaxies, or of portions of galaxies, for which the basic assumption of the present work is satisfied—namely, that the stars of the group in question all condensed at essentially the same epoch. This might well be the case for elliptical galaxies and for the nuclei of Sa and Sb spirals.

Although there is much scope for improvement in the theoretical basis of this work, particularly in that whole families of theoretical tracks are needed, the results are already sufficient to expose an erroneous argument concerning the elliptical galaxies. It has sometimes been argued, from the small dispersion in the colours of elliptical galaxies ($+0{\cdot}85 \pm 0{\cdot}05$) that their ages must be closely similar. The values given in Table IV show that the integrated colour is insensitive to age, and that a range from $+0{\cdot}8$ to $+0{\cdot}9$ corresponds to a variation in age by almost a factor 2.

The present considerations raise the interesting possibility of determining ages of extragalactic systems from their integrated colours. To implement such a programme, much remains to be done. Better star counts than those of M67 are required. These can very likely be supplied by the cluster 47 Tucanae, which appears to possess stars of the M67 type. The need for more theoretical work has already been mentioned. And some means of allowing for halo stars projected against the nuclei of spiral galaxies would be necessary. Finally, since age is sensitive to colour, the effects of interstellar reddening must be very accurately allowed for. For this reason only observations made near the galactic poles would be useful in such a programme.

Girton College,
Cambridge:
1960 *September.*

St John's College,
Cambridge.

References

(1) Morgan, W. W., *Stellar Populations*, Rome 1957, 325 (North-Holland).
(2) Crampin, J., *M.N.*, **121**, 17, 1961.

NOTE ON THE MAGNETIC STRUCTURE OF THE GALAXY

F. Hoyle and J. G. Ireland

(Received 1960 September 7)

Summary

The picture of the magnetic field of the Galaxy discussed in earlier papers is unsatisfactory in that it does not provide for an outflow of gas from the galactic nucleus. The observed lack of any inward flow of gas suggests that the interstellar medium must constantly gain angular momentum. But unless the galactic halo holds the main reservoir of gas and angular momentum, it is difficult to see how this can be the case.

It is now suggested that, instead of the spiral arm field being primary and the halo field secondary, as it was in our earlier work, the situation may be reversed. In a model in which lines of force of the halo cross the interarm regions of the galactic plane, it is possible for the whole interstellar medium to gain angular momentum at a comparatively rapid rate. The windings of the spiral arms then move outwards, thereby preventing the arms from becoming more tightly wound with time. When the field intensity in the halo is 3×10^{-6} gauss, the windings move out to the periphery of the Galaxy in a time scale of order 5×10^{8} years.

The structure of the spiral arm field, according to this new picture, is briefly discussed. It seems that a helical structure is to be preferred to the usual cylindrical model. A well-known difficulty concerning the direction of the local spiral arm is then overcome.

---

1. *Introduction.*—The attempt made in two previous papers (**1**, **2**) to understand the spiral structure of the Galaxy was based on the conventional picture of the spiral arms as magnetic tubes of force. The magnetic field in the halo was regarded as derivative to that in the arms, lines of force escaping from, and returning to, the arms. Strict spiral structure became replaced by a general tendency towards spirality (**1**). In our second paper, the possibility of angular momentum transfer through the agency of the spiral arm magnetic field was considered. It turned out that transfer of angular momentum in the disk of the Galaxy is always small, except under a special condition operative at one, or perhaps two, particular distances from the galactic centre.

The idea that the halo field is chaotic, being built out of a complex of lines of force that break out of, and return to, the galactic disk, avoids a pole strength problem. If the halo field possesses large scale regularity, its pole strength must be of order 3×10^{39} gauss cm^2, which is greater by a factor $\sim 10^2$ than the pole strength of a spiral arm. (The pole strength of the halo is given in such a case by a field with intensity of order 10^{-6} gauss maintained over the area of the galactic disk, viz. 3×10^{45} cm^2, whereas the pole strength of a spiral arm is given by a field with intensity of order 10^{-5} gauss maintained over a cross-section of the arm, viz $\sim 3 \times 10^{42}$ cm^2.) Since two magnetic systems with widely different pole strengths cannot be connected it would follow that, if the halo field is closed (so as to confine cosmic rays and relativistic electrons), it must be closed within itself. The problem of the topology of the halo field then arises in an acute form.

XUM

Particularly, we might ask whether the lines of force of the halo field cross over from the northern galactic hemisphere to the southern hemisphere. The lines of force would then cut through the galactic plane, and this might well have important observable effects.

These awkward questions were avoided in our picture. But our picture suffers from the disadvantage that it hardly seems possible to explain the efflux of material from the galactic nucleus that has been observed by the Dutch radio-astronomers. In (**2**) it was seen that such an outward motion can only be explained, in our picture, in terms of an angular momentum transfer from one part of the galactic disk to another—outward motion at one place implying inward motion at another. No such inward motion is observed.

Then, although a case can be made for the existence of spirality, rather than of a strict spiral structure, in the case of our own galaxy, a question arises as to whether this is really satisfactory in all cases—particularly in Sc galaxies. And if we admit the existence of a coherent spiral structure in such a galaxy as M51 the winding problem discussed in (**1**) is immediately reinstated. Why are such spiral structures not more tightly wound?

These difficulties seem strong enough for a reassessment of the situation to be worth while. This will be attempted below.

2. *The angular momentum problem.*—If it is accepted that the Galaxy possesses a connected spiral structure, rather than a mere spirality, the appropriate degree of winding of the arms is established in a time interval of order 5×10^8 years (**1**). Why then is the spiral structure not more tightly wound? It was our failure in (**1**) to answer this question that led us to reject strict spiral coherence in favour of a disconnected spirality. A review of our argument reveals one weak point, however.

The possibility was considered that the spiral structure continues to be wound for periods of time in excess of 5×10^8 years, and that the system loses turns of its spiral structure. This might happen through an inward motion of the whole spiral pattern, turns being lost at the galactic centre, or through an outward motion—turns being lost in this case at the periphery of the Galaxy. The first of these possibilities was considered in (**1**) and was, we believe, properly rejected. The second possibility was dismissed on much weaker grounds, however, namely that we could see no source for the large supply of angular momentum that would be necessary to drive the whole gaseous component of the Galaxy to its periphery in a time interval of order 5×10^8 years. If such a source of angular momentum could be found the whole course of the argument would be changed.

Since the interstellar gas cannot be separated from the magnetic spiral structure, any proposal that turns of the spiral structure are lost at the periphery of the Galaxy requires the interstellar gas also to flow to the outside of the Galaxy. Write $U(r)$ for the outward velocity at central distance r. Tentatively, we set $U(r)$ proportional to r^{-1},

$$U(r) = a/r. \qquad (1)$$

(A reciprocal dependence on r is suggested by the requirement of continuity of flow, which would be maintained by (1) in a gaseous disk of uniform density and thickness.) Taking the radius of the Galaxy to be 10 kpc, it is easily verified that material flows, in accordance with (1), to the edge of the Galaxy in a time of 5×10^8 years if $a \cong 3 \times 10^{28}\,\mathrm{cm^2\,sec^{-1}}$. With this value, (1) gives an outward

velocity of $\sim 30\,\mathrm{km\,sec^{-1}}$ at $r = 3\,\mathrm{kpc}$. At $r = 8\,\mathrm{kpc}$ the outward velocity $\sim 10\,\mathrm{km\,sec^{-1}}$.

Although the idea of a total outflow of gas to the edge of the Galaxy in a time scale as short as 5×10^8 years seems extremely radical, the present simple result tends to support it. We obtain immediately a speed of outflow of the required order at $r = 3\,\mathrm{kpc}$. And a radial outflow of gas at the solar distance, at a speed of a few kilometres per second, is consistent with the observed dynamical motions of A and B type stars. The implication is that both the interstellar gas and the spiral structure are evanescent—they are both replaced in a time scale that is short compared with the age of the Galaxy.

Two problems arise immediately, as to the source of the gas and the source of the angular momentum. Of these, the angular momentum appears to be the more stringent requirement. The gas might be supplied by mass loss from the stars of the galactic nucleus. But no process in the nucleus can supply the necessary angular momentum. For this, it seems essential to assign to the halo a far more dominant role than it has hitherto been usual to do.

We take the average density in the halo to be about 10^{-2} atom $\mathrm{cm^{-3}}$, maintained throughout a volume of $10^{69}\,\mathrm{cm^3}$. This yields a total halo mass of order $10^{10}\odot$, which is about ten times the mass of gas in the galactic disk. On this basis the halo contains the main gaseous reservoir of angular momentum. It is therefore possible, at any rate in principle, for the interstellar medium to be much changed by a supply of gas and angular momentum from the halo. The supply of gas appears at the nucleus however, and hence should not be regarded as carrying the angular momentum. Rather does it seem as if angular momentum is transferred from halo to disk through the agency of a magnetic process. This will now be considered.

The halo magnetic field produces a magnetic stress on the material of the halo. (Because of the low halo density, the resulting body force can be comparatively large.) In general, the body force possesses a component perpendicular to the axis of rotation, and intersecting the axis. Now if the lines of force of the field are pinned through the galactic nucleus, and if they tend to contract towards the nucleus—being held out by the gas—the component towards the axis of rotation will be positive in the inward sense. In such a case the magnetic body force increases the circular rotational velocity of the gas. Since the increase can be very considerable (because of the low gas density) it is possible that the rotational velocity of gas in the halo is greater than that in the galactic plane. We assume this to be the case.

We are now regarding the halo magnetic field as possessing a large scale structure. The pole strength argument given in the introduction requires the lines of force to be mainly closed in themselves—if indeed the halo field is closed. We assume that this is the case, at any rate for an appreciable fraction of the lines of force, and that the lines of force connect between the two galactic hemispheres. We regard the lines of force from the halo as crossing the galactic plane through the interarm regions.

In this picture the lines of force of the halo must be dragged backwards as they cross the galactic plane, owing to the lower circular velocity of the gas in the disk. This property is quite independent of the detailed form of the field. The effect of the dragging of the lines of force is to cause the interstellar gas to gain angular momentum. This takes place over the whole face of the galactic

plane. There is no question of one part of the galactic disk gaining angular momentum at the expense of another part. Thus there is no inward motion anywhere in the disk.

These considerations can be subject to simple semi-quantitative checks. From the intensity of radio emission from the Galaxy, and from its spectrum, it is known that the magnetic intensity in the halo cannot exceed 3×10^{-6} gauss. Now in order that the magnetic body force shall appreciably increase the circular velocity in the halo, we evidently require the hydromagnetic velocity, $(H^2/4\pi\rho)^{1/2}$, to be of order 100 km sec^{-1}. With $H = 3 \times 10^{-6}$ gauss, $\rho = 10^{-26}$ gm cm^{-3}, this is indeed the case.

The maximum force that can be exerted by the halo field in the direction of rotational motion is $H^2/4\pi$ per unit area of the face of the Galaxy. The total force over the whole galactic plane can thus be as high as $\frac{1}{4}H^2R^2$, where R is a suitable galactic radius. This force has a moment of order $\frac{1}{4}H^2R^3$ about the galactic centre. This is the possible gain per unit time of angular momentum by the interstellar medium. Now the total angular momentum of the interstellar medium is of order MVR, where M is the mass of the medium, and $V \cong 250$ km sec^{-1} is an average value of the circular velocity in the disk. The magnetic force is therefore capable of changing radically the angular momentum of the gaseous disk of the Galaxy in a time T given by

$$\tfrac{1}{4}H^2R^3T \cong MVR. \qquad (2)$$

With $R = 10$ kpc, $H = 3 \times 10^{-6}$ gauss, $M = 10^9 \odot$, $V = 250$ km sec^{-1}, (2) gives $T \cong 2 \times 10^{16}$ sec—a value that falls satisfactorily close to the time scale of 5×10^8 years.

3. *The spiral arm field.*—The spiral arm field is no longer intimately connected with the halo. It is usually assumed that the lines of force of the spiral arm field run parallel to the direction of the spiral arm itself. A serious question arises now as to whether this picture is correct.

According to the rotation curve of (**2**), the rotation period in the inner nucleus of the Galaxy must be less than 10^7 years. Of the order of 10^2 rotations of the inner nucleus relative to the outer parts of the Galaxy must accordingly take place in a time scale of 5×10^8 years. If the spiral arm field passes through the inner nucleus—as in M31 it appears to do—a highly complex situation must arise. We find it difficult to believe that any very strict winding of the arms could prove stable. Rather will the field be twisted into a tangled ball. If this ball remained inside the nucleus there would be no need to suppose any great complexity in the spiral arm fields in the outer parts of the Galaxy. But if the picture described in the previous section is correct, some twisting of the spiral arm fields is to be expected throughout the Galaxy—simply because a twisted complex field is carried outwards from the nucleus. Is there any observational evidence for believing that this is indeed the case?

It seems worth recalling a well-known discrepancy between two methods of determining the orientation of the local spiral arm. According to the 21 cm hydrogen line data, the arm is nearly transverse to the radial direction—the inward going direction is in about galactic longitude $l = 54°$. Maximum polarization of starlight occurs, on the other hand, in about $l = 102°$. Since maximum polarization is expected in directions at right angles to the magnetic lines of force, this implies that the lines of force are directed in about $l = 12°$.

Hence if the lines of force are parallel to the spiral arm, the arm is also directed in $l = 12°$. A discrepancy of some 40° therefore exists between the two methods of estimating the orientation of the spiral arm. The likely resolution of the discrepancy is that the lines of magnetic force do not point along the spiral arm.

That this is the case, is shown by other features of the polarization data. If the spiral arm were really directed in $l \cong 12°$, with the lines of force parallel to the arm, the directions of polarization at $l = 40°$, say, should be nearly parallel to the galactic plane. But if the arm really is in $l \cong 54°$, longitudes near 40° are directed towards interarm regions (the sun lies on the inside of the arm). Thus in the latter case we might expect polarizations near 40° to be irregularly distributed—and this is exactly the case. Indeed near $l = 50°$ the polarizations take on more or less random directions, some being nearly normal to the galactic plane—as they would be if a halo field were to cut through the galactic plane in the interarm regions.

The problem of interstellar polarizations will be considered in detail by one of us in a further paper, where a helical model for the spiral arm field will be studied, on the basis that the true direction of the arm lies near $l = 54°$.

A helically twisted model for the spiral arm field has the property of providing far greater arm stability than the cylindrical model of Fermi and Chandrasekhar. In a helically twisted field there is a force per unit volume of order $H^2/4\pi a$ tending to oppose the shearing effect of galactic rotation, where H is here the intensity of the spiral arm field, and a is the average arm radius. With $H = 5 \times 10^{-6}$ gauss, and $a = 300$ pc, this force is of order 2×10^{-33} gm cm^{-2} sec^{-2}. The differential gravitational field of the Galaxy across an arm that lies transverse to the radial direction is $Fa\rho/r$, where F is the radial gravitational acceleration—about 3×10^{-8} cm sec^{-2}, ρ is gas density—about 2×10^{-24} gm cm^{-3}, and r is the distance from the galactic centre. Putting $r \cong 3 \times 10^{22}$ cm we again obtain $\sim 2 \times 10^{-33}$ gm cm^{-2} sec^{-2}. Thus a helically twisted spiral arm field with intensity of order 5×10^{-6} gauss is able to resist the shearing effect of the main gravitational field of the Galaxy. The arm can therefore maintain its identity in a way that the simple cylindrical structure cannot.

St John's College,
Cambridge:
1960 *September.*

Emmanuel College,
Cambridge.

References

(1) Hoyle, F., and Ireland, J. G., *M.N.*, **120**, 173, 1960.
(2) Hoyle, F., and Ireland, J. G., *M.N.*, **121**, 253, 1960.

EXPANDING GALACTIC SYSTEMS AND A NEW APPLICATION OF EINSTEIN'S GENERAL THEORY OF RELATIVITY

Nicola St. Kalitzin

(Communicated by D. W. Sciama)

(Received 1960 September 8)*

Summary

A model for a hierarchical universe, in which the density of matter within any unit is so much greater than the average density on the next larger scale that the unit may be treated as though it were in an empty space, is assumed. This model is applied in turn to the multiple galaxies, the superclusters of galaxies, and the metagalaxies. The Hubble effect of the recession of the galaxies in our metagalaxy is obtained, and similar effects are found at the superclusters of galaxies and at the multiple galaxies.

---

1. In contemporary astronomy the concept that the galaxies form systems of a different order more and more prevails. Galaxies form multiple galaxies and clusters of galaxies; these in turn evidently form superclusters of galaxies (Vaucouleurs 1959). The superclusters of galaxies probably form metagalaxies.

Following Einstein and Friedmann, the majority of cosmologists postulate that on a sufficiently large scale the universe has everywhere the same density. Formerly it was supposed that the stars fill space uniformly, later the same was assumed for the galaxies; then it became clear that the galaxies form clusters of galaxies and the postulate of uniform distribution was transferred to the clusters. Now it is evident that the clusters gather in superclusters, so it is necessary to transfer the same postulate to the superclusters.

The historical development of our knowledge about the universe shows that the idea of constant density of matter in the whole universe can, with difficulty, be reconciled with the astronomical data. Inherent in this idea is the concept of the "whole universe", which is for us at the present time a very obscure notion.

As opposed to the theory of Einstein and Friedmann for an expanding or contracting universe with constant mean density, we propose in this paper a theory in which the vague concept of the "whole universe" is nowhere used. Our theory is based on the hierarchical structure of the clusters of galaxies. We shall first assume that a multiple galaxy is embedded in a space which is Euclidean at infinity and is only a local disturbance of the Euclidean field. That is to say, it is embedded in a "flat space". Later we assume the same for a supercluster of galaxies, and finally, for a metagalaxy.

The model which we investigate is the following: we consider a spherical region G in which we have a spherically symmetric distribution of matter. Inside the region G we assume that the pressure is zero and that the density depends only on the time, whilst outside the density of matter vanishes and the field is asymptotic to Euclidean (or rather Minkowskian) space at infinity.

* Received in original form 1960 June 13.

XUM

The idea of our model for a hierarchical universe is, as D. W. Sciama points out, that the density within any unit is so much greater than the average density on the next larger scale that the unit may be treated as though it were in an empty space.

We apply this model to the multiple galaxies, the superclusters of galaxies and the metagalaxies. This model obviously corresponds better to the hierarchical structure of the visible part of the universe than the solution of Friedmann, which supposes the determination of the mean density of matter in the "whole universe". In this way we obtain not only the Hubble effect of recession of the galaxies in our metagalaxy, but a similar effect at the superclusters of galaxies and at the multiple galaxies. Such effects of "recession" and "repulsion" have recently been discovered.

2. The model with spherically symmetric distribution of matter and with vanishing pressure in the general theory of relativety is considered by McVittie (1933), Tolman (1934), (1938), Datt (1938) Oppenheimer and Volkoff (1938), Oppenheimer and Snyder (1939), Jaernefelt (1940, 1942), Einstein and Strauss (1945), Bondi (1947), Omer (1949), Just (1956). The most general solution of this problem is given by Bondi (1947).

According to our assumption that the density ($\rho = \epsilon/c^2$) in the region G depends only on the time, it follows that in a system of coordinates, which at each point, moves with the matter at this point (the so-called "cosmic coordinates" or "comoving coordinates") we have the following well known particular solution of Einstein's gravitational equations in G

$$ds^2 = c^2dt^2 - T^2(dr^2 + r^2d\theta^2 + r^2\sin^2\theta d\phi^2) \tag{1}$$

where r, θ, ϕ are "spherical" space coordinates, t-time coordinate, ds^2 is the square of the four dimensional distance between two neighbouring points, and T^2 is a function of ct alone.

Since T represents the relative measure of metric distance between two points in G as a function of the time, then

$$\frac{1}{T}\frac{dT}{d(ct)} = \frac{\dot{T}}{T} = H \tag{2}$$

gives the expansion (or the contraction) in the region G.

The Einstein gravitational equations for the region G take in this case the form

$$2\dot{H} + 3H^2 = 0 \tag{3}$$

$$3H^2 = \frac{8\pi\kappa}{c^4}\epsilon\,. \quad (\kappa - \text{Newton's Constant}). \tag{4}$$

According to our assumption the density of matter vanishes outside the region G. Therefore the field outside G must be given by the Schwarzschild exterior solution.

The boundary conditions of our problem are that at the boundary of G the field (1) shall go over continuously up to the first derivative into the field of Schwarzschild in his conformally Euclidean representation. This problem for the line element (1) is solved by Einstein and Strauss (1945), but in this work the region with uniform density is outside G and the Schwarzschild exterior solution holds inside G. Nevertheless the boundary considerations of Einstein and Strauss (1945) hold also for our case (non-vanishing density inside G and

vanishing density outside G)*. This proves that (1) together with (2), (3) and (4) is a correct solution of our problem and can represent the physical properties of our model.

3. In the preceding chapter we found an exact solution to the following problem. Matter with uniform density $\rho = \epsilon/c^2$ which can depend on the time is distributed throughout a spherically symmetric region G, the pressure in the region being zero. Outside the region the density vanishes, and the metric tensor assumes its Galilean values at infinity. We have found our solution in the so-called "cosmic coordinates" in which the space coordinates are chosen such that for a fixed particle they are independent of the time.

As we saw in Section 2, the equation (2) gives the expansion (or the contraction) in the region G. (According to (4) H can have positive as well as negative values: in the first case we have expansion in G; in the second, contraction.) The expressions (2) and (4) for the quantity H correspond exactly to the expression of Friedmann for Hubble's quantity h (see Einstein 1953) for a flat space.

The relation between the expansion quantity H and the average density ϵ/c^2 in the region G given in equation (4) can be compared, at least with respect to the order of the quantities involved, with the experimental data.

To connect the velocity of expansion V of unit distance with the quantity H we note from (2)

$$V = Hc. \tag{5}$$

From (4) and (5) we have

$$V = \sqrt{\left(\frac{8\pi\kappa}{3}\rho\right)} \tag{6}$$

where $\rho = \epsilon/c^2$ is the rest density of matter in G.

We shall apply the expression (6) to the multiple galaxies and then to the superclusters of galaxies.

The linear dimensions of multiple galaxies are of the order 5×10^4 parsecs, whilst the distances between neighbouring multiple galaxies are of the order of $10^6 - 5 \times 10^6$ parsecs. Since the distances between multiple galaxies are about 50 times greater than their linear dimensions our model can certainly be applied to the multiple galaxies. As is well known the majority of the galaxies are clustered in multiple galaxies.

According to Vorontsov-Velyaminov (1958), the majority of the multiple galaxies exhibit a clearly expressed "repulsion" among their components. This "repulsion" reveals itself in the following facts:

(i) In general, the tails of galaxies are directed outside the system and are larger than the filament connections between neighbouring galaxies. The spiral structure can clearly be seen on the outer side of the system, whilst it is absent, or considerably fainter, among the galaxies of the system.

(ii) The destruction of the facade, i.e. the absence of spiral or other structure, or alternatively the decreased brightness of such structures, on the side of a galaxy which faces another galaxy of the system is a very widespread phenomenon. On the sides of the galaxies facing each other the brightness is generally fainter, whereas the gravitational tide wave should give rise to a confluence of stars towards these sides and a consequent increase in brightness. The

* Some inessential errors of Einstein and Strauss (1945) which were corrected in Einstein and Strauss (1946) do not change the validity of their results.

destruction of the facade is a phenomenon which has nothing to do with the tides, but which emphasises the "repulsion," between the components of the multiple galaxy. This "repulsion" is illustrated most clearly by the presence of bright tails.

(iii) The new data published in recent years for the radial velocities of the components of the multiple galaxies has given direct confirmation that some multiple galaxies expand. Examples are:

(*a*) Stephan's quintet: the difference in the radial velocities between the near components NGC 7318a and NGC 7318b is 1000 km/sec.

(*b*) The triple system of Zwicky consisting of IC 3481, Anon and IC 3483. The components of this system are connected by spanning filaments, on account of which an accidental projection is excluded. The radial velocities of these components are respectively, +7304 km/sec, +7278 km/sec, +108 km/sec. It is clear that the last component recedes from the remaining couple, towards us, with enormous velocity. Zwicky, who considers this fact in detail, comes to the conclusion that the interpretation based on the assumption of the accidental approach of the galaxy IC 3483 with the other two encounters great difficulties. For that reason the interpretation of this system as expanding is, for the time being, the only possible one (Ambartsumian 1959).

(*c*) In the radio galaxy NGC 1572 there are two objects which separate with velocity 3000 km/sec.

The investigations of Vorontsov-Velyaminov (1958) show that the interacting multiple galaxies have common origin and that the components of these multiple galaxies have been quite near to each other in the past.

According to Ambartsumian (1959, p. 11) we can estimate the diameter of such a system to be 5×10^4 parsecs. The mean density of matter in this system we can take as 10^{-24} gm/cm^3. 6×10^{-24} gm/cm^3 is the density in the spiral arms of our Galaxy (see report of A. A. Wlassov (1959)).

Substituting these values in (6) we get for the periphery velocity

$$V = \sqrt{\left(\frac{8\pi 6{\cdot}67\,10^{-8}}{3}\,10^{-24}\right)} . 3{\cdot}08 . 10^{18} . 5 . 10^4 = 1150 \text{ km/sec.} \qquad (7)$$

Thus the velocity of recession on the periphery of the system is 1150 km/sec. Of the same order are the above mentioned velocities of recession of some multiple galaxies.

This effect of expansion at the multiple galaxies, which can be explained on the basis of the general theory of relativity without additional hypotheses, represents a new application of Einstein's theory of gravitation. On account of the few effects confirming the general theory of relativity, namely: the advance of the perihelion of Mercury, the gravitational shift of spectral lines at the Sun and at the heavy companion of Sirius, and the gravitational deflexion of light at the Sun, this new application is worthy of our attention. The galaxies behave in this "recession" as independent units.

According to G. de Vaucouleurs (1959) our Galaxy belongs to the so-called Local Supercluster of galaxies. The nucleus of this Supercluster is the Virgo cluster which is situated at a distance 12·6 Mpc from us. The overall diameter of this supersystem is about 30 megaparsecs; its mass is about 10^{15} solar masses. de Vaucouleurs (1959) has observed a similar supercluster with diameter of the order of 30 Mpc, and other superclusters with diameters of the same order have been observed by Abell.

de Vaucouleurs (1959) states that the Local Supercluster of galaxies expands and the velocity of recession is

$$V_l = Bl \tag{8}$$

where $B = 140$ km/sec/Mpc, and l is the distance from the centre of the Supercluster, situated in the Virgo cluster. (According to Sandage

$$B = 80 \text{ km/sec/Mpc.})$$

We may apply our model of insular accumulation of matter in a spherically symmetric region G which is embedded in an Euclidean four-dimensional space to the superclusters of galaxies. We assume that the density ρ in the region G is constant. From the diameter of the Local Supercluster—30 Mpc, and from its mass 10^{15} solar masses we calculate $\rho = \cdot 482 \,.\, 10^{-29}$ gm/cm^3. Substituting this value in formula (7) we get

$$B = 50{\cdot}5 \text{ km/sec/Mpc.} \tag{9}$$

Considering the inexactness of our present day knowledge of the mass and the linear dimensions of the superclusters of galaxies, and similarly of the constant B, we think that the coincidence of (9) with the value of de Vaucouleurs, and even more with that of Sandage, is satisfactory.

We can assume that our Metagalaxy, which consists of superclusters of galaxies, is also embedded in an Euclidean four-space. In the same Euclidean space at great distances from our Metagalaxy are perhaps other metagalaxies which also consist of superclusters of galaxies. These metagalaxies expand according to our equation (6). In this way we come to a new cosmological concept based on the hierarchical structure of the visible part of the universe in which the vague notion of mean (average) density of matter in the "whole universe" is avoided.

According to our theory we can have expansion as well as contraction of the matter in the region G. After Lifshitz (1946) we can assume that the expanding model is stable and the contracting model unstable. This is in good agreement with the experimental data according to which at the multiple galaxies, clusters of galaxies and superclusters of galaxies, expansion predominates.

From (3) and (4) we see that for $\rho(=\epsilon/c^2)$ non-vanishing $\dot{H}$ is everywhere negative; this excludes a pulsating model, in our solution.

The author wishes to acknowledge the help given by M. Kalinkov and the criticism and the suggestions of Dr D. W. Sciama. He is indebted to Professor Chr. Christov and to D. Stojanov for helpful discussions.

Institute of Physics,
Bulgarian Academy of Sciences,
Sofia, Bulgaria:

1960 *September* 1.

References

G. O. Abell, Communication to A.S.P. meeting of June 19 in Los Angeles.
V. A. Ambartsumian, 1959, Reports on the Sixth Conference on the Problems of Cosmogony, Moscow.
H. Bondi, 1947, *M.N.*, **107**, 410.
B. Datt, 1938, *Zs. f. Phys.*, **108**, 314.
A. Einstein and E. G. Strauss, 1945, *Rev. Mod. Phys.*, **17**, 120.

A. Einstein and E. G. Strauss, 1946, *Rev. Mod. Phys.*, **18**, 148.
A. Einstein, 1953, *The Meaning of Relativity*, 4th edition, Princeton.
G. Jaernefelt, *Ann. Acad. Sci. Fenn., Ser. A*, **45**, 3, (1940); *Ser. A*, **45**, 12 (1942).
K. Just, 1956, *Zs. f. Phys.*, **145**, 235.
E. M. Lifshitz, 1946, *Journal-Experimentalnoj i Theorethicheskoj Fisiki*, **16**, 587.
G. C. Omer, 1949, *Astrophys. J.*, **109**, 164.
J. Oppenheimer and G. Volkoff, 1938, *Phys. Rev.*, **55**, 374.
J. Oppenheimer and Snyder, 1939, *Phys. Rev.*, **56**, 455.
R. C. Tolman, *Proc. Nat. Ac. Sci. U.S.A.*, **20**, 169 (1934); *Phys. Rev.*, **55**, 364 (1938).
G. de Vaucouleurs, 1959, *Astronomitcheski Journal*, **36**, 977.
G. C. McVittie, 1933, *M.N.*, **93**, 325.
B. A. Vorontsov-Velyaminov, 1958, *Astronomitcheski Journal*, **35**, 858.
A. A. Wlassov, 1959, Reports on the Sixth Conference on the Problems of Cosmogony, Moscow.

CAN GRAVITATIONAL FORCES ALONE ACCOUNT FOR GALAXY FORMATION IN A STEADY STATE UNIVERSE?

Martin Harwit

(Communicated by F. Hoyle)

(Received 1960 September 10)

Summary

Steady-state cosmology requires galaxy formation at the present epoch. It is shown that, unless matter is preferentially created in the presence of existing galaxies, a stationary galaxy cannot gravitationally attract a sufficient amount of matter from the extragalactic medium to double its own mass within a time $T/3$, where $H=1/T$ is Hubble's constant. An approximation shows that a moving galaxy is also incapable of accreting extragalactic matter at this required rate. By summing over the contributions of all galaxies, one concludes that gravitational forces alone cannot bring about galaxy formation at the required rate if matter is created uniformly throughout a steady state universe. If the steady state theory is to survive, one must postulate that either (1) creation is a markedly localized process, or (2) there exist forces, other than gravity, which can lead to galaxy formation.

---

1. *Introduction.*—The requirements of steady state cosmology are very stringent. One of the predictions of the theory is that galaxies must be formed at a rate that permits regeneration of all galaxies within a time $T/3$, where $H=1/T$ is Hubble's constant (**1**), (**2**), (**3**). It has usually been assumed that gravitational forces play a predominant role in galaxy formation. In contrast, the present paper shows that cosmic expansion interferes with the accretion of matter, and that gravitational forces are not sufficiently powerful to bring about galaxy formation at the rate required by steady state theory.

To prove this, one can consider galaxy formation under the most favourable conditions. A galaxy, whose mass is M, is placed in an expanding universe in which the extragalactic gas is at zero temperature. One examines whether or not the galaxy is able to accrete an equal mass M of extragalactic matter, within a time $T/3$.

If it were possible to condense this amount of matter, one would try to find processes which could separate the condensation from the parent galaxy and lead to the formation of a new daughter galaxy. However, these further considerations are unimportant because a galaxy cannot condense enough extragalactic matter within the theoretically required time.

2. *The equation of motion.*—Consider a galaxy of mass M placed at the origin of a coordinate system. One wishes to examine the motion of a gas particle in the neighbourhood of the galaxy. The most direct method of obtaining the equation of motion in an easily handled form is to start with Pirani's (**4**) expression

$$ds^2=(1-\epsilon)c^2dt^2-(1-\epsilon)^{-1}dr^2-r^2(d\theta+\sin^2\theta d\phi^2) \qquad (1)$$

where $\epsilon\equiv 2\gamma M/c^2r+H^2r^2/c^2$, and r is the proper radial distance. For weak fields,

such as those to be considered here, and particle velocities small compared to the speed of light, this line element implies (5) a Newtonian potential

$$V = -c^2/2\epsilon \tag{2}$$

which immediately leads to the velocity relationship

$$(dr/dt)^2 - (dr_0/dt)^2 = H^2(r^2 - r_0^2) + 2\gamma M(r^{-1} - r_0^{-1}) \tag{3}$$

where γ is the gravitational constant.

In order to fix boundary conditions, one assumes that before time $t=0$ a particle moves freely, receding from the origin of any given coordinate system with a velocity Hr. At time $t=0$, the field of the galaxy is switched on. For $t>0$

$$(dr/dt)^2 = H^2r^2 + 2M\gamma(r^{-1} - r_0^{-1}) \tag{4}$$

If r_0 is small, the attractive force of the galaxy is able to decelerate and eventually reverse the motion of gas particles, so that, sooner or later, they fall into the galaxy. Matter initially at a large distance r_0 from the galaxy is never sufficiently decelerated to assume negative values of dr/dt. In order to determine the amount of matter eventually falling into the galaxy one needs to know the value of r_0 for which the direction of motion can just be reversed.

An element of gas is instantaneously at rest provided the function $X \equiv (dr/dt)^2$ is equal to zero. Restricting oneself to the physically meaningful positive values of r_0 and r, one finds X to be a monotonically increasing function of r_0. For sufficiently large values of r_0, X always remains positive. The largest value of r_0 for which X has a real root is given by the condition that the functions have a minimum value at $X=0$, i.e. $dX/dr=0$ and $X=0$ must be true simultaneously. These two conditions yield a maximum value for r_0

$$r_{0\max} = (8M\gamma/3H^2)^{1/3} \tag{5}$$

A particle at arbitrary initial position r_0 and initial recession velocity Hr_0 will eventually reverse the direction of its motion, if and only if, $r_0 \leqslant r_{0\max}$.

Gas initially at a distance greater than $r_{0\max}$ must recede indefinitely and hence cannot be captured by the galaxy. The amount of matter originally contained in the sphere of radius $r_{0\max}$ is

$$(4\pi/3)\rho r_0{}^3{}_{\max} \tag{6}$$

where ρ is the initial gas density. In a steady state universe* $\rho_{\text{tot}} = 3H^2/8\pi\gamma$ where the total density $\rho_{\text{tot}} > \rho$. Hence the amount of matter which eventually can fall into the galaxy has mass $< 4M/27$ where M is the mass that must be condensed in order adequately to regenerate galaxies during each period $T/3$. In this treatment it has been assumed that the amount of matter initially contained by a sphere of radius $r_{0\,\max}$ is constant. Actually, since matter is continually being created, one may expect slightly more mass to be condensed by the galaxy; but the total mass captured cannot be doubled on this score, so that still less than 1/3 of the required mass is condensed.

Since not all authors (7) agree with the density expression $3H^2/8\pi\gamma$, or $3H^2/4\pi\gamma$, it may be of interest to insert here a numerical estimate of the density of intergalactic matter necessary to allow (gravitational) galaxy formation at the required rate.

* In some models of the steady state universe (10), (11), $\rho_{\text{tot}} = 3H^2/4\pi\gamma$; but the total mass that can be gathered still is less than $8M/27$.

The desired density is $81H^2/32\pi\gamma$. With $H \sim 2{\cdot}5 \times 10^{-18}\,\mathrm{sec}^{-1}$ one obtains $\rho \sim 8 \times 10^{-29}$ g/cc which is an order of magnitude greater than the usual upper limit estimated for the extragalactic gas density.

3. *Accretion of matter by a moving galaxy.*—One might wonder whether or not a moving galaxy would be able to gather a greater amount of matter than a stationary one, especially since Sciama (**6**) suggested some years ago that galaxies might be formed in this manner. However, Sciama was concerned only with orders of magnitude and a factor of 4/27 would have gone unnoticed. If one continues his calculations, within the Newtonian approximation that he adopts, one finds once again that an insufficient amount of matter is gathered. Sciama considers that the cosmic expansion can be neglected (i.e. that the Newtonian equations hold) out to a distance r_N from the galaxy.

$$r_N = \tfrac{1}{2}\left(\frac{3M\gamma}{8\pi\rho}\right)^{1/3} = \tfrac{1}{2}(M\gamma H^{-2})^{1/3} \tag{7}$$

The particle trajectory becomes

$$a^2v^2/\gamma Mr = 1 + \cos\theta + (av^2/\gamma M)\sin\theta \tag{8}$$

where a is the initial distance of the particle from the axis of symmetry, and v is the velocity of the galaxy. A particle crosses the axis when $\theta = 0$, at a distance $d = a^2v^2/2\gamma M$ from the galaxy. At this point one digresses from Sciama's argument by stipulating that $d \leqslant r_N$, which is no more than requiring the particles to cross the axis of symmetry within the region where the equation of motion holds. The amount of matter gathered in unit time is proportional to a^2v. Hence, for a fixed value of d, a^2v is inversely proportional to v, and a slowly moving galaxy is able to gather a maximum amount of matter. Again, $a \leqslant r_N$, and in order to gather the maximum amount of matter the condition

$$r_Nv^2/2\gamma M = 1 \tag{9}$$

has to hold.

In a time $T/3$, matter from a volume $\pi r_N^2 vT/3$ crosses the axis of symmetry within a distance r_N in the wake of the galaxy. By substituting from equation (9) for v one finds that this volume is only $\pi\gamma M/6H^2$ and contains a mass $M/16$, even less than the mass captured by a stationary galaxy.

Of course, the amount of mass gathered in this manner can be raised somewhat by assuming the Newtonian region to extend to greater distances r_N. In fact, the principal difficulty in making this approximation lies in properly choosing the dimensions of the Newtonian region. However, one notes that, within the present approximation, the condensed mass is inversely proportional to the velocity v. One, therefore, can argue that the maximum possible amount of matter accreted by a galaxy equals that accreted by a stationary galaxy, and for that case the mass can be rigorously derived. One concludes that a galaxy cannot gather an appreciable fraction of its own mass within a time $T/3$.

A more rigorous mathematical treatment of the non-stationary case involves no new physical concepts, but the mathematics becomes involved. A first step towards the solution of particle trajectories in a steady state universe has been worked out by Pirani (**4**) who presents the differential equation governing the motion of a particle about an attracting central mass. Complications arise in attempting to integrate this equation.

4. *Discussion.*—Arguments have been presented to show that a galaxy cannot condense sufficient amounts of matter from the extragalactic medium to double its own mass within a time $T/3$. By summing over all galaxies, one concludes that galaxy formation by means of gravitational forces alone is impossible, if matter is created at a uniform rate throughout a steady state universe.

If the steady state theory is to survive, one of two alternatives must be true:

(i) Matter may be preferentially created in the neighbourhood of galaxies. Bondi (**7**) states that the creation rate cannot be proportional to the density, since otherwise the mass of individual stars would double in a time $T/3$. However, observations do not rule out the possibility, say, of a uniform, unusually high rate of creation within galaxies, with little or no creation in extragalactic space.

(ii) There may exist other forces which could lead to galaxy formation. Recently Hoyle (**8**) and Gold and Hoyle (**9**) have proposed a hot universe in which matter is created in the form of neutrons which decay into energetic protons and electrons. Gold and Hoyle suggest that the pressures exerted by the extragalactic gas, whose temperature is 10^7 to 10^9 °K, could compress cool regions of gas to form new galaxies.

A discussion with Professor T. Gold led to this research which was started while the author was in the Physics Department at the Massachusetts Institute of Technology. Professor F. Hoyle very kindly suggested improvements in the manuscript.

The author wishes to thank the N.A.T.O. countries for the award of a post-doctoral fellowship. He is also grateful to Cambridge University for its hospitality.

Department of Applied Mathematics
and Theoretical Physics,
The University,
Cambridge:
1960 *September.*

References

(**1**) H. Bondi and T. Gold, *M.N.*, **108**, 252, 1948.
(**2**) F. Hoyle, *M.N.*, **108**, 372, 1948.
(**3**) F. Hoyle, *M.N.*, **109**, 365, 1949.
(**4**) F. A. E. Pirani, *Proc. Camb. Phil. Soc.*, **50**, 637, 1954.
(**5**) L. Landau and E. Lifshitz, " The Classical Theory of Fields ", p. 302. Translated by M. Hammermesh, Addison Wesley, 1959.
(**6**) D. Sciama, *M.N.*, **115**, 3, 1955.
(**7**) H. Bondi, *Cosmology*, Cambridge, 1960.
(**8**) F. Hoyle, 11th Solvay Congress (R. Stoops, Ed.), 1958.
(**9**) T. Gold and F. Hoyle, I.A.U./U.R.S.I. (1958) Paris Symposium on Radio Astronomy (R. N. Bracewell, Ed.), p. 583, 1959.
(**10**) F. Hoyle, *Proc. Roy. Soc.* A, **257**, 431, 1960.
(**11**) R. A. Lyttleton and H. Bondi, *Proc. Roy. Soc.* A, **257**, 442, 1960.

THE SURFACE BRIGHTNESS OF RADIO SOURCES AT GALACTIC LATITUDES GREATER THAN 20°

Patricia R. R. Leslie

(Communicated by M. Ryle)

(Received 1960 September 20)

Summary

The new interferometric radio-telescope at Cambridge has been used both as a total power instrument and as an East–West interferometer to survey the sky between declinations of $-05°$ and $+61°$ for sources having flux densities greater than 6×10^{-26} wm^{-2} (c/s)$^{-1}$ at a frequency of 178 Mc/s; a comparison of the two surveys allows estimates to be made of angular diameters.

The area $|b| > 20°$, which contains 629 sources, has been examined in detail. The results are consistent with a model in which 83 per cent of the sources have brightness temperatures (T_b) greater than 6×10^4 °K and 98 per cent have $T_b > 10^4$ °K. Two per cent of the sources have $100 < T_b < 200$ °K and these have been identified with nearby normal galaxies.

1. *Introduction.*—A survey of radio sources has been carried out at the Mullard Radio Astronomy Observatory to measure the angular diameters, and hence the radio surface brightness, of a large number of radio sources. A detailed knowledge of the surface brightness is important for two reasons. First, it may be useful in deciding the nature of individual sources and relating them to optical objects, since brightness temperature is a physical property which is independent of distance and is, at the moment, the only basis for classifying sources. Secondly, it may allow a distinction to be made between different classes of sources, so that their distributions in space may be studied separately.

The present observations, at a frequency of 178 Mc/s, were made using two different arrangements of the aerial system which has already been described in connection with the principle of "aperture synthesis" (Ryle 1960). The survey covered most of the sky between declinations $-05°$ and $+61°$, a total area of 5·8 steradians which included 3·9 steradians in the region $|b| \geqslant 20°$. Circular symmetry of the sources was assumed and the observations enabled angular diameters greater than 2′ to be measured. Values of the angular diameter, flux density and position were obtained for 910 sources having flux densities $S \geqslant 6 \times 10^{-26}$ wm^{-2} (c/s)$^{-1}$. A preliminary account of all the observations is given but only the region $|b| > 20°$, which contained 629 sources, is discussed in detail. At lower galactic latitudes a larger fraction of the sources have measurable angular diameters; the relation between these additional sources and H II regions, supernova remnants and other galactic features will be discussed in a separate paper.

Since more accurate positional measurements using the instrument with its full resolving power will soon be available (Scott, Ryle and Hewish 1961), a detailed list of sources is not given. The positions of all sources observed are, however, shown in a map in Section 5 (Fig. 7).

2. *The method of diameter measurement.*—Two sets of observations were used to measure angular diameters. In one, the long element of the aerial system was connected to a receiver which measured the total aerial power, and values of angular diameters were estimated from the broadening of the recorded trace. This aerial had a fan beam whose width to half-power was $4^{\circ}{\cdot}6$ in δ and $13'{\cdot}6$ in α, and angular diameters $>9'$ could be measured for sources with flux density $S \geqslant 6 \times 10^{-26}\,\mathrm{wm^{-2}\,(c/s)^{-1}}$. For sources of angular diameter $>15'$ a progressive increase in the minimum detectable flux density occurred due to difficulties in the analysis caused by irregularities in the background emission; a source of angular diameter $120'$, for example, could only be reliably detected if its flux density exceeded $50 \times 10^{-26}\,\mathrm{wm^{-2}\,(c/s)^{-1}}$; such a source would have a brightness temperature of 25 °K. Sources having angular diameters $>120'$ were excluded from the present analysis.

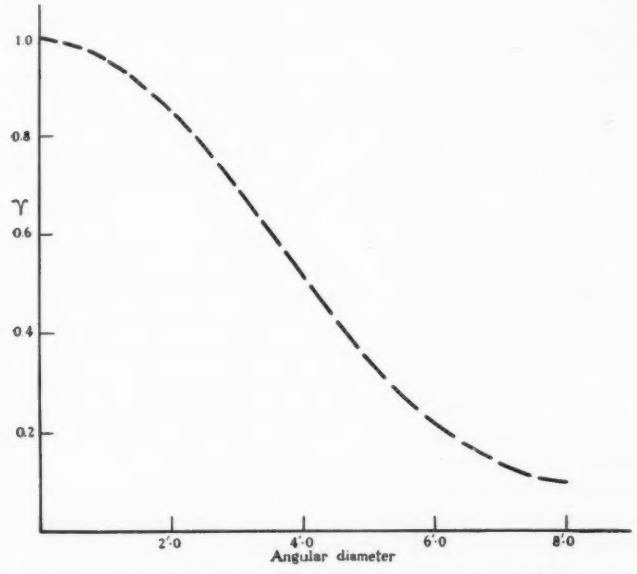

FIG. 1.—*The variation with angular diameter of the ratio of the amplitude of a source on the interferometric system to that on the total power system.*

Angular diameters falling in the range $2'$–$8'$ were measured by combining the total power measurements with another set of observations made using both elements of the aerial system as an interferometer aligned on an East–West axis. A phase-switching receiver was used and this arrangement gave an interference pattern with lobes separated by $7'{\cdot}6$ inside an envelope whose width to half-power was $4^{\circ}{\cdot}6$ in δ and $15'$ in α. Here, values of angular diameters were derived from the ratio (γ) of the deflections obtained with the interferometric and total power recording systems. The variation of γ with angular diameter for a circularly symmetrical Gaussian source is shown in Fig. 1.

The range of spatial frequency included in the combined observations is depicted in Fig. 2. In cases where the brightness distribution does not approximate to a Gaussian profile the parameter γ represents only a part of the data

available on the record. Further information may be derived from the precise variation of amplitude, phase, and periodicity of the record. It may be shown, for example, that a double source can be distinguished from a single extended source provided that the components are separated by not less than 5′ in α and have flux densities whose ratio does not exceed 2.

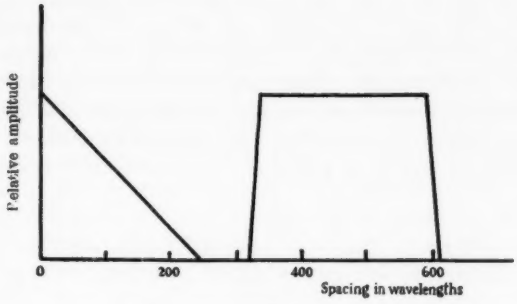

FIG. 2.—*Aerial spacings used in the present observations.*

3. *The observations.* (*a*) *Total power measurements.*—In the first set of observations the large element of the radio-telescope was connected to a total power receiving system as shown in Fig. 3. The input to the preamplifier was connected alternately at 275 c/s to the aerial and to a matched load kept at constant temperature. This load was connected to the input by a coaxial cable, having the same attenuation and supported in the same way as the aerial cable, so that variations in ambient temperature were compensated.

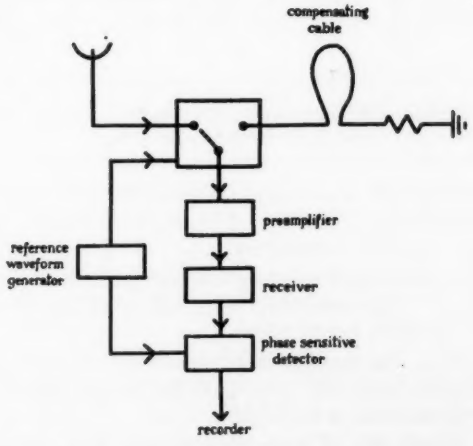

FIG. 3.—*Schematic diagram of the total power system.*

Observations were made at intervals of 3° over a range −05° to +61° in declination. The system was calibrated daily by replacing the aerial by a diode noise generator which had previously been calibrated against a thermal source.

The sensitivity remained constant to within 5 per cent throughout the survey. Since the measurement of total aerial power was more affected by solar emission and terrestial sources of interference than were the interferometric measurements, two days' observations were made at each declination setting.

A typical record is shown in Fig. 4 (*a*). By comparing records at adjacent declination settings the positions of all sources having $S \geqslant 6 \times 10^{-26}\,\mathrm{wm^{-2}\,(c/s)^{-1}}$ were deduced; at this level there is approximately one source per 20 beam areas.

(*b*) *Interferometric measurements.*—For the second set of observations the outputs from the two elements of the radio-telescope were combined in a phase-switching receiver (Ryle 1952). The overall sensitivity was measured by observing two small diameter sources, 3C409 and 3C438 (Edge, *et al.*, 1959; Elsmore, Ryle and Leslie 1959), at weekly intervals throughout the survey; the sensitivity remained constant to within 5 per cent. A section of record is shown in Fig. 4 (*b*).

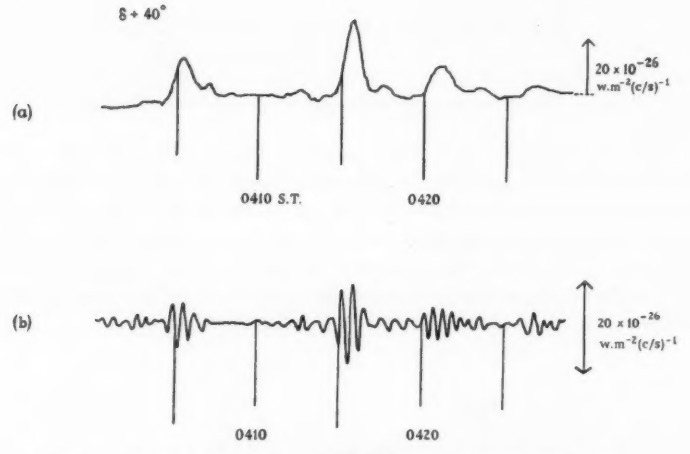

FIG. 4.—*Sections of typical record taken with (a) the total power system and (b) the interferometric system.*

The receiver contained an automatic gain control so that the sensitivity varied with the mean temperature of the sky. In order to correct for this effect, calibration records were taken at declinations $-05°$, $+04°$, $+19°$, $+31°$ and $+42°$, during which known correlated noise signals were periodically fed into the inputs of the preamplifiers. The correction required rarely exceeded 10 per cent in the area of sky analysed.

A small correction was applied to allow for the effect of using a fixed time constant of 4 seconds, while the period of the fringes varied from 30 seconds at the equator to 60 seconds at declination $+60°$.

Although the sensitivity of both surveys was maintained constant it was necessary to establish an absolute scale and an accurate relative scale of flux density for the two surveys for the derivation of angular diameters. Both calibrations were based on the recorded amplitudes of 15 intense sources known to be unresolved from earlier measurements (Morris, Palmer and Thompson 1957; Elsmore, Ryle and Leslie 1959).

4. *Limitations set by noise and confusion.*—It is necessary to determine the effect on γ of noise and weak confusing sources within the reception pattern of the aerial. This problem has been considered by Ryle (1958), who showed how the probable error in the amplitude obtained with an interferometer could be determined from the statistical properties of the records. Similar methods may be used in the case of a total power record but difficulties arise owing to the presence of gradients and curvature on the trace caused by irregularities in the background emission. In the absence of these the record will exhibit fluctuations about a mean level whose power spectrum has the same form as for an isolated source and whose probability distribution is similar to that obtained with an interferometer of the same beam area (Hewish 1961). The presence of gradients and curvature make it difficult to determine the mean level in the vicinity of a source and so the amplitude was measured relative to the intensities recorded in the regions of the first minima of the expected response. The method of analysis is illustrated in Fig. 5. Under these conditions the measured flux density will, on the average, exceed the true value by an amount which may be determined from the deflections on the corresponding interferometric record.

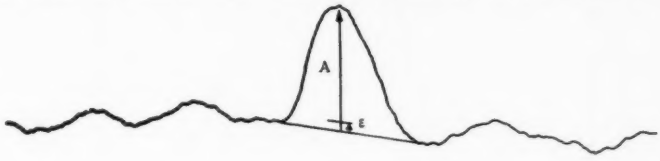

FIG. 5.—*The method adopted for analysis of the total power records. A denotes the measured deflection; in this particular example the true base-level might have been as indicated. The probability distribution of the error (ε) may be derived from a statistical analysis of the interferometric records.*

By sampling 48 hours of record at 1-minute intervals a histogram of interferometric record deflections was formed. This curve was used to predict the distribution of errors in the apparent amplitude of a source on both total power and interferometric systems and hence to establish the distribution in γ which arises from the presence of weak confusing sources. In Fig. 6, the result of making this analysis for a model containing only point sources is shown for two values of flux density, $S = 7{\cdot}5 \times 10^{-26}\,\mathrm{wm^{-2}\,(c/s)^{-1}}$ and $S = 17{\cdot}5 \times 10^{-26}\,\mathrm{wm^{-2}(c/s)^{-1}}$; the curves show clearly the dispersion of γ and also the decrease in the maximum of the curve. In the next section, these theoretical distributions will be compared with the histogram of observed γ, in order to set limits on the percentage of sources having appreciable angular diameters.

5. *Results*—The positions and approximate flux densities of all sources observed are shown in a map in Fig. 7*. The positional accuracy is $\pm 0^{m}{\cdot}15$ in α and $\pm 0^{\circ}{\cdot}75$ in δ for $S > 15 \times 10^{-26}\,\mathrm{wm^{-2}\,(c/s)^{-1}}$ and $\pm {}^{m}0{\cdot}3$ in α and $\pm 1^{\circ}{\cdot}0$ in δ for $6 \leqslant S \leqslant 15 \times 10^{-26}\,\mathrm{wm^{-2}\,(c/s)^{-1}}$. The area of sky analysed is also shown in Fig. 7; a strip of sky having $|b| < 05^{\circ}$ has been excluded from the analysis since, with the high sensitivity of the present survey, the total power records were off-scale. No detailed analysis of the distribution of surface brightness amongst sources having $|b| < 20^{\circ}$ is included in the present paper.

* Due to solar emission the regions $13^{h} < \alpha < 16^{h}$, $30^{\circ} < \delta < 60^{\circ}$ and $11^{h} < \alpha < 13^{h}$, $-05^{\circ} < \delta < 30^{\circ}$ may be incomplete.

XUM

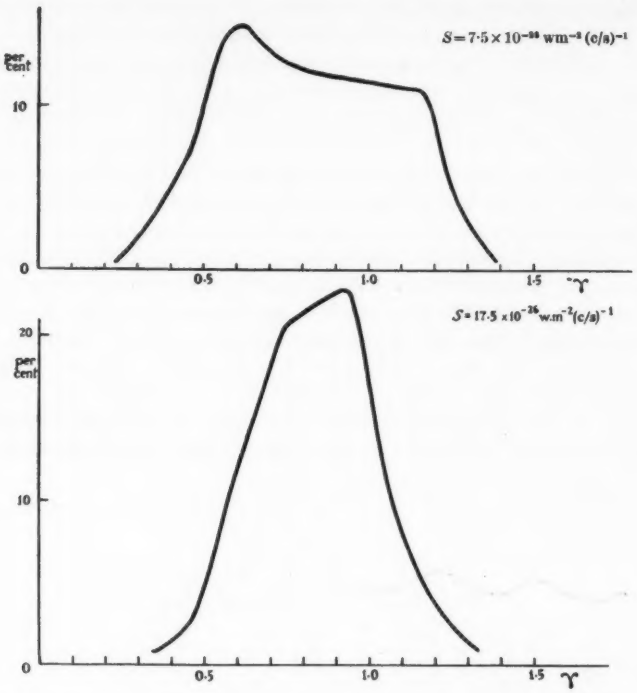

FIG. 6.—*Theoretical curves showing the distribution of γ due to confusion for two values of flux density, assuming that only point sources are present; the two values of flux density correspond to one source every 30 and 150 beam areas respectively.*

The sources in the area $|b| > 20°$ have been divided into three ranges of flux density, $6 \leqslant S \leqslant 10$, $10 < S \leqslant 15$, and $S > 15 \times 10^{-26}$ wm^{-2} (c/s)$^{-1}$. In each range the recorded amplitudes have been used to derive a value of γ for each source and the distribution of γ has been plotted as a histogram (Fig. 8). The sources which have angular diameters greater than 9′·0 have been included as $\gamma = 0$ in the two higher ranges of flux density. In the lowest range of flux density, however, the histogram is incomplete, since, as described in Section 2, weak sources having angular extents greater than 15′·0 cannot always be reliably detected; this histogram is still of use in establishing the distribution of sources of smaller angular extent. For comparison, the appropriate theoretical curves are also shown for a model in which all sources have negligible angular diameters.

From the agreement between these curves and the histograms, it is immediately clear that few sources in any of the flux density ranges have angular diameters as great as 5′·0; the presence of such sources would introduce an excess of those having small γ. Among sources with $S > 10 \times 10^{-26}$ wm^{-2} (c/s)$^{-1}$, only three out of 207 have diameters greater than 9′·0 ; the corresponding brightness temperatures of these three sources lie in the range 100–200 °K.

The limits on the distribution of brightness temperature amongst the sources of smaller angular diameter may be established by comparing the observed

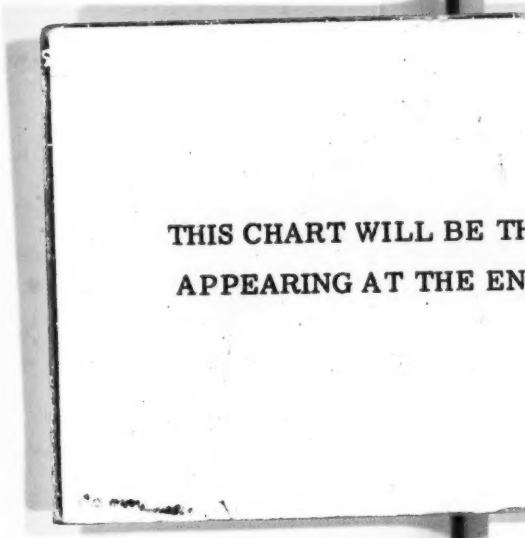
THIS CHART WILL BE TH
APPEARING AT THE EN

LL BE THE FIRST CHART
T THE END OF THIS FILM

XUM

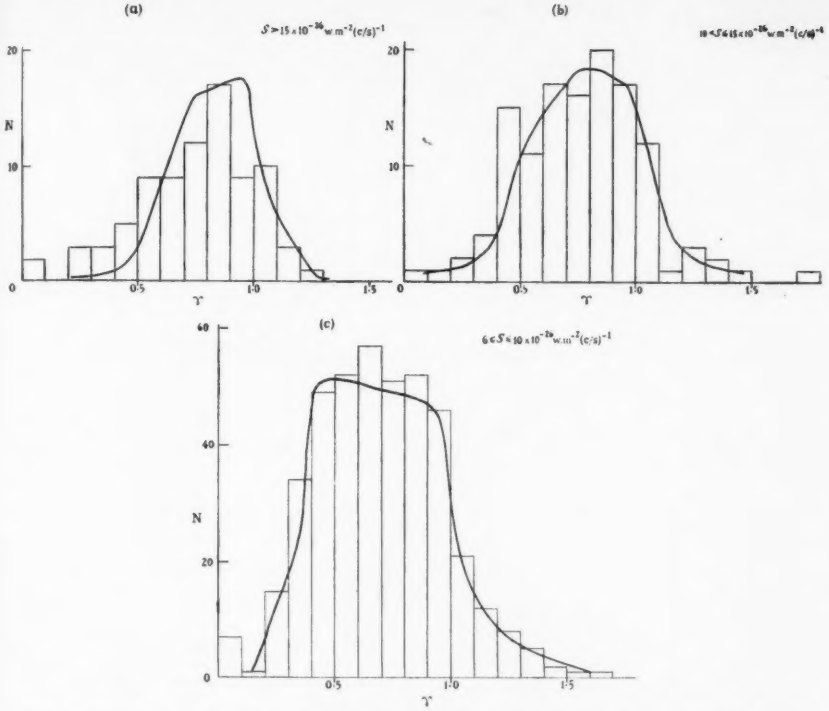

FIG. 8.—*Observed histograms for three ranges of flux density, together with the theoretical curves assuming that all sources are of small angular diameter.*

histograms of γ with those derived for a series of theoretical models. Initially the range $10 < S \leqslant 15 \times 10^{-26}\,\mathrm{wm^{-2}\,(c/s)^{-1}}$ was investigated. In Fig. 9 (*a*) and 9 (*b*) the observations are compared with theoretical curves for models which include different percentages of sources having angular diameters of 3′·5 and 2′·5; these diameters correspond to brightness temperatures of 10^4 °K and 2×10^4 °K respectively. The remaining sources are assumed to be of small angular diameter. It may be concluded from Fig. 9 that a negligible percentage of the sources have a brightness temperature as low as 10^4, and not more than 15 per cent have a brightness temperature in the range $10^4 - 2 \times 10^4$ °K.

In Fig. 10 the theoretical distributions are shown for a model based on these limits, in which 2 per cent of the sources have T_b in the range 100–200 °K, 15 per cent in the range $10^4 - 2 \times 10^4$ °K, and 83 per cent have $T_b > 6 \times 10^4$ °K. The latter figure was adopted because in comparing the theoretical and observed curves for the highest flux density range (a total of 83 sources) it may be concluded that most of the sources must in fact have $T_b > 8 \times 10^4$ °K; for the lower flux ranges the lower limit can only be set at 2×10^4 °K.

6. *Discussion.*—The observations have shown that only a very small percentage of sources (3 out of 207 having $S > 10 \times 10^{-26}\mathrm{wm^{-2}\,(c/s)^{-1}}$) have a brightness temperature $T_b < 200$ °K; these sources have been identified with the nearby normal galaxies M31, M101 and NGC 4258. The remaining sources have

XUM

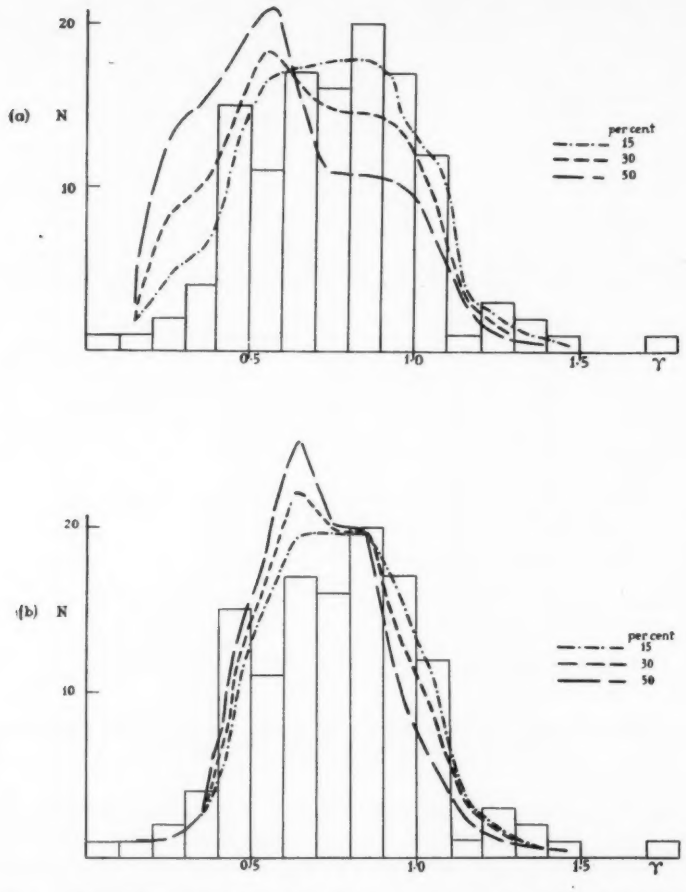

FIG. 9.—*Theoretical curves for the range* $10 < S \leqslant 15 \times 10^{-26}$ *wm*$^{-2}$ *(c/s)*$^{-1}$ *for models containing different percentages of sources with angular diameters of (a)* 3′·5 *arc and (b)* 2′·5 *arc. The observed histogram is also shown.*

$T_b > 10^4$°K, and 85 per cent have $T_b > 2 \times 10^4$°K. From an analysis of 83 sources having $S > 15 \times 10^{-26}$ wm^{-2} (c/s)$^{-1}$, it is concluded that most of the latter group in fact lie in a range $T_b > 8 \times 10^4$°K.

An analysis of the relationship between the optical and radio magnitudes of the identified sources (Long and Marks 1961) has indicated a clear distinction between two classes of extra-galactic radio sources. One class, which includes 3 per cent of the sources falling in a given range of flux density, represents normal galaxies, whose radio emission corresponds closely to that from the Galaxy; the remainder represent galaxies whose radio emission is some 10^3 to 10^6 times greater.

The present results confirm this distribution and support the conclusion that most of the unidentified sources should be associated with very distant galaxies.

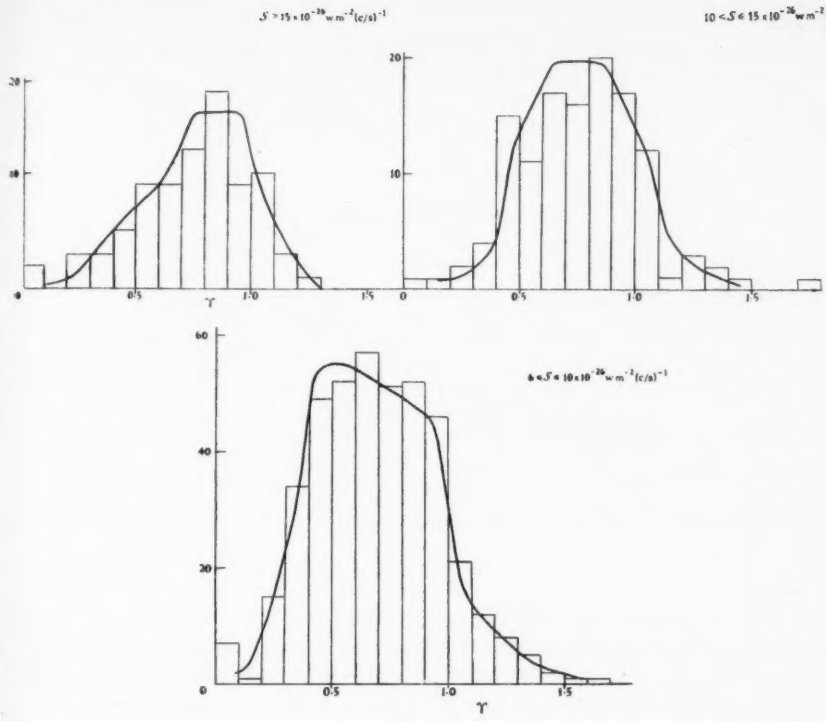

FIG. 10.—*Comparison of observations with theoretical curves for all three ranges of flux density assuming that* 15 *per cent of the sources have* $T_b = 2 \times 10^4$ °K *and the rest* $T_b > 6 \times 10^4$ °K.

The author wishes to thank Dr J. E. Baldwin and Mr A. J. Turtle for their assistance with the total power observations and Professor M. Ryle for his help and encouragement.

The author is indebted to the Trustees of the Robert Cormack Bequest for a Fellowship.

Mullard Radio Astronomy Observatory,
Cavendish Laboratory,
Cambridge:
1960 *September*.

D. O. Edge, J. R. Shakeshaft, W. B. McAdam, J. E. Baldwin and S. Archer, 1959, *Mem. R.A.S.*, **68**, 37.
B. Elsmore, M. Ryle and P. R. R. Leslie, 1959, *Mem. R.A.S.*, **68**, 61.
A. Hewish (in preparation).
R. J. Long and D. R. Marks, 1961, *M.N.*, **122**, 61.
D. Morris, H. P. Palmer and A. R. Thompson, 1957, *Observatory*, **77**, 163.
M. Ryle, 1952, *Proc. Roy. Soc. A*, **211**, 351.
M. Ryle, 1958, I.A.U. Symposium, Paris, p. 475.
M. Ryle, 1960, *J.I.E.E.*, **6**, 14.
P. F. Scott, M. Ryle and A. Hewish, 1961, *M.N.*, **122** (in the press).

THE RELATION BETWEEN THE OPTICAL AND RADIO MAGNITUDES OF GALAXIES

R. J. Long and D. R. Marks

(Communicated by M. Ryle)

(Received 1960 September 20)

Summary

The first observations with the new large interferometric radio telescope at Cambridge have provided positions of good accuracy for several hundred radio sources. Some 200 of these positions have been examined on the prints of the 48-inch Sky Survey, and a number of new identifications have been made. In addition lower limits have been set to the optical magnitude of the objects which are related to the remaining radio sources.

The results are combined with those of earlier searches, and are used to derive information on the distribution of intrinsic radio luminosity among the sources. It is concluded that at least 70 per cent of those observed above a given limit of flux density have luminosities greater than 10^{25} w.(c/s)$^{-1}$ ster^{-1} at 178 Mc/s; only about 3 per cent are normal galaxies with a luminosity of 10^{22} w.(c/s)$^{-1}$ ster^{-1} or less.

1. *Introduction.*—Discrete sources of cosmic radio emission have been studied for a number of years and several extensive surveys have been made, yet it has proved difficult to establish their nature with certainty. Two classes of sources, which are only observed near the galactic equator, have been attributed to the emission from H II regions and from the remnants of supernovae; it is now clear, however, that most of the sources must be extragalactic (Ryle 1958).

Several sources have been identified with external galaxies, and using the optical red-shift their distances and hence their radio luminosities have been found. In order to be able to draw conclusions about the nature of the remainder, it is important to derive the distribution of the radio luminosity for as large a sample as possible.

In the present paper the evidence provided by two recent surveys in the northern hemisphere is examined, and the results are combined with those obtained by Dewhirst (1961) from earlier surveys, with a view to establishing this distribution.

The new radio observations, which include the first results obtained with the full resolution of the large interferometric radio telescope at Cambridge, are summarized in Section 2. The optical search has so far been limited to an examination of the prints of the 48-inch Sky Survey. In most cases it has only been possible to establish lower limits for the optical magnitude of any related object; the radio luminosity function cannot therefore be derived completely, although useful limits can be determined.

The analysis also provides an estimate of the number of optical identifications which are likely to be made from the more accurate radio information which is now becoming available and indicates to what optical magnitude it will be necessary to work.

A value of Hubble's constant of 100 km sec^{-1} Mpc^{-1} has been adopted.

XUM

2. *The observational material.*—In addition to previous surveys, three new sets of observations at a frequency of 178 Mc/s are now available from the high resolution radio star interferometer at the Mullard Radio Astronomy Observatory. These are:

(i) A special investigation of 64 intense sources (Elsmore, Ryle and Leslie, 1959) whose positions could be established with an error of the order of $\pm 1^{s}\cdot 5$ in right ascension and $\pm 1'\cdot 5$ in declination.

(ii) A survey of an area of 1·35 steradians using the full resolution available from the technique of "aperture synthesis" (Scott, Ryle and Hewish, 1961). The positions of sources having flux densities $\geqslant 2\cdot 5 \times 10^{-26}$ w.m^{-2}(c/s)$^{-1}$ were determined with errors of about $\pm 3^{s}\cdot 0$ in R.A. and $\pm 3'\cdot 0$ in Dec.; an area between declinations $+40°$ and $+52°$ is considered in the present paper.

(iii) An investigation at reduced resolving power of the surface brightness of radio sources with integrated flux densities $\geqslant 12 \times 10^{-26}$ w.m^{-2}(c/s)$^{-1}$ over an area of 5·5 steradians (Leslie 1961a). Probable errors in position were $\pm 0^{m}\cdot 15$ in R.A. and $\pm 0°\cdot 75$ in Dec. In these observations a special search was also made in the positions of all galaxies brighter than 11th photographic magnitude (Leslie 1961b).

The first set of observations together with the *A sources in the third Cambridge survey (Edge *et al.* 1959) have been examined by Dewhirst (1961), using the plates of the 48-inch Sky Survey and in some promising cases plates taken with the 200-inch telescope. All the certain identifications are given in Table I.

TABLE I

3C number	Optical object	Radio angular diameter	Estimated m_{pg}	m_r
28	Anon.	$<3'\cdot 0$	17·5	8·4
33	,,	$<1'\cdot 0$	16·5	7·2
75	,,	$4'\cdot 0$	14	8·1
84	NGC 1275	$<1'\cdot 5$	12·8	7·0
98	Anon.	$<1'\cdot 0$	15·5	7·5
218 (Hydra A)	,,	$2'\cdot 3$	15·9	5·8
274 (Virgo A)	M 87	$4'\cdot 7$	9·6	4·0
*295	Anon.	$<0'\cdot 2$	21·5	6·8
310	,,	$<2'\cdot 0$	16·4	7·1
315	,,	$<4'$	17·5	8·1
317(1)	,,	$<1'\cdot 0$	14·5	7·5
317(2)	,,	$<4'\cdot 0$	15	8·7
338	NGC 6166	$<2'\cdot 0$	13·9	8·5
386	Anon.	$<2'\cdot 5$	15	8·1
405 (Cygnus A)	,,	2 disks each 40″ diam. separated by 85″	15	2·1
430	,,	$6'$	17·5	6·6
433	,,	$<1'\cdot 0$	17	7·1

* We are indebted to Professor J. G. Bolton for details of this recent identification.

Lower limits have been found for the optical magnitudes of the remaining 59 radio sources. For each source this is the magnitude of any suggested but uncertain identification; where there appears to be no brighter object a figure of 19 m_{pg} has been taken, since at this level spurious identifications caused

by chance coincidence of position become important (Dewhirst, private communication).

The presence of dense star fields and obscuration make it difficult to maintain a uniform magnitude limit at low galactic latitudes. The analysis which follows in Section 3 has therefore been restricted to $|b| > 20°$, although a few sources, with $|b| < 20°$, whose identification is certain are included in Table I; the inclusion of these sources is allowed for in deriving the histogram in Section 3.

The photo-red magnitudes measured by Dewhirst have been corrected approximately to blue magnitudes (in *UBV*) by adding $1^m{\cdot}0$ to the photo-red value, and are corrected for obscuration. Radio flux densities are expressed, following Hanbury Brown and Hazard (1952), as radio magnitudes, here defined as

$$m_r = -53{\cdot}5 - 2{\cdot}5 \log S$$

where S is the flux density in $\text{w.m}^{-2}\ (\text{c/s})^{-1}$ at 178 Mc/s. This definition differs by $0^m{\cdot}1$ from that used by Hanbury Brown and Hazard to take account of the small change in the frequency of observation.

Two areas of sky from the second set of observations (those taken using the method of "aperture synthesis") have been examined by one of us (D.R.M.), using the prints of the 48-inch Sky Survey at the Cambridge Observatories. The two areas cover declinations 40°–44° and 48°–52°, and all sources in those regions more than 20° from the galactic equator (approximately $11^h{\cdot}5$ and 13^h in R.A. respectively) were examined.

Whilst it is hoped in the future to carry out a more thorough examination and to investigate a larger area of sky, the method adopted in the present search has provided a reliable lower limit to the optical magnitude of the object which is related to each of the radio sources. In this method an area of sky (8·5 square minutes of arc), somewhat larger than that indicated by the estimated positional errors, has been examined at each radio source position in order to allow for any unexpected error in radio position and to cover any possible difference between the radio and optical centres of emission such as occurs in Cygnus A.

The sources examined include 78 with $m_r \leqslant 10{\cdot}6$ on the 40°–44° strip and 53 with $m_r \leqslant 10{\cdot}5$ on the 48°–52° strip, and cover a total area of sky of 0·32 steradians. Within these sensitivity limits there were a further 15 sources on each strip which showed effects of confusion with adjacent sources, and accurate positions could not be obtained; these sources are therefore omitted from the analysis in Section 3, allowance being made in the final statistics. For each source the lower limit on m_{pg} has been taken as the magnitude of the brightest galaxy observed in the adopted error rectangle of 8·5 square minutes of arc, magnitudes being estimated to the nearest $0^m{\cdot}5$. The results are presented in Section 3.

Since it is important that the adopted error area shall include all objects that represent true associations, a further test was made. The search was repeated using an error rectangle of 34 square minutes of arc; the additional number of galaxies recorded corresponded with the increase expected for random coincidences calculated from the counts of galaxies given by Hubble (1934). It was concluded therefore that the 8·5 square minutes of arc search area was large enough to include all true associations. The numbers recorded in the rectangles of 8·5 square minutes of arc were too small for a reliable estimate of the proportion of true associations among them to be made.

Fewer sources were recorded with galaxies of about 18^m in their search areas than would be expected from random coincidences; this is almost certainly due to errors in estimating the magnitudes of galaxies near the magnitude limits of the Sky Survey prints.

The third set of observations, although limited to sources having $m_r \leqslant 8{\cdot}8$, was not restricted to sources of small angular size, and therefore permitted a study of all sources in this range of flux density; the positional accuracy is however considerably worse. The observations included the whole sky between declinations -05° and $+61^\circ$, and in addition a special examination was made in the positions of all galaxies brighter than 11 m_{pg} (Leslie 1961b); in this way it was possible in many cases to set a lower limit on the radio emission than could be achieved throughout the whole area.

The 9 galaxies detected in the special search are listed in Table II, with values of m_r, m_{pg}, and the absolute photographic magnitude M_{pg} in cases where the distance of the galaxy is reliably known. The value of m_{pg} quoted for NGC 4526 is that given by Pettit (1954), and values given by Holmberg (1958) are quoted for the remainder. Obscuration by the galaxy has been allowed for in the one case (NGC 224) in which it is important. Unlike the galaxies listed in Table I, none of these galaxies shows marked optical peculiarities, although NGC 598, 1068, and 4258 are Seyfert emission objects.

Radio emission was not detected from 24 other galaxies. All these have $m_r \geqslant 9{\cdot}8$.

TABLE II

NGC	m_r	m_{pg}	M_{pg}
*224	5·8	3·7	−20·4
598	9·0	5·8	...
†1068	8·5	9·6	−20·5
2903	10·0	9·4	...
4254	9·9	10·4	−21·4
*4258	9·5	8·9	...
4490	9·6	10·1	...
4526	10·0	10·7	...
*5457	8·3	8·2	...

* First observed by Hanbury Brown and Hazard (1952).
† First observed by Mills (1955).

Apart from this special search 17 sources with angular diameters $\geqslant 3'{\cdot}0$ and $m_r \leqslant 8{\cdot}8$ were located at galactic latitudes $>20^\circ$; six of these are among the sources considered by Dewhirst. A search for the remaining 11 was made on the Sky Survey prints, and lower limits to their optical magnitudes were determined except in two cases where obscuration prevented this. Owing to the greater positional errors of this survey a search area of about 600 square minutes of arc was adopted, with a corresponding limiting optical magnitude of approximately 16 m_{pg}.

3. *The distribution of radio luminosity.*—Since recessional velocities have only been measured for a few of the galaxies identified with radio sources, it is convenient, initially, to examine the distribution of $m_r - m_{pg}$; if the spread of the absolute optical magnitude M_{pg} can be assumed to be small, and if a small correction

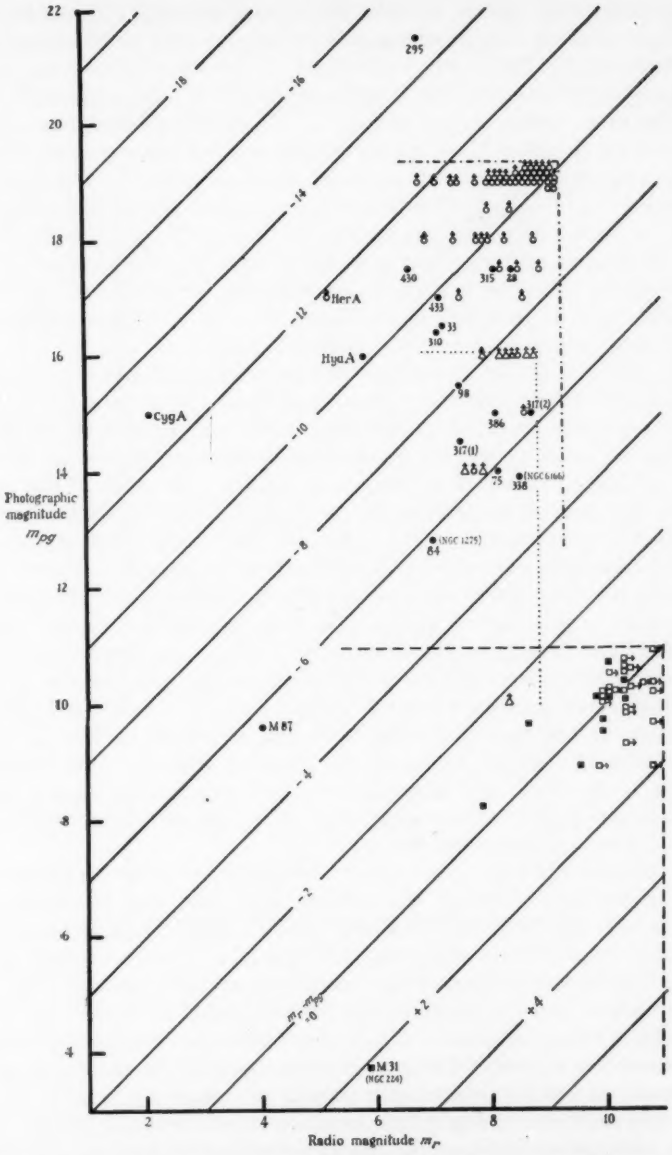

FIG. 1.—*Radio and optical magnitudes of sources observed between declinations −05° and ±61° at 178 Mc/s and the •A sources in the third Cambridge catalogue.*

- ● *Identified sources given by Dewhirst (1961).*
- ○↑ *Limits on m_{pg} of unidentified sources (Dewhirst 1961).*
- ■ *Normal galaxies observed at 178 Mc/s (Leslie 1961b).*
- □→ *Limits on m of normal galaxies not observed.*
- △↑ *Limits on m_{pg} of unidentified sources with angular diameters ⩾3′·0 (Leslie 1961a).*
- ——·—— *Approximate sensitivity limits for sources considered by Dewhirst.*
- – – – – *Approximate sensitivity limits in search for normal galaxies.*
- ····· *Sensitivity limits for unidentified sources with angular diameters ⩾3′·0.*

Except where otherwise noted the numbers refer to the third Cambridge catalogue.

for the differential effects of radio and optical red-shifts is made, then the distribution of $m_r - m_{pg}$ corresponds closely to that of the absolute radio magnitude M_r.

(*a*) *Identified sources.*—The distribution of $m_r - m_{pg}$ is conveniently displayed by a plot of m_r against m_{pg} as in Fig. 1. On this figure the sources at present identified are shown as filled-in symbols, the analysis being restricted, except for the 3C sources considered by Dewhirst, to observations at 178 Mc/s north of declination $-05°$. Earlier identifications and those identified by Dewhirst are shown as black circles and the normal galaxies in Table II as black squares. Lines of constant $m_r - m_{pg}$ have been drawn, showing the variation of $m_r - m_{pg}$ from -15 for 3C 295 to $+2$ for the Andromeda Nebula. It will be noted that all normal galaxies have $m_r - m_{pg}$ between $+3$ and -1, while galaxies showing optical peculiarities have $m_r - m_{pg}$ generally below -5.

The limits of $m_r - m_{pg}$ obtained here for normal galaxies may be compared with those obtained by Hanbury Brown and Hazard (1952) and by Mills (1955). The four galaxies observed by Hanbury Brown and Hazard fall in this range; Mills has been able to obtain a greater radio sensitivity, so that his observations extend to higher values of $m_r - m_{pg}$. It is likely that many of the 23 normal galaxies not observed by radio in the northern sky, for which lower limits on m_r are shown as open squares on Fig. 1, have similarly high values of $m_r - m_{pg}$.

(*b*) *Unidentified sources.*—The lower limits on m_{pg} established for unidentified sources in the three sets of observations may be plotted in exactly the same way to derive an upper limit on $m_r - m_{pg}$ for each unidentified source. On Fig. 1 the lower limits on m_{pg} for the unidentified sources considered by Dewhirst are shown as open circles and the lower limits on the unidentified sources in the lower resolution survey are shown as open triangles; the sensitivity limits are $m_r = 9{\cdot}2$ for the former and $m_r = 8{\cdot}8$ for the latter, and are shown on Fig. 1.

The sources observed by means of "aperture synthesis" are the results of a survey to $m_r = 10{\cdot}6$, and although restricted to a smaller area of sky (0·32 steradians as opposed to approximately 4), the results have comparable statistical weight. They are plotted on Fig. 2.

All the results in Figs. 1 and 2 may now be combined, taking account in each survey of the area observed, the limiting sensitivity, and any sources whose positions were insufficiently well known for an optical search, in order to derive limits on the distribution of $m_r - m_{pg}$ amongst all radio sources down to a given limit of flux density. These limits are shown as a histogram in Fig. 3. For the purposes of later discussion the figures correspond to the number of sources per steradian having $m_r \leqslant 10{\cdot}6$. The upper limit to the contribution from normal galaxies is shown shaded. The most conservative limits for the remaining sources are derived, except for sources with angular diameters $\geqslant 3'{\cdot}0$, from the data in Fig. 2, and are shown in Fig. 3 by continuous lines. By using the data from the sources examined by Dewhirst, the limits may be moved to lower values of $m_r - m_{pg}$, as shown by the dotted lines in Fig. 3. Since, however, these sources are not a complete sample above a given limiting flux density, there is some risk of observational selection in using them.

Extended sources (with angular diameters $\geqslant 3'{\cdot}0$) which would be missed or observed at seriously reduced flux density by the high resolution survey, except when at great distances, are included using the results from the lower resolution survey.

The most striking feature of the distribution is that most sources have $m_r - m_{pg}$ more negative than -8. Less than one third have $-4 > m_r - m_{pg} > -8$, a range which includes a number of identified sources having optical peculiarities (M87, NGC 1275, NGC 6166). Less than 3 per cent of the sources have $m_r - m_{pg} > -2$ (normal galaxies).

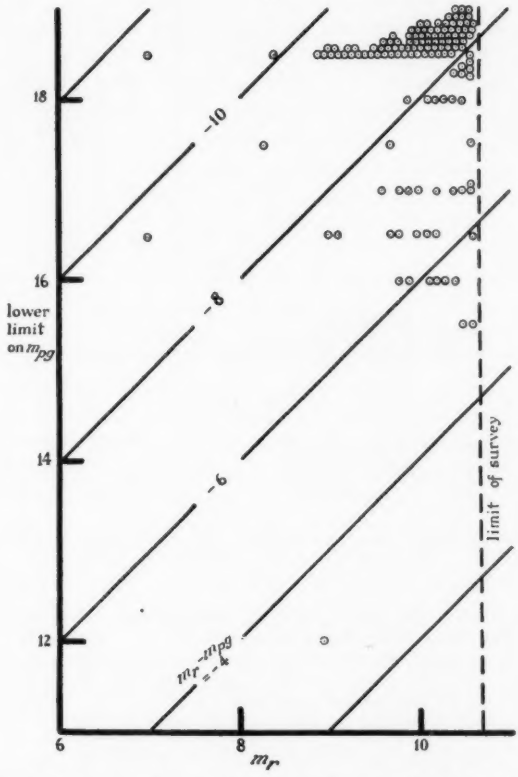

FIG. 2.—*Lower limits on m_{pg} for 131 sources with $m_r \leqslant 10{\cdot}6$ observed with high resolution over 0·32 steradians at 178 Mc/s.*

(*c*) *Relation between $m_r - m_{pg}$ and radio luminosity.*—So far the concept of $m_r - m_{pg}$ has been used only to classify radio sources, the procedure being justified by the correspondence between this classification and any optical peculiarities in the case of identified sources. It becomes a more useful concept if the variation of M_{pg} among radio sources is proved to be small. This appears to be so among those identified.

Over the northern and southern sky the distances of 7 radio sources having optical peculiarities have been measured, and all these have M_{pg} within the limits $-20{\cdot}6 \pm 1{\cdot}0$. The three galaxies in Table II for which M_{pg} has been calculated also fall within these limits. It seems permissible therefore to derive the radio luminosity from the measured value of $m_r - m_{pg}$.

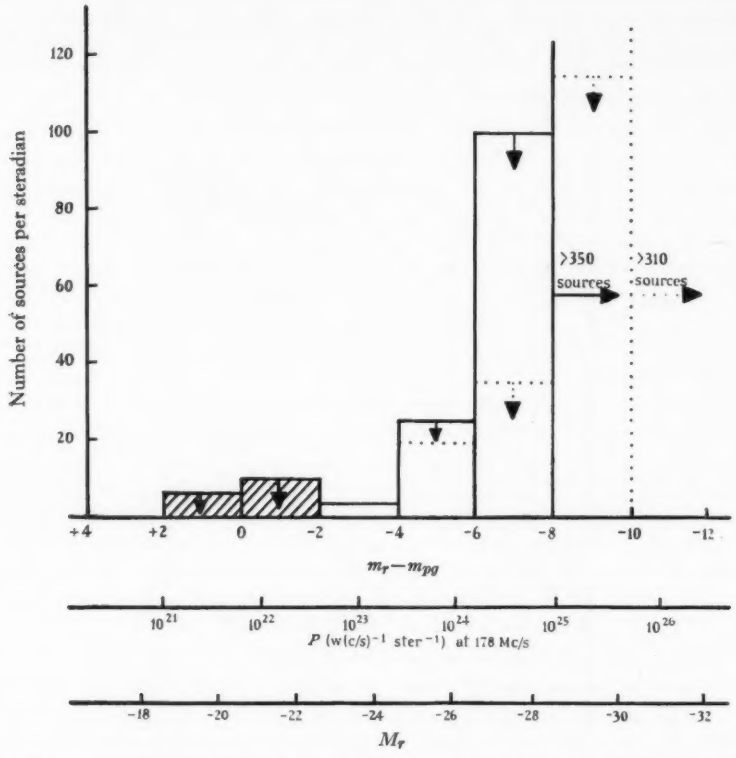

FIG. 3.—*Limits to the distribution of $m_r - m_{pg}$ among all radio sources observed at* 178 *Mc/s with $m_r \leqslant 10{\cdot}6$. The shaded area represents the upper limit to the contribution from normal galaxies. The areas shown in continuous lines represent the most conservative estimate based on the "aperture synthesis" results. These are modified as shown by the dotted lines, by using the results given by Dewhirst. The vertical arrows indicate upper limits.*

It is important to note that this conclusion is based only on identified sources other than objects such as the Magellanic Clouds and NGC 55 which are of considerably lower optical luminosity and have $m_r - m_{pg} = +4$ approximately (Mills 1955). No other irregular galaxies have been detected at radio wavelengths and the number of such sources is in any case too small to affect the histogram in Fig. 3 appreciably.

The existence of an entirely different class of extragalactic object, having negligible optical emission, would of course affect conclusions based on the distribution of $m_r - m_{pg}$ among the unidentified sources. The minimum optical emission expected on theoretical grounds to occur from an extragalactic radio source has however been discussed by Tunmer (1960), who concludes that even in the absence of stellar emission appreciable free–free emission from the gaseous material should occur. Since no such objects have been found even among the more intense sources, it may be concluded that an entirely new class of extragalactic source is unlikely.

In the following analysis it will therefore be supposed that there is only a small dispersion in M_{pg}.

(*d*) *Correction for red-shift.*—$M_r - M_{pg} = m_r - m_{pg}$ only if the effects of the red-shift on the optical and radio magnitudes may be assumed to be equal.

To investigate this the effect on the radio magnitudes has been calculated assuming that the spectral distribution may be represented by $S \propto \lambda^{0.7}$. The correction for the optical magnitude is less certain, since many of the sources have strong emission lines. If, for example, an appreciable fraction of the total optical emission were in the $\lambda 3727$ line, the correction would be somewhat less than for an assumed black-body spectrum. This uncertainty is, however, unlikely to introduce an error in the derivation of $M_r - M_{pg}$ of more than $0^{m}{\cdot}5$ for sources having $m_{pg} < 22$, and the upper limit of the differential red-shift correction has been used to provide a conservative estimate of M_r.

Using this correction, scales of radio luminosity have been added to Fig. 3, expressed both in terms of M_r, and in terms of $P(\text{w.(c/s)}^{-1}\,\text{ster}^{-1})$ as used previously (Ryle 1958).

4. *Discussion.*—From the histogram plotted in Fig. 3 it may be seen that at least 70 per cent of the sources are of very great luminosity, having $P > 10^{25}$ w.(c/s)$^{-1}$ ster^{-1}. Most of the 30 per cent or less that remain have $10^{25} > P > 10^{23}$, while only 3 per cent or less are normal galaxies with $P \sim 10^{22}$. This latter result is confirmed by the distribution of "surface brightness" among 305 sources with $S > 10^{-25}$ w.m^{-2} (c/s)$^{-1}$ whose angular diameters have been measured (Leslie 1961a); only about 2 per cent have a surface brightness comparable with that of the Galaxy, the rest having considerably greater values.

The predominance of sources having $P > 10^{25}$ is in good agreement with the conclusions reached by Tunmer (1960) from considerations of the problems of accounting for the radio emission from extragalactic sources. From an examination of the angular diameter and radio spectrum of the sources, the supply of energy and the conditions for gravitational stability, she was able to show that it was difficult to account for sources having $P < 2 \times 10^{25}$ w.(c/s)$^{-1}$ ster^{-1}.

It is interesting to examine, on the basis of these results, the possibilities of increasing the number of identified sources. There is little chance of observing a large sample of normal galaxies, unless the radio sensitivity can be extended appreciably below the present limits. In a search to $19\,m_{pg}$ further identifications of abnormal galaxies are only likely to be made among those with $P < 10^{25}$ w.(c/s)$^{-1}$ ster^{-1}; of sources whose flux density at 178 Mc/s exceeds $2{\cdot}3 \times 10^{-26}$ w.m^{-2} (c/s)$^{-1}$ 30 per cent might fall into this category, or about 125 per steradian. It must be remembered, however, that the histogram of P represents conservative lower limits for abnormal galaxies, and the number having $P < 10^{25}$ may be considerably less than 30 per cent; in this case a smaller number of sources would be brighter than $19\,m_{pg}$.

It would be of the greatest interest to extend the search to objects having $P > 10^{25}$ w.(c/s)$^{-1}$ ster^{-1}. To do this objects fainter than $19\,m_{pg}$ must be examined on red sensitive plates using the most refined methods. Under these conditions the present optical limit might be taken as $22\,m_{pg}$. A source such as 3C 295 having $P = 10^{27{\cdot}5}$ w.(c/s)$^{-1}$ ster^{-1} would then correspond (when corrections have been made for the red-shift), to $m_r = 7{\cdot}2$ or $S = 50 \times 10^{-26}$ w.m^{-2} (c/s)$^{-1}$.

Allowing for the fraction of sources which are of smaller luminosity, it may be concluded that over the whole northern and southern sky (excluding the

area near the galactic plane) there could be 10 to 15 such sources which might be identifiable.

The discovery of even such a small number of sources of large P would seem to be sufficiently important to justify a very careful investigation of the most intense sources whose positions have been established with considerable accuracy (Elsmore, Ryle and Leslie, 1959).

5. *Acknowledgments.*—We should like to thank Professor M. Ryle and Dr D. W. Dewhirst for much helpful discussion and advice. We should also like to thank Dr D. W. Dewhirst, Miss P. R. R. Leslie, and Mr P. F. Scott for making results of recent observations available before publication.

Mullard Radio Astronomy Observatory,
Cavendish Laboratory,
Cambridge:

1960 *September* 9.

References

Brown, R. Hanbury, and Hazard, C., 1952, *Phil. Mag.*, **43**, 137.
Dewhirst, D. W., 1961, in preparation.
Edge, D. O., Shakeshaft, J. R., McAdam, W. B., Baldwin, J. E., and Archer, S., 1959, *Mem. R.A.S.*, **68**, 37.
Elsmore, B., Ryle, M., and Leslie, P. R. R., 1959, *Mem. R.A.S.*, **68**, 61.
Holmberg, E., 1958, *Medd. Lunds Astron. Obs.*, Ser. II, **136**.
Hubble, E., 1934, *Ap. J.*, **79**, 8.
Leslie, P. R. R., 1961a, *M.N.*, **122**, 51.
Leslie, P. R. R., 1961b, *Observatory* (in the press).
Mills, B. Y., 1955, *Aust. J. Phys.*, **8**, 368.
Pettit, E., 1954, *Ap. J.*, **120**, 413.
Ryle, M., 1958, *Proc. Roy. Soc. A*, **248**, 289.
Scott, P. F., Ryle, M., and Hewish, A., 1961, *M.N.*, **122** (in the press).
Tunmer, H. E. C., 1960, *M.N.*, **120**, 360.

A COMPARISON OF THREE SURVEYS OF RADIO STARS

A. S. Bennett and F. G. Smith

(Received 1960 September 30)

Summary

The reliability of a recent survey of radio stars using a pencil-beam radio telescope at 178 Mc/s (Leslie 1961) is established by comparison with a high-resolution survey using an interferometer (Scott, Ryle, and Hewish 1961). The pencil-beam survey is then used to check the accuracy of surveys by Mills, Slee, and Hill (1958) and by Edge *et al.* (1959) known as the MSH and 3C surveys, at 85 Mc/s and 158 Mc/s respectively.

It is shown that these two surveys are substantially correct for flux densities greater than 20×10^{-26} w.m^{-2} (c/s)$^{-1}$ at 85 Mc/s, and 8×10^{-26} w.m^{-2} (c/s)$^{-1}$ at 159 Mc/s. There is some doubt about the reliability of the MSH survey at lower flux densities, since considerable errors are already found at this level.

Some of the extended sources included in the MSH survey appear to represent clusters of unresolved sources.

Introduction.—This paper is an analysis of the accuracy and reliability of the surveys known as MSH (Mills, Slee and Hill 1958) and 3C (Edge *et al.* 1959). This analysis has been made possible by the completion of two new and more powerful surveys at Cambridge. We refer to a survey PRRL in which Miss Leslie (1961) used a single aerial with a beam 13′·6 in α by 4°·6 in δ at 178 Mc/s, covering the sky from declination $-05°$ to $+61°{\cdot}5$, and to a survey SRH in which Scott, Ryle and Hewish (1961) used the same aerial as part of an aperture synthesis radio telescope, covering three strips in the Northern sky with a high-resolution interferometer with primary resolution 25′ in α by between 33′ and 48′ in δ depending on the declination. Since the SRH survey is not sensitive to extended sources, it is used here only as a check of the accuracy and completeness of PRRL for point sources; the latter is then used as the standard against which MSH and 3C may be tested.

Detailed comparisons of surveys must take into account the different circumstances of resolution, sensitivity, and frequency. Further, it is not always clear how complete a survey is intended to be, since uniform coverage over a large area of sky may be difficult to achieve. For this reason we have examined primarily the correctness of the published lists of MSH and 3C rather than their completeness. We have not attempted any search of the MSH list for other sources listed in PRRL, although some such search has been made of the 3C list.

1. *Comparison of PRRL with SRH.*—A comparison was made of all sources observed in the PRRL and SRH surveys in the three areas between declinations $+2°{\cdot}2$ and $+7°{\cdot}2$, $+40°$ and $+44°$, $+48°$ and $+54°$; the total solid angle of these three areas is 1·0 steradian. The maximum difference allowed in position was $\pm 15''$ in α and $\pm 1°{\cdot}5$ in δ, approximately 3/2 times the quoted accuracy of PRRL. The PRRL survey lists all sources observed with a flux density greater than $6{\cdot}0 \times 10^{-26}$ w.m^{-2} (c/s)$^{-1}$, while the SRH survey extends down to $2{\cdot}5 \times 10^{-26}$ w.m^{-2} (c/s)$^{-1}$.

A total of 151 sources are found by PRRL in the three areas; of these 147 occur on the SRH survey, 19 being resolved into 2 sources and 2 into 3 sources. The remaining 4 all have flux density less than 8×10^{-26} w.m^{-2} (c/s)$^{-1}$; their absence from the SRH survey is probably due to the uncertainty in declination, which may place them outside the SRH survey areas.

The reverse comparison shows that only two sources, each with flux density $6{\cdot}0 \times 10^{-26}$ w.m^{-2} (c/s)$^{-1}$, are missing from the PRRL list. Since there is no reason to doubt that a corresponding sensitivity and reliability is attained in PRRL for extended sources, we may take PRRL as a reliable standard.

2. *Comparison of MSH with PRRL.*—These two surveys cover areas overlapping between declinations $-5°$ and $+10°$. Separate comparisons were made of sources listed by MSH as extended, and those with a small angular diameter. The analysis also distinguished between regions well away from the galactic plane, namely R.A. 21^h–00^h–05^h and R.A. 09^h–15^h, and the remaining regions near or in the galactic plane. The area R.A. $11^h\,10^m$–$12^h\,15^m$ was excluded from PRRL owing to the position of the Sun at the time of observation; also the galactic plane in the region $17^h\,20^m$ to $19^h\,37^m$ is not included in PRRL.

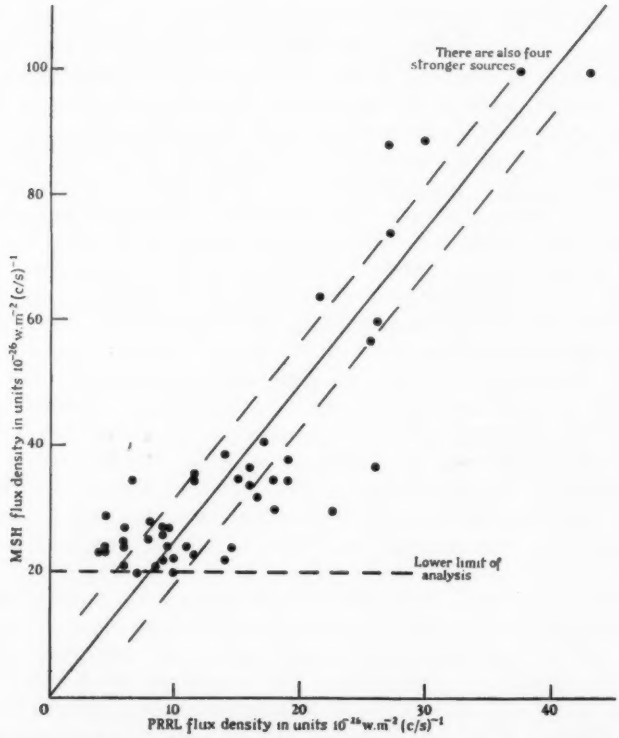

FIG. 1.—*Comparison of flux densities for sources recorded on both the PRRL and MSH surveys. The full line represents a ratio of 2·5, while the broken lines show the expected r.m.s. error*

Since the two surveys are at 85 Mc/s and at 178 Mc/s respectively, discrepancies might arise from a large dispersion in spectral index. Harris and Roberts (1960) show however that the spectral indices of most discrete sources, apart from H II regions, are contained in a spread of 0·6. Consequently the ratio of flux density between the two frequencies may be taken as constant within ±25 per cent, and we may therefore use with some confidence an average value for this ratio. Some of the extended sources at low galactic latitude may however be expected to have a lower spectral index, corresponding to thermal emission. In the comparison any source in MSH which has a lower spectral index than average will have a greater chance of being detected by PRRL, so that a test of the correctness of MSH is not affected by such sources.

We first establish the mean ratio of flux density as measured in the two surveys. Fig. 1 shows a plot of the two flux densities for 50 sources which clearly correspond in the MSH and PRRL lists. In the MSH survey the r.m.s. error in flux is not clearly stated, but appears to be about 5×10^{-26} w.m^{-2} (c/s)$^{-1}$ at 85 Mc/s (referred to hereafter as 5 units at 85 Mc/s). The PRRL survey is usually only limited by the "confusion level" from the combination of deflections from weak sources; this corresponds to an uncertainty of about 2 units at 178 Mc/s. After allowing for the spectral ratio derived below, this is roughly equivalent to the MSH error, and may be combined with it to give a resultant r.m.s. error in any comparison of 7 units at 85 Mc/s or 3 units at 178 Mc/s. The spread in the ratio appearing in Fig. 1 is accounted for by the combination of this error with the ±25 per cent spread in spectral index. The two dashed lines represent the combined limits of error if the mean ratio is 2·5 (derived from the stronger agreeing sources) and we shall adopt this value.

(i) *MSH "small diameter" sources.*—This analysis included only those sources not listed by MSH as extended or possibly extended. The limit of 6 units at 178 Mc/s for the PRRL survey corresponds to 15 units at 85 Mc/s, but if we include the combined error of 7 units as a Gaussian error we would expect some 20 per cent of MSH sources listed as 20 units to be missing from the PRRL list on account of errors in flux density alone. The analysis was therefore limited to MSH sources with flux densities $\geqslant 20$ units at 85 Mc/s, and in all cases of disagreement the original records of the PRRL survey were searched to a flux density of 2 units at 178 Mc/s.

Owing to the different beam shapes, a number of sources resolved by MSH appear as blends in the PRRL survey, while other MSH sources have been resolved into two or more by PRRL.

There are 87 relevant MSH sources listed in the region surveyed by PRRL. Of these 42 agreed directly with sources in the PRRL list, and 19 were apparently blends in one or other list, the total flux density being in reasonable agreement. One source was found to be in a region obscured for PRRL by solar interference (just outside the listed region). The remaining 25 were searched for on the PRRL survey records, as follows:

8 agreed with sources just below the PRRL limit.

5 corresponded each to several weak sources, resolved in R.A. by the PRRL survey.

12 corresponded to nothing greater than the confusion limit of 2 units at 178 Mc/s These sources are listed in Table I,

Of these 12 sources, only 09+02 was originally suspect, although two others had been observed once only. Including these, we find that 3 out of 53 sources away from the plane, and 9 out of 33 close to the plane, are missing. The high proportion of spurious sources near the plane is indicative of the difficulty of interpreting the complicated records obtained in this region. Possibly some of the missing sources should be classified along with 09+02 as sidelobe responses to other sources.

TABLE I

Sources reported by MSH and not found on PRRL records

	MSH	Flux density at 85 Mc/s	MSH remarks	Comments from PRRL evidence
Away from plane	09+02	40	Possibly sidelobe of 09S1A	...
	14+01	28	...	...
	22−016	20	Perhaps forms one extended source with 22−015	No evidence for extended source.
Near plane				
	05+03	20	...	...
	06+09	29	...	Corresponds to feature of extent 4°–5° in galactic background.
	15+011	22	One record only	...
	16+08	23	One record only	...
	06−012	24	...	...
	15−014	23	...	...
	17−05	31	...	...
	19−012	20	...	...
	19−013	22	...	...

(ii) *MSH "extended" sources.*—For each extended source the MSH list gives both the total flux density and the peak deflection as observed by a 1° beam, and it is possible from this to estimate the angular extension of the source in R.A. Since the resolution of the PRRL survey is 13′·6 in R.A., giving the possibility of a greatly reduced peak deflection, it is necessary to search the original records over the same extent of R.A., where we would expect to find a corresponding integrated deflection for each extended source. With the improved resolution it becomes possible to distinguish between a true extended source and a blend of two or more small sources, but in either case the integrated deflection should correspond with the MSH total flux density.

Since extended sources are more difficult to confirm than unresolved sources a limit of 40 units at 85 Mc/s was used in testing the correctness of the MSH list. Sources near the galactic plane were not examined in detail, since it is often difficult to distinguish them from irregularities in the background.

There are 10 extended sources to be examined in the area away from the galactic plane. For each source the relevant record on the PRRL survey extends over about 8 beamwidths. One source (14+10) corresponds to an extended source on the PRRL records (Fig. 2, (i)). As shown by the interferometer

records, there are also some small diameter sources present in this region. The observed flux density suggests that the spectrum may be the flat spectrum typical of a thermal source. In the figure the broken line indicates the deflection to be expected from a source as reported by MSH, if the spectrum is the same as that of the small diameter sources.

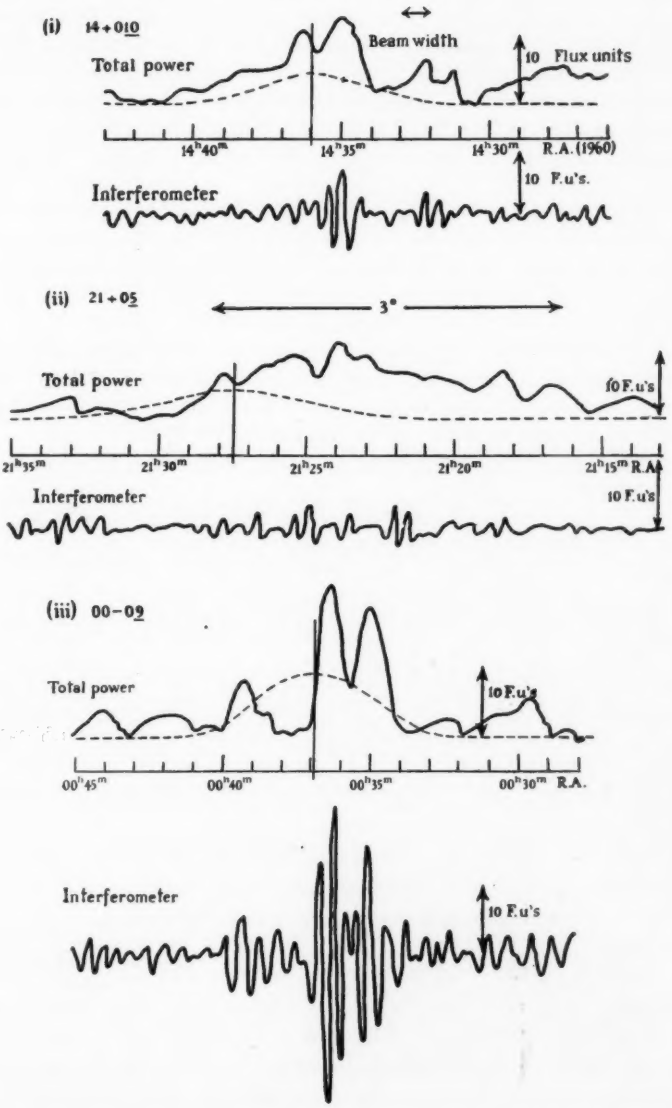

FIG. 2.—*Records obtained near MSH "extended sources". For each of the three sources the PRRL total power and interferometer records are shown. The interferometer spacing was 465 λ. The broken line represents the trace to be expected from the MSH survey.*

A second source (21+5) appears to be associated with an extended feature on the PRRL record (Fig. 2 (ii)). The MSH position here corresponds with the late edge of the feature, which is about 3° wide and has an integrated flux density of about 100 units at 178 Mc/s.

All the remaining eight MSH extended sources were found not to correspond to any extended source on the PRRL records. In each position, however, several small diameter sources were found, with a total flux density sufficient to account for the MSH source. Comparison with other sections of the PRRL records indicates that some of these groups of sources may be sufficiently outstanding to be regarded as discrete clusters, but further analysis is required before these groups can be regarded as distinct from fluctuations in a random distribution. The records for the most convincing example are shown in Fig. 2 (iii).

3. *Comparison of 3C with PRRL.*—These two surveys cover areas overlapping between declinations −05° and +61°·5. Following the same procedure as for the comparison of MSH with PRRL, but ignoring the difference in frequencies (the 3C survey was at 159 Mc/s), we search the PRRL list for all sources listed in 3C for regions covered by the PRRL survey.

Direct agreement was obtained for 181 out of 376 sources, and 74 more agreed after applying a "lobe-shift" correction as described in the 3C catalogue. A further 48 were resolved by PRRL into double sources, or otherwise differently interpreted as a result of the increase in primary resolving power.

The remaining 73 were searched for using the PRRL records, with the following results:

11 were found to be in regions where the PRRL survey was affected by solar radiation, or by sidelobe responses of various intense sources.

14 agreed with sources at or just below the PRRL limit of 6 units.

9 more agreed similarly after application of a "lobe-shift" correction.

23 were resolved on the PRRL records into two or more sources below the limit of 6 units.

16 corresponded to nothing greater than 3 units on the PRRL records.

Regrouping these, out of 365 sources which could be checked 278 (75 per cent) agreed, 71 (20 per cent) agreed partly, and 16 (5 per cent) do not exist. This result may be compared with the statement in the 3C paper that: "It is believed that not more than 15 per cent of the sources included in the catalogue are seriously in error".

The 16 cases of clear disagreement are listed in Table II.

TABLE II

Sources reported by 3C and not found on PRRL records.

3C number	7	50	70	80	81	148	150
Flux density	13·5	8·0	8·0	8·0	9·5	11	8·5

3C Number	151	156	214	260	312	373	399	426	427
Flux Density	8·0	14·0	8·5	9·5	8·5	11·0	8·0	9·5	12·0

A partial check of the completeness of the 3C catalogue shows that it is practically complete down to 12 units of flux density, only 4 sources each with a flux density about 17 units having been missed. One further source with flux density 31 units lies in a region obscured by solar radiation just outside the region reported in the 3C paper.

A comparison of flux densities recorded by PRRL and 3C is shown in Fig. 3, which includes only those sources whose angular diameters are not appreciably resolved by the 3C interferometer. The spread on this plot is accounted for by the probable error of ± 2 units on both surveys; the broken line represents a combined error of $\pm 2{\cdot}8$ units. The mean slope is close to unity.

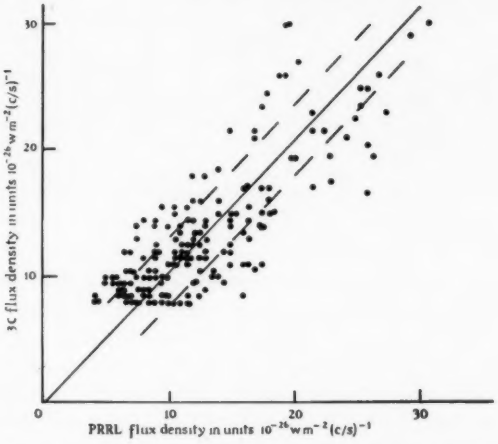

FIG. 3.—*Comparison of flux densities for sources recorded on both the PRRL and 3C surveys. The full line represents a ratio of 1·0, while the broken lines show the expected r.m.s. error.*

4. *Conclusions.*—We note first that our results confirm the general accuracy of positions quoted in all lists referred to, and also that most sources with flux densities in excess of 20 units at 85 Mc/s and 8 units at 178 Mc/s are correctly listed.

The MSH list does however contain considerable errors at this level, and the validity of this list at lower flux densities must therefore be doubted. The majority of MSH sources have a flux density below 20 units, with quoted values reaching to 7 units. The errors are greater near the plane of the Galaxy, where about a quarter of the sources listed with a flux density greater than 20 units cannot be found. The extended sources are more difficult to check, but at least it is clear that the majority of extended sources away from the plane are small clusters of point sources rather than true extended sources.

The 3C catalogue has been checked to its limit of 8 units of flux density. About 5 per cent of the listed sources do not exist, and 20 per cent appear to be blends. The catalogue is practically complete to 12 units of flux density.

Mullard Radio Astronomy Observatory,
Cavendish Laboratory,
Cambridge:
September 1960.

References

Edge, D. O., Shakeshaft, J. R., McAdam, W. B., Baldwin, J. E. and Archer, S., 1959, *Mem. R.A.S.*, **68**, 37.
Harris, D. E. and Roberts, J. A., Cal. Inst. Tech. Radio Observatory, 1960.
Leslie, P. R. R., 1961, *M.N.*, **122**, 51.
Mills, B. Y., Slee, O. B. and Hill, E. R., 1958, *Aust. J. Phys.*, **11**, 360.
Scott, P., Ryle, M. and Hewish, A., 1961, *M.N.*, **122** (in the press).

STONY METEORITE ORBITS

John A. Wood

(Received 1960 October 3*)

Summary

The observed distribution of apparent radiants and diurnal variation in frequency of meteorite falls, taken together, are shown to be consistent only with a bombardment of the Earth by *fast* meteorites (velocity of approach, independent of acceleration by the Earth's gravitational field, approximately 8 km/sec). This lends support to the traditional view that meteorites pursued asteroid-like orbits before being captured by the Earth.

---

1. *Introduction.*—It has been generally supposed that the meteorites are closely related to the asteroids: in fact that they are probably asteroidal fragments produced by collisions in the densely populated asteroid belt. The little that is known of the astronomy of meteorite falls bears out this idea. Orbital elements computed for three competently witnessed falls are presented in Table I (Wylie 1948), and it can be seen that all three pursued asteroid-like orbits.

TABLE I

Orbital elements computed for three stony meteorite falls in the United States (*Wylie* 1948)

Fall	Tilden (Illinois)	Paragould (Arkansas)	Archie (Missouri)
a	1·72 a.u.	2·50 a.u.	1·52 a.u.
e	0·45	0·63	0·47
ω	141° 53′	143° 57′	110° 24′
Ω	110° 24′	328° 2′	138° 2′
i	1° 22′	19° 3′	7° 34′
Period	2·25 yr.	3·96 yr.	1·87 yr.

On the other hand, Urey (1959) has pointed out that measurements of the abundance of He^3 and H^3 in stony meteorites have consistently yielded cosmic ray exposure ages in the range 10–100 million years, an order of magnitude lower than the range of ages encountered in iron meteorites. Because of this, Urey has postulated two very different sources for these two classes of meteorites. The irons are asteroidal in origin, as above, and travel in asteroid-like orbits. But the stones are fragments of the surface of the Moon, blasted loose and accelerated beyond escape velocity by impacts of crater-forming planetesimals. Because these stone fragments subsequently follow near-circular orbits, closely coincident with that of the Earth–Moon system, they are more readily captured by the Earth than are the irons; hence the discrepency in the cosmic ray exposure ages of the two groups.

Theoretical calculations made by Öpik (1951) of the average time-before-capture of particles in asteroid-like and Earth-like orbits support Urey's hypothesis.

* Received in original form 1960 June 2.

XUM

In proposing this hypothesis, Urey questions either the accuracy of calculated orbits such as Wylie's, or the assumption that the orbits of these three falls are typical of the majority of stony meteorites. In any case, even the gross characteristics of the average stony meteorite orbit are regarded as open to question.

It appears worthwhile to examine the astronomical data more closely, in order to try to make some definite statement about the character of meteorite orbits. There seems little point in speculating on the early history of a meteorite, when we do not know even approximately where it was in the solar system six months before it fell to Earth.

We have at our disposal two sets of statistical meteorite fall data, from which it should be possible to determine at least the gross characteristics of meteorite orbits. These are the distribution of apparent radiants of the falls, taken with respect to the apex of the Earth's way; and the distribution of falls over the hours of the day. Both distributions will obviously be affected, in different ways, by the manner in which meteorites approach the Earth. Our plan is to use them to solve for two unknowns: an average velocity, and a distribution of angles of incidence with which meteorites bombard the Earth.

2. *Observational data.*—The distribution of apparent radiants to be used is taken from Newton's compilation of 116 radiants available in the literature in 1888. Unfortunately Newton does not tabulate his falls and calculations, but presents his results in the form of true radiants plotted on a stereographic net. In 1888 an association between meteorites and comets seemed certain, so Newton assumed parabolic velocity in computing his true radiants. For the purposes of the present work, these are reduced back to apparent radiants, and are presented in Fig. 1 plotted on equal-area nets.

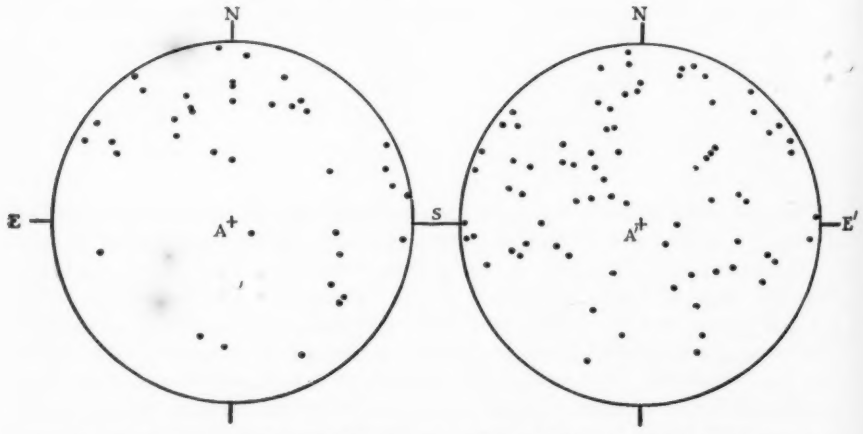

FIG. 1.—*Apparent radiants of 116 meteorite falls compiled by Newton (1888), plotted on equal-area nets. A, apex of Earth's way; A', antapex; EASA'E', plane of ecliptic; N, north pole of ecliptic plane; S, Sun.*

We will be concerned with only a single parameter in employing the radiant distribution: the angle between the apparent radiant and the antapex. (ϕ and Φ will be used to designate the angles between an apparent radiant and, respectively, the incident direction and the antapex; similarly, λ and Λ will be measured

between the vector from the Earth's centre to the point of impact on the surface of the Earth, and the same two reference directions (see Fig. 4). The incident direction is parallel to the asymptote of the hyperbola which an approaching meteorite attempts to describe about the centre of the Earth. The angle between the incident direction and the antapex (angle of incidence) will be denoted by I.) Accordingly, Fig. 1 is reduced in Fig. 2 to a plot of the relative density of radiants (δ_ϕ; radiants per unit solid angle) against Φ.

Many of the radiants assembled by Newton are admittedly approximate, and Fig. 1 must contain a substantial number of errors of several tens of degrees. There is, however, no reason to think that the errors in Fig. 1 are not essentially random in direction, and so they should not greatly affect the shape of the density curve in Fig. 2.

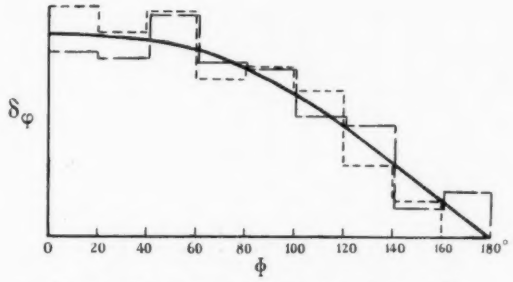

FIG. 2.—*Plot of observed density of radiants vs.* Φ.
— — — *from all 116 falls in Fig. 1.*
– – – – – *from 46 falls with radiants in northern-sunlit quadrant of celestial sphere.*
——— *smoothed distribution.*

It can be seen that radiant density in Fig. 1 is not symmetrical about the axis apex–antapex. This follows from the concentration of the world's land area and population in the northern hemisphere and, to a lesser degree, from the smaller likelihood of recovering meteorites which fall at night. That this asymmetry does not seriously affect the δ_ϕ–Φ distribution is demonstrated in Fig. 2, where a plot assembled from all 116 radiants is shown to differ little from a plot based only on the 46 radiants in the northern-sunlit quadrant of the celestial sphere.

The distribution of 357 falls over the hours of the day (Fig. 3) was compiled from the *Catalogue of Meteorites* (Prior and Hey 1953). Only the daylight falls are included, as darkness must clearly bias the probability of recovery. There is a clear-cut tendency for more meteorites to fall in the afternoon than in the morning. The great majority of meteorite falls are seen by farmers, who work the fields from dawn to dusk; there is no reason to believe that this distribution is biased by any increase in probability of observation and recovery of falls later in the day.

Only about 7 per cent of all the meteorites observed to fall are irons. 5 per cent of the 357 falls compiled in Fig. 3 are irons, and it is assumed that Newton's compilation of radiants, including as it did all available reports of falls up to 1888, must have contained a similarly small proportion. Thus, the distributions presented above cannot be significantly affected by the orbital characteristics of the irons. Our results will be meaningful only for stony meteorites.

3. *Derivation of theoretical distributions.*—We will consider the two-body problem where a particle of negligible mass (meteorite) approaches a fixed massive body (the Earth; see Fig. 4), and seek expressions for λ and ϕ as functions of v_0, the velocity of the particle an infinite distance from the Earth; and y, the

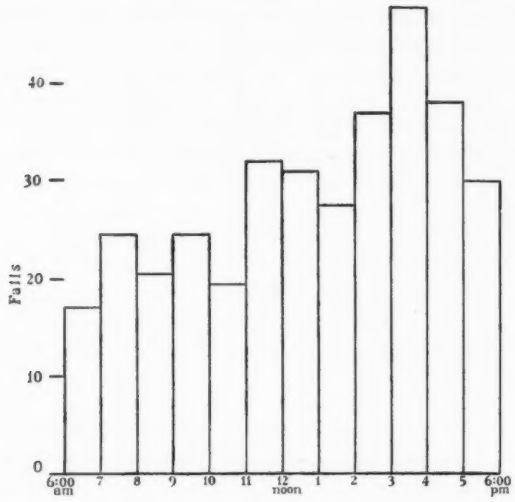

FIG. 3.—*Histogram showing number of meteorites which have been seen to fall and reported during each hour of daylight (compiled from Prior and Hey, 1953).*

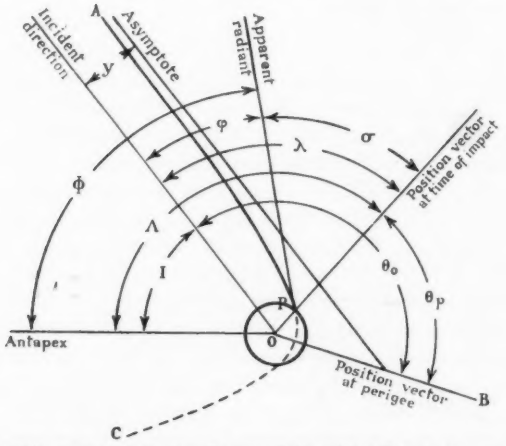

FIG. 4.—*Particle attempting to describe hyperbolic orbit APC about centre of Earth; P, point of impact.*

length of a perpendicular from the asymptote of the particle's motion to the centre of the Earth. Equations of celestial mechanics, for hyperbolic motion, which will be required:

$$r = \frac{a(e^2 - 1)}{1 + e\cos\theta} \qquad (1a)$$

(θ reads counterclockwise from $\theta = 0$ along OB);

$$\frac{v^2}{2} - \frac{\mu}{r} = \frac{\mu}{2a}, \tag{1b}$$

from which

$$v_0^2 = \mu/a; \tag{1c}$$

and

$$rv \sin\sigma = \sqrt{\mu a(e^2-1)}, \tag{1d}$$

where σ is the angle between the position vector $\mathbf{r}$ and the velocity vector $\mathbf{v}$ for the particle; μ is the product of the gravitational constant and the mass of the Earth.

In (1 *a*), as r becomes infinitely long, $(1+e\cos\theta)$ must approach zero; hence, referring to Fig. 4,

$$\cos\theta_0 = -1/e. \tag{2}$$

Noting that as $r\to\infty$, $r\sin\sigma\to y$, (1 *c*) and (1 *d*) yield

$$e = \sqrt{1 + \frac{v_0^4 y^2}{\mu^2}}. \tag{3}$$

From (1 *a*), (1 *c*) and (3),

$$\cos\theta_P = \frac{F}{e}, \tag{4}$$

where

$$F = \frac{v_0^2 y^2}{\mu r_e} - 1, \tag{5}$$

r_e being the radius of the Earth. Then, from (2) and (4),

$$\lambda = \theta_0 - \theta_P = \cos^{-1}\left(-\frac{1}{e}\right) - \cos^{-1}\left(\frac{F}{e}\right), \tag{6}$$

where e (eccentricity) and F are given in terms of v_0 and y in (3) and (5).

As y increases, for a given value of v_0, a limiting y_l will be reached, at which r at perigee equals the radius of the Earth, and beyond which particles will escape being captured by the Earth. At perigee $\theta = 0$, so the limiting value of y can be derived from (1 *a*), (1 *c*) and (3):

$$y_l = \sqrt{r_e^2 + \frac{2r_e\mu}{v_0^2}}. \tag{7}$$

Given a uniform, parallel (at a large distance from the Earth) flux of meteorites, we now derive the relative density of falls (falls per unit area–unit time) on the surface of the Earth, δ_λ, as a function of λ. Referring to Fig. 5,

$$\delta_\lambda \propto \frac{\text{elemental source area in plane } S}{\text{corresponding elemental fall area on Earth}}.$$

Thus, eliminating constants,

$$\delta_\lambda \propto \frac{y}{\sin\lambda\left(\frac{d\lambda}{dy}\right)}. \tag{8}$$

Differentiating (6) with respect to y, and inserting in (8),

$$\delta_\lambda \propto \frac{e^2}{\sin\lambda}\left[\frac{2\mu e^2}{v_0^2 r_e\sqrt{e^2-F^2}} - \frac{F}{\sqrt{e^2-F^2}} - \frac{1}{\sqrt{e^2-1}}\right]^{-1}. \tag{9}$$

ϕ is given by

$$\phi = \lambda - \sigma, \tag{10}$$

where from (1 *b*), (1 *c*), and (1 *d*)

$$\sin\sigma = \frac{1}{r_e v_0}\sqrt{\frac{\mu(e^2-1)}{2\left(\frac{1}{r_e}+\frac{v_0^2}{2\mu}\right)}}. \tag{11}$$

Finally, we need a relationship between δ_λ, the derived density of falls (falls per unit area–unit time, equivalent to falls per unit solid angle of the Earth–unit time) and δ_ϕ, the density of radiants in radiants per unit solid angle (of the celestial sphere)–unit time, since our observational data are in the latter form. Referring to Fig. 5,

$$\frac{\delta_\lambda}{\delta_\phi} = \frac{\text{elemental radiant area on celestial sphere}}{\text{elemental fall area on earth}} = \frac{\sin\phi\, d\phi}{\sin\lambda\, d\lambda}.$$

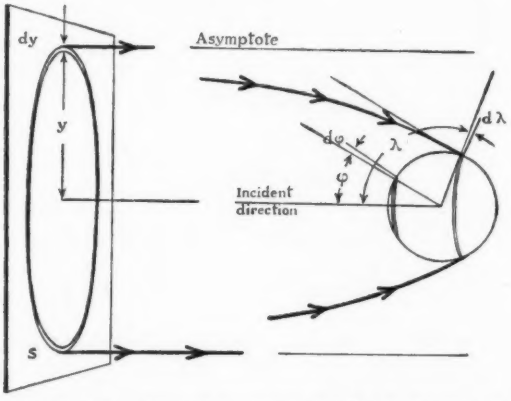

FIG. 5.—*From left to right: elemental source area in plane S, elemental radiant area on celestial sphere, and elemental fall area on Earth, all for a particular y and* v_0.

It is easier to show by numerical calculation than to prove that $d\phi/d\lambda$ for any given v_0 is constant or very nearly constant (see Fig. 7). Thus little error is introduced by assuming

$$\delta_\phi \propto \frac{\sin\lambda}{\sin\phi}\,\delta_\lambda. \tag{12}$$

4. *Computations.*—We are now in a position to compute the density of falls as a function of position on the Earth, and density of radiants as a function of the apparent radiant, for any v_0 (initial velocity) and angle of incidence.

First, we examine models in which uniform parallel fluxes of meteorites bombard the earth at three different initial velocities:

$v_0 = 0{\cdot}06$ km/sec (so slow that trajectories are profoundly influenced by the Earth's gravity),

$v_0 = 1{\cdot}49$ km/sec (an intermediate velocity), and

$v_0 = 16{\cdot}6$ km/sec (so fast that effects of the Earth's gravity are small).

Results of computations are presented graphically in Fig. 6. In Fig. 7, ϕ is plotted against λ for the three models to justify the derivation of equation (12). Finally, equation (12) is employed in plotting δ_ϕ against ϕ in Fig. 8.

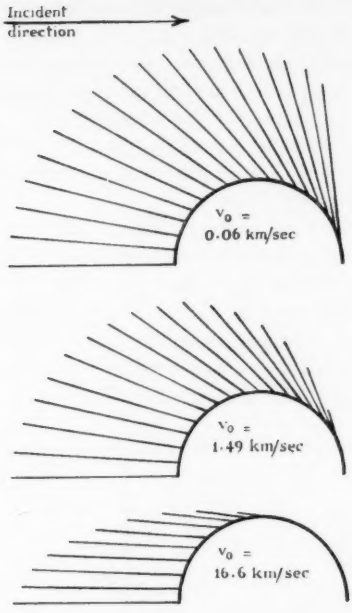

FIG. 6.—*Vector diagram, illustrating relationship between point of impact on Earth's surface, apparent radiant, and relative density of falls* (δ_λ, *proportional to length of vectors*).

It is apparent from the differences between Fig. 2 and any of the curves plotted in Fig. 8 that the observed radiant distribution cannot be caused by a flux of meteorites approaching the Earth parallel to the line apex–antapex, but that the flux must be distributed over a range of angles of incidence.

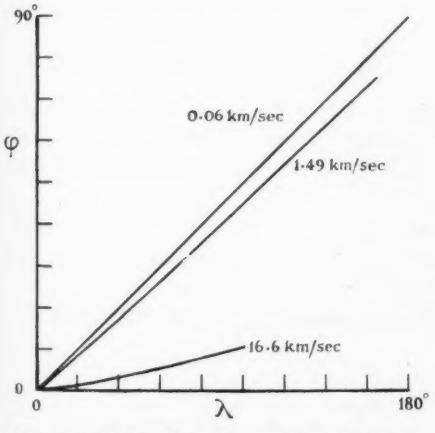

FIG. 7.—*Relationship between apparent radiant,* ϕ, *and position of impact,* λ.

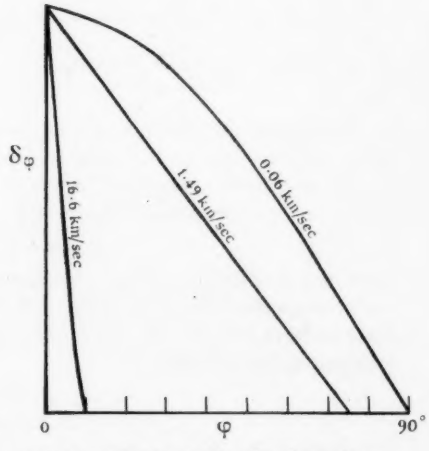

FIG. 8.—*Relative density of radiants,* δ_ϕ, *as a function of* ϕ, *for three initial velocities of approach.*

From each of the δ_ϕ–ϕ relationships illustrated in Fig. 8 it is possible to derive graphically a δ_ϕ–Φ relationship (i.e. with respect to the Earth's antapex instead of to the incident direction) for any angle of incidence. For each of the three velocity models, we perform such transformations at several values of I. Then, for each v_0, it is possible by the solution of simultaneous equations to partition the falls among these angles of incidence, such that the summed effect of each model is an apparent radiant distribution which closely simulates Fig. 2. The three models are given in Table II.

Having used the observed radiant distribution in constructing the three models, it only remains to test them by computing the fall density–time of day relationship for each and comparing it with that observed (Fig. 3).

The δ_λ–λ curves in Fig. 9 can be converted graphically into δ_λ–Λ relationships for the various angles of incidence called for in Table II. These may then be weighted as indicated in Table II, and summed to yield the three overall δ_λ–Λ dependencies appropriate to the three models (Fig. 10).

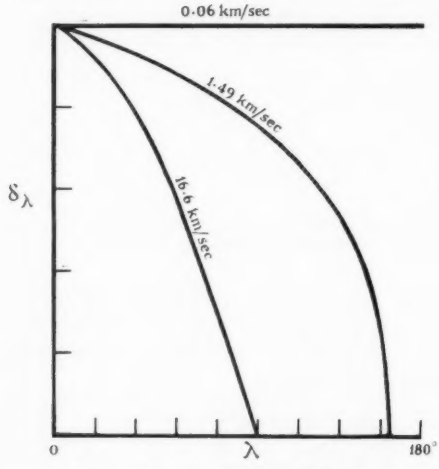

FIG. 9.—*Relative density of falls, δ_λ, as a function of λ.*

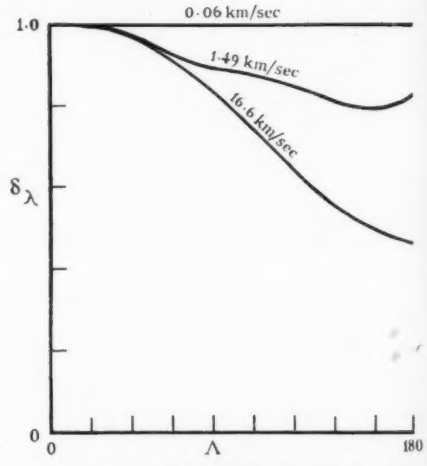

FIG. 10.—*Relative density of falls, δ_λ, as a function of Λ, for the three summed models.*

We specify the position of a fall on the surface of the Earth by γ, its latitude taken with respect to the ecliptic plane rather than the Earth's equator; and ψ, a "longitude" measured from the antapex, hence (neglecting the tilt of the Earth's axis) equivalent to time of day. Then

$$\cos\Lambda = \cos\gamma\cos\psi. \tag{13}$$

Knowing Λ, therefore δ_λ, as a function of latitude and time of day, it is possible to compute the relative average fall density over a whole gore of the Earth's surface, from pole to pole, corresponding to a particular time of day, by graphically integrating the equation

$$\delta_\psi \propto \int_0^{\pi/2} \delta_\lambda \cos\gamma\, d\gamma. \tag{14}$$

Theoretical fall density–time of day curves for the three velocity models are presented, then, in Fig. 11. The observed falls–time of day histogram shows a marked resemblance to the high-velocity model.

TABLE II

Three meteorite-bombardment models capable of reproducing the observed apparent radiant distribution

Velocity v_0	Angle of incidence I	Proportion of meteorites approaching at I
0·06 km/sec	30°	·300
	60°	·065
	90°	·635
1·49 km/sec	35°	·346
	70°	·227
	105°	·427
16·6 km/sec	10°	·023
	20°	·046
	30°	·068
	40°	·087
	50°	·102
	60°	·112
	70°	·115
	80°	·113
	90°	·106
	100°	·094
	110°	·080
	120°	·064
	130°	·046
	140°	·031
	150°	·018
	160°	·008
	170°	·002

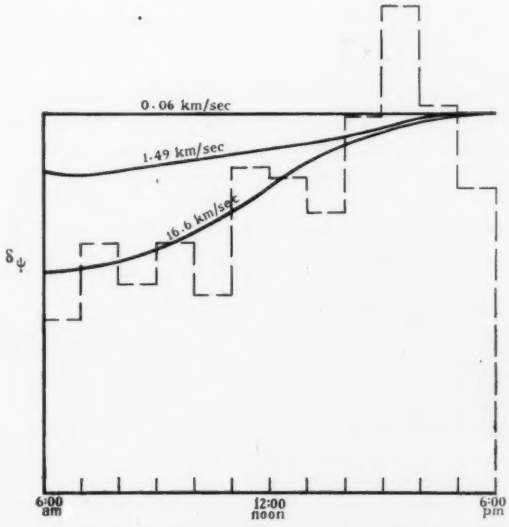

FIG. 11.—*Theoretical curves of fall density vs. time of day, compared with the observed distribution of falls (dashed line from Fig. 3).*

The value 16·6 km/sec attached to this model is not particularly meaningful, because the δ_ψ–ψ curve plotted for it in Fig. 11 is very nearly the limiting relationship approached as velocities increase and the effect of the Earth's gravity (i.e. the zenith attraction) becomes negligible. H. C. Urey (private communication) has pointed out that it is quite unrealistic to think in terms of a velocity as high as 16·6 km/sec, for in such a case meteorites with small apparent radiant angles ($\phi < 42°$) would have to approach at greater than solar system escape velocity; a meteorite capable of falling at $\phi = 180°$, on the other hand, would have to pass within 0·1 a.u. of the Sun, and the primeval gases which are found in meteorites could not have survived the high temperature at this small perihelion distance.

An 8 km/sec model escapes these difficulties. At this velocity, $\phi = 0°$ falls would come from orbits with aphelion at 3·96 a.u. and $\phi = 180°$ falls from orbits with perihelion at 0·36 a.u. The fall density–time of day curve for such a model will lie above but close to the 16·6 km/sec curve in Fig. 11.

The δ_ψ–ψ curve given for the 0·06 km/sec model in Fig. 11 is also a limiting case approached as velocities become very low. Since δ_λ for $v_0 = 0{\cdot}06$ km/sec (Fig. 9) is constant, it is obvious that δ_ψ for that velocity must also be constant, regardless of angle or angles of incidence.

These computations have not taken into account the fact that the Earth's axis is tilted $23\frac{1}{2}°$ to the pole of the ecliptic, hence that the aspects the Earth's time zones present to the meteorite bombardment change with the seasons. The effect that this tilt has on the δ_ψ–ψ relationship was investigated, and the error introduced by its neglect proved to be small (about 1 per cent).

5. *Conclusion.*—The statistical distributions of meteorite falls among the hours of the day, and over the range of apparent radiant angles, are consistent only with a bombardment of the Earth by "fast" meteorites ($v_0 \sim 8$ km/sec, subject to the condition that meteorites do not come from interstellar space).

A fall for which $v_0 = 8$ km/sec and $I = 70°$ is equivalent to an orbit of $a = 1{\cdot}31$ a.u., $e = 0{\cdot}32$, whose perihelion lies inside Venus's orbit and whose aphelion is beyond Mars. Clearly it is impossible to reconcile the high-velocity model with Earth-like orbits.

To the extent that the two statistical distributions we have employed are true distributions, then, it is possible to conclude that the stony meteorites pursue asteroid-like orbits, and were not derived from the surface of the Moon.

Acknowledgments.—An expression of gratitude is due to P. J. Message for reading this work in manuscript and offering helpful suggestions. The research was carried out while the writer studied under an American Chemical Society Petroleum Research Fund fellowship.

Department of Geodesy and Geophysics,
Madingley Road,
Cambridge:
1960 *September* 29.

Smithsonian Astrophysical Observatory,
60 *Garden Street,*
Cambridge 38,
Mass., U.S.A.

References

Newton, H. A., 1888. Relation which the former Orbits of those Meteorites that are in our Collections and that were seen to fall, had to the Earth's Orbit, *Amer. J. Sci.* (Series III), **36**, 1–14.

Öpik, E. J., 1951. Collision Probabilities with Planets and the Distribution of Interplanetary Matter, *Armagh Obs. Contrib.* No. 6, 165–199.

Prior, G. T. and Hey, M. H., 1953. *Catalogue of Meteorites*, British Museum of Natural History, London, 432 pp.

Urey, H. C., 1959, Primary and Secondary Objects, *J. Geophys. Res.*, **64**, 1721–1737.

Wylie, C. C., 1948. The Orbits of three Stone-Dropping Meteors: Tilden, Paragould, and Archie, *Pop. Astron.* (Northfield, Minnesota), **56**, 273–274.